2-11-2015

Development of Functionalized Nanoporous Materials for Biomass Transformation to Chemicals and Fuels

Iman Noshadi
noshadi.iman@gmail.com

Development of Functionalized Nanoporous Materials for Biomass Transformation to Chemicals and Fuels

Iman Noshadi, PhD

University of Connecticut, [2015]

Abstract

An ever increasing global energy demand and evolving geopolitical scenarios has put the non- renewable and depleting petroleum resources under pressure. This, coupled with a concern for the environment, make the development of alternative and renewable sources of fuel, as a replacement for fossil fuels, an imperative task for the transition to a sustainable energy future. The production of biofuels from waste and renewable biomass needs to be catalyzed by acids and bases. However, homogenous acids, while efficient, come with concomitant problems of product purification, equipment corrosion, non-reusability while being environmental hazards. These issues are mitigated by heterogeneous catalysts.

This thesis explores the development and application of several novel nanoporous heterogeneous solid acids and solid bases that successfully catalyze the conversion of renewable and waste biomass feedstock such as vegetable oils, cellulose, algae, brown grease and acidulated bone oil into fuels and biorenewable chemicals. The catalysts were used for developing and optimizing renewable resource utilization processes. As an example, the 100% transformation of a municipal waste such as brown grease into biodiesel, synthesis gas and bio-oil illustrates the prototype blue print of a process which can be used for power generation and biofuel production from a low grade feedstock and a potential health hazard with high municipal management costs and little alternative avenues for usage.

The novel chemistries employed in the synthesis of these structures results in nano materials with very high surface area, mesoporosity and superhydrophobic character with catalytic activities superior to all corresponding commercially available solid catalysts. In some studies, the catalytic activity was found to be superior to even homogenous catalysts. In addition, the limited reduction in catalytic activity over cycles of usage make these nanoporous heterogeneous catalysts attractive and sustainable candidates for the development of scaled up reactor modules to commercialize biofuels and biorenewable chemical production with minimal ramifications on the environment and production equipment.

Development of Functionalized Nanoporous Materials for Biomass Transformation to Chemicals and Fuels

Iman Noshadi

B.S., Shiraz University, **[2006]**

M.S., University Technology Malaysia, **[2011]**

A Dissertation

Submitted in Partial Fulfillment of the

Requirements for the Degree of

Doctor of Philosophy

at the

University of Connecticut

[2015]

APPROVAL PAGE

Doctor of Philosophy Dissertation

Development of Functionalized Nanoporous Materials for Biomass Transformation to Chemicals and Fuels

Presented by:

Iman Noshadi, B.S., M.S.

Co-Major Advisor _____
Richard Parnas

Co-Major Advisor _____
Steven Suib

Associate Advisor _____
Luyi Sun

Associate Advisor _____
Ranjan Srivastava

Associate Advisor _____
George M. Bollas

University of Connecticut
[2015]

Acknowledgements

I thank the Department of Chemical and Biomolecular Engineering at the University of Connecticut for the opportunity to work towards a Ph.D. I thank my advisory committee, Prof. Steven Suib, Prof. Richard Parnas, Prof. Luyi Sun, Prof Ranjan Srivastava and Prof. George Bollas for their support, guidance and valuable suggestions over the course of my study. I thank Dr. Fujian Liu of Shaoxing University for his excellent collaboration.

I thank Prof. Yao Lin for his valuable suggestions and collaborations on several projects.

I thank Mrs. YoungHee Chudy of the Polymer Program, Institute of Materials Science, for her constant encouragement, motivation and support.

I would like to thank my friends and colleagues, Baishali, Eddy and Ranjan for their friendship and collaboration. I would like to thank Prof. Alex Asandei's group Joon Sung, Vignesh, Chris and Olu for their support. I also thank all friends in the department and outside the department whose friendship supported me through the course of this PhD, in particular Hasan, Hamid and Noureddin.

I owe my gratitude to Prof. Kazerounian and the Uconn School of Engineering for their support and encouragement.

I thank Prof. Ali Khademhosseini of Harvard and MIT Division of Health Sciences and Technology for the opportunity to work with him during my PhD and his valuable advice.

I am indebted to my Father Mr. Manoucher Noshadi, mother Mrs. Manijeh Yousefi, brother Mohsen and sister Anis for their support of me and belief in me, despite overcoming struggles and vicissitudes of life. It is their respect for education that prompted me to pursue the direction of research and higher studies.

It is to my family that I dedicate my thesis

Table of contents

Chapter 1.1 Transesterification Catalyzed by Superhydrophobic–Oleophilic Mesoporous Polymeric Solid Acids: An Efficient Route for Production of Biodiesel

Introduction

Increase in energy demand and environmental concerns coupled with depletion in world petroleum reserves have been the primary drivers for the development of alternative and renewable sources of energy. Biodiesel is a renewable fuel comprising of alkyl esters. It is made from vegetable oil and animal fat and proffers advantages of renewability, better lubricity and biodegradability. Additionally, in comparison to petro diesel, its use results in decreased particulate emission, unburned hydrocarbons and carbon monoxide [1-5].

Acid catalysts can simultaneously catalyze both esterification and transesterification without forming any soap, unlike base catalysts [6-8]. Thus they can be employed to produce biodiesel from low-quality and low cost feedstock such as waste cooking oil or renewable plants oil [6-8]. Although conventional mineral acids such as H_2SO_4 or HCl are excellent catalysts for converting crude oils to biodiesel, they are environmentally unfriendly and difficult to recycle in addition to being highly corrosive. This restricts their application [9-14]. Solid acids such as sulfated zirconia, heteropolyacids and acidic resins, on the other offer advantages of recyclability and reduced corrosion. Additionally, being environmentally friendly, they have been widely used for production of biodiesel at laboratory scale [9-14]. However their poor porosity restricts their catalytic capabilities and largely constrains their application in biodiesel production [9-14]. Mesoporous solid acids, with high BET surface areas and abundant and uniform mesoporosity overcome the disadvantage of porosity limitations [15-17] and hence exhibit very good catalytic

activities in various acid-catalyzed reactions. Typical mesoporous solid acids such as sulfonic group functional mesoporous silica (SBA-15-SO_3H) and mesoporous sulfated ZrO_2 [18,19] have been studied with good results in esterification and transesterification [18, 19]. The limitation on their catalytic activity arises from their inorganic hydrophilic framework and hence low miscibility for various organic substrates [20-22]. Very recently, Liu et al. have successfully synthesized mesoporous polydivinylbenzene (PDVB) based solid acids, which showed superhydrophobicity and good oleophilicity, which result in their excellent catalytic activities towards transesterification to biodiesel. The superhydrophobicity and good oleophilicity results in superior wettability and good miscibility with organic substrates, favorable characteristics for enhanced catalytic activity in transesterification [22]. Thus, synthesis of mesoporous solid acids with good oleophilic polymer network may be considered as an important step towards improvement of their catalytic activities for biodiesel production. This work demonstrates successful preparation of sulfonic group-functionalized, stable mesoporous solid acids with excellent hydrophobicity by copolymerization of divinylbenzene (DVB) with sodium *p*-styrene sulfonate (H-PDVB-SO_3H-*x*s) under solvothermal conditions without using any surfactant templates. H-PDVB-SO_3H-*x*s samples have high BET surface areas, large pore volumes, adjustable active site concentrations, and exhibit excellent hydrophobicity. Catalytic tests have shown that H-PDVB-*x*-SO_3H's exhibit extraordinary catalytic activities and recyclability in transesterification for production of biodiesel as compared with those of conventional solid acid of ZMS-5 zeolite, carbon solid acid and Amberlyst 15.

Experimental section

Preparation of Mesoporous H-PDVB-x-SO_3H's

Sodium 4-vinylbenzenesulfonate (SVBS) was copolymerized with DVB by using AIBN initiator under hydrothermal conditions. As a typical run, 2.0 g of DVB was added to 0.5 g of SVBS. This monomer mixture was added to a mixture of 0.065 g AIBN, 25 ml THF and 2.5 ml distilled water and stirred for 2 hours at room temperature, followed by autoclaving at 100 °C for 1 day and evaporating of the solvents. The resultant solid obtained is white in color. Then the resulted sample was ion exchanged by using sulfuric acid as follows: 1.0 g of this solid acid was added into a mixture of 30 ml distilled water, 10 ml ethanol and 5 ml sulfuric acid, vigorously stirred for 24 hours and filtered. The residue on the filter paper was washed thoroughly with water and dried at 80°C for 6 hours prior to use, giving the sample of H-PDVB-SO_3H-0.16.

For comparison, ZMS-5 zeolite and carbon solid acid were synthesized according to the literature [23, 24].

Characterizations

Nitrogen isotherms were measured using a Micromeritics ASAP 2020 M system. The samples were outgassed for 10 h at 150 °C before the measurements. The Barrett–Joyner–Halenda (BJH) model was used to calculate the pore-size distribution for mesopores. A Bruker 66 V FTIR spectrometer was used for FTIR spectral measurements. Acid−base titration with standard NaOH solution was employed to estimate the acid exchange capabilities of the catalysts. Elemental analyses (C, H, N & S) were performed on a Perkin–Elmer series II CHNS analyzer 2400.

Catalytic reactions

Model transesterification reactions were carried out on triolein with methanol, respectively. As a typical run, 2 g of triolein was added into a three-necked round flask equipped with a condenser and a magnetic stirrer, and then the temperature was increased to 65 °C. 10.9 mL of ethanol and 0.05 g of catalyst were quickly added under strong stirring, the reaction was kept at 65 °C for 16 h. The molar ratio of triolein/methanol was 1:120 and the mass ratio of catalyst/triolein was 0.05.The reaction products were analyzed by gas chromatography (Agilent 5390) with a flame ionization detector (FID).

Results and discussion

Catalyst characterization

Figure 1.1 shows the N_2 isotherms and pore size distribution of *p*-PDVB-SO_3H. Clearly, *p*-PDVB-SO_3H shows a type-IV curve with a sharp capillary condensation step at P/P_0=0.8-0.95, indicating the formation of obviously mesoporous in the sample, which exhibits relative high BET surface area (171 m^2/g) and large pore volume (0.52 cm^3/g), much higher than those of Amberlyst 15 and carbon based solid acid (Table 1). Correspondingly, *p*-PDVB-SO_3H shows very uniform pore size centered at 21.2 nm, in good agreement with the results published by us previously [20]. Additionally, the S content and H concentration of *p*-PDVB-SO_3H were 1.3 and 1.8 mmol/g respectively, higher than those of H-Beta and H-ZSM-5, lower than those of Amberlyst 15, H-USY and C-SO_3H. In general, the increasing of the concentration of active site usually results in the decreasing of BET surface areas of the samples [20].

Figure 1.2 shows the FT-IR spectrum of *p*-PDVB-SO_3H. Notably, the peaks at around 620 and 1092 cm^{-1} associated with S-O, and S=O bond could be clearly seen; In the meanwhile, the peak at 1042 cm^{-1} assigned to the formation of C-S bond could also be clearly observed. Above results confirmed that the sulfonic group has been successfully introduced into *p*-PDVB-SO_3H.

Figure 1.3 shows the contact angles of p-PDVB-SO_3H for water and triolein. Notably, the water droplet contact angle of 150°, on the surface of p-PDVB-SO_3H indicates its superhydrophobic nature; On the contrary, the contact angle of soybean oil or methanol droplet on the surface of p-PDVB- SO_3H is nearly 0° indicating its super wettability for oil and methanol. Interestingly, the contact angle of 120° for glycerin on the same surface indicates a good anti-wettability for glycerin. The super wettability of p-PDVB-SO_3H for oil and good anti-wettability for glycerin and water were favorable for enhancement of its catalytic activities in transesterification of oil with methanol. To the best of our knowledge, solid acids with good hydrophobic and oleophilic properties have not been reported previously.

Figure 1.4 shows TG curves of p-PDVB-SO_3H and Amberlyst 15, both of them demonstrate the weight loss associated with the desorption of adsorbed water, destruction of sulfonic group and polymeric network ranged from 30 to 150, 200 to 440 and 440 to 540 °C; Notably, the weight loss assigned to destruction of sulfonic group and polymeric network were centered at around 364 and 497 °C, which were much higher than those of Amberlyst 15 (295–439 °C), indicating the better thermal stability of p-PDVB-SO_3H than that of commercial Amberlyst 15. Similar results have also been reported previously [22, 23].

Catalytic reactions

Figure 1.5 shows the catalytic kinetics curves in transesterification of soybean oil with methanol using various catalysts. Clearly, *p*-PDVB-SO_3H showed very good catalytic activities when compared with those of ZMS-5 zeolite, carbon solid acid and Amberlyst 15. After only 4 hours of reaction, the conversion of soybean oil catalyzed by *p*-PDVB-SO_3H was much higher than those of H-form mesoporous ZSM-5, Amberlyst 15, and carbon based solid acid. After 16 hours of reaction time a conversion of 78 % was achieved with *p*-PDVB-SO_3H, which was much higher than those of H-form mesoporous ZSM-5, Amberlyst 15 and carbon solid acid (57.32 %, 43.23 % and 40.23 % respectively), suggesting the excellent catalytic activities of *p*-PDVB-SO_3H in transesterification for production of biodiesel.

Figure 1.6 shows the recyclability of *p*-PDVB-SO_3H in transesterification of soybean oil with methanol. Interestingly, compared with fresh *p*-PDVB-SO_3H (conversion at 78.3%), even after recycled for one time, the sample showed the conversion at 72.3%, further recycled for two times, the conversion of soybean oil was still up to 71.0 %. The decrease in catalytic activities of *p*-PDVB-SO_3H was not very large confirming that *p*-PDVB-SO_3H do not suffer instant deactivation.

Conclusions

An efficient solid acid of *p*-PDVB-SO_3H with hydrophobic and good oleophilic network was successfully prepared through copolymerization of DVB with sodium 4-vinylbenzenesulfonate. The solid acid exhibited the characteristics of high BET surface area, large pore volume, a stable and hydrophobic network and a high concentration of active sites, which result in their superior catalytic activities and recyclability in

transesterification of triglyceride or plant oil with methanol for production of biodiesel as compared with those of conventional solid acid including H-form mesoporous zeolite, Amberlyst-15 and carbon based solid acid. The successful synthesis of H-PDVB-SO_3H-*x*s will open new avenues for preparation and application of efficient solid acid catalysts for production of biodiesel towards transesterification.

References

[1] Jaliliannosrati H, Amin NAS, Talebian-Kiakalaieh A, Noshadi I (2013). Bioresource Technology. In press

[2] Talebian-Kiakalaieh, A, Amin, NAS., Zarei, A, Noshadi, I (2013) Applied Energy. Article in Press.

[3] Liu F, Zhengb A, Noshadi I, Xiao FS (2013) J App. Cata.:Envorom. **136** , 193–201

[4] Molaei Dehkordi A, Ghasemi M (2012) Fuel Pro. Tech., **97**, 45-51

[5] Wilson K and Lee AF. (2012) Catal. Sci. Technol.,**2**, 884-897

[6] Lacome T, Hillion G, Delfort B, Revel R, Leporc S, Paille F, Pat FR (2005) 2855518-A1.

[7] Hillion G, Delfort B, Durand I, Pat FR (2005) 2866653-A1.

[8] Corma A (1995) Chemical Reviews, **95** 559.

[9] Corma A (1997) Chemical Reviews **97** 2373.

[10] De Vos DE, Dams M, Sels B.F, Jacobs PA, (2002) Chemical Reviews, **102** 3615.

[11] Dioumaev VK, Bullock RM ,(2003) Nature **424** 530.

[12] Gates BC (Ed.), (1992) Catalytic Chemistry, Wiley, New York.

[13] Davis ME, Nature, (2002), **417** 813–821.

[14] Chai F, Cao FH, Zhai FY, Chen Y, Wang X.H, Su ZM (2007) Advanced Synthesis and Catalysis , **349** 1057.

[15] Wan Y, Zhao DY (2007) Chemical Reviews **107** 2821.

[16] Xing R, Liu N, Liu YM, Wu HH, Jiang YW, Chen L, He MY, Wu P (2007) Advanced Functional Materials, **17** 2455.

[17] Liu FJ, Li CJ, Ren LM, Meng XJ, Zhang H, Xiao FS (2009) Journal of Materials Chemistry, **19** 7921.

[18] Melero JA, Van Grieken R, Morales G (2006) Chemical Reviews, , **106** 3790.

[19] Arata K (1996) Applied Catalysis A: General, **146** 143.

[20] Liu FJ, Kong WP, Qi CZ, Zhu LF, Xiao FS, (2012) ACS Catalysis, **2** 565.

[21] Liu FJ, Meng XJ, Zhang YL, Ren LM, Nawaz F, Xiao FS (2010) Journal of Catalysis, **271** 52.

[22] Liu FJ, Li W, Sun Q, Zhu LF, Meng XJ, Guo YH, Xiao FS (2011) ChemSusChem, **4** 1059.

[23] Liang X, Yang J (2009) J. Catal Lett, 132:460–463.

[24] Liu FJ, Willhammar T, Wang L, Zhu L, Sun Q, Meng X, Carrillo-Cabrera W, Zou X, Xiao FS (2012) J. Am. Chem. Soc. **134** 4557−4560.

Table 1.1 The textural and acidic parameters of various solid acid catalysts.

Run	Samples	S content (mmol/g) [a]	Acid sites (mmol/g) [b]	S_{BET} (m^2/g)	V_p (cm^3/g)	D_p (nm)[c]
1	*p*-PDVB-SO_3H	1.3	1.8	171	0.52	21.5
2	Amberlyst 15	4.30	4.70	45	0.31	40
3	SBA-15-SO_3H	1.36	1.26	820	1.40	7.3
4	C-SO_3H	1.91	2.0	10<	-	-
5	H-ZMS-5-OM	-	0.92	368	0.31	14.5
6	H-Beta [e]	-	1.21	550	0.20	0.67
7	H-USY [f]	-	2.06	623	0.26	14.7
8	H_2SO_4	10.2	20.4	-	-	-

[a] Measured by elemental analysis.

[b] Measured by acid-base titration.

[c] Pore size distribution estimated from BJH model.

[d] The sample after being recycled for five times in esterification of acetic acid with cyclohexanol.

[e] Si/Al ratio at 12.5.

[f] Si/Al ratio at 7.5.

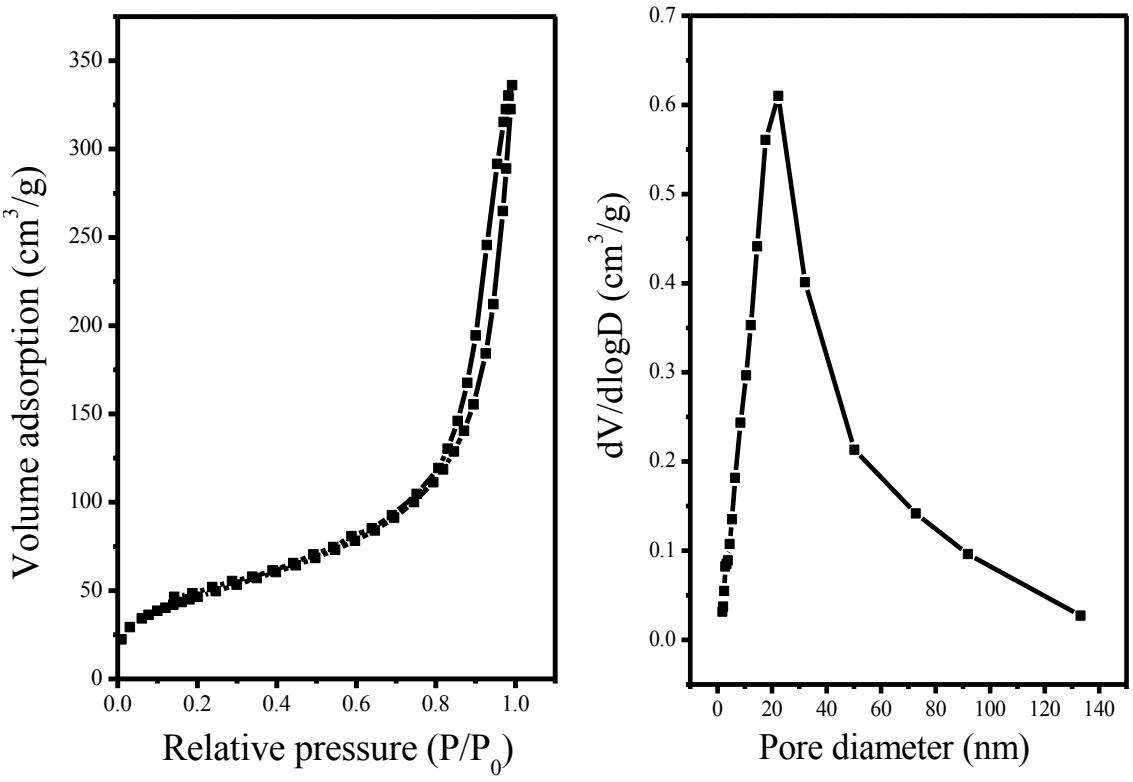

Figure 1.1 N_2 isotherms and pore size distribution of *p*-PDVB-SO_3H.

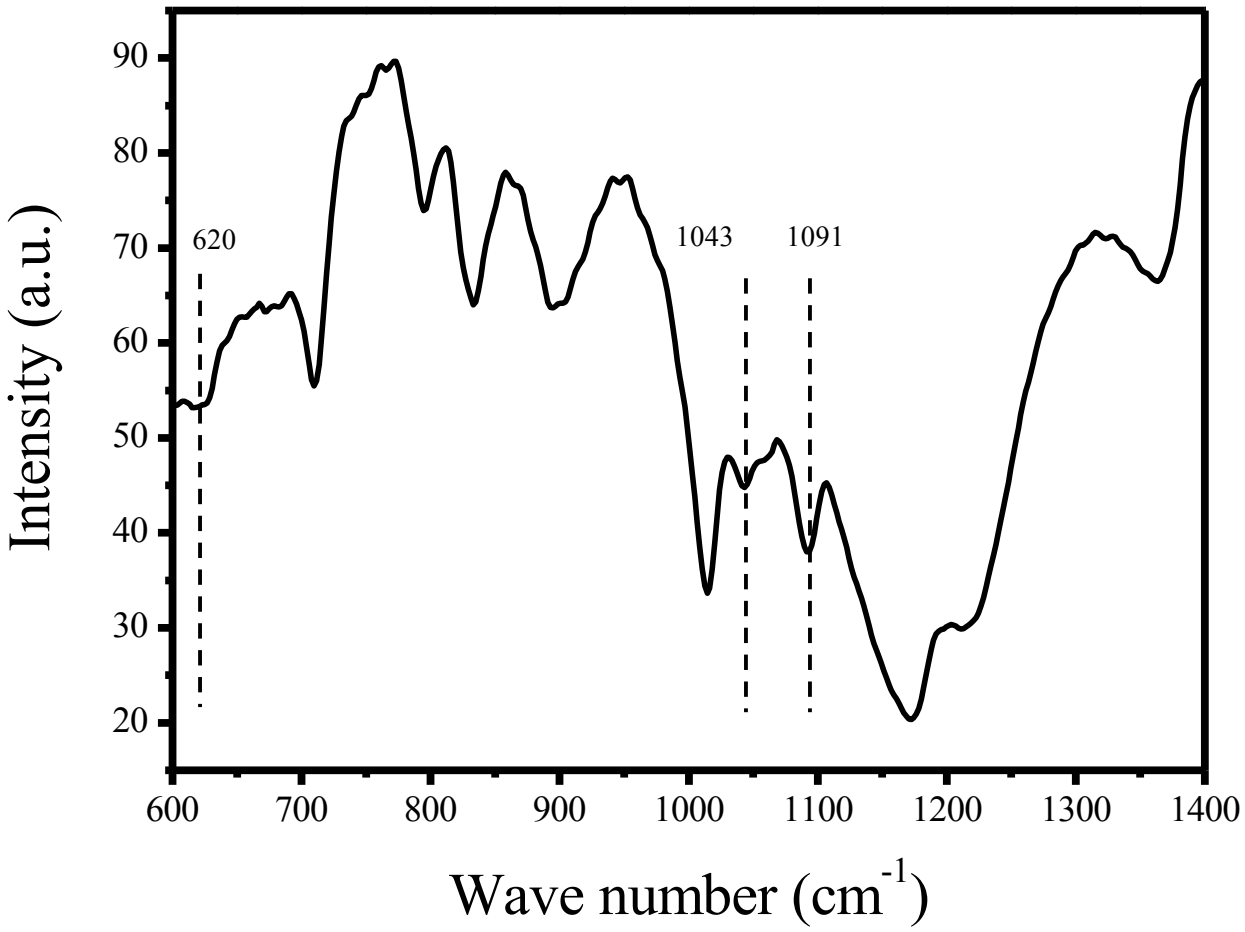

Figure 1.2 FT-IR spectrum of *p*-PDVB-SO_3H.

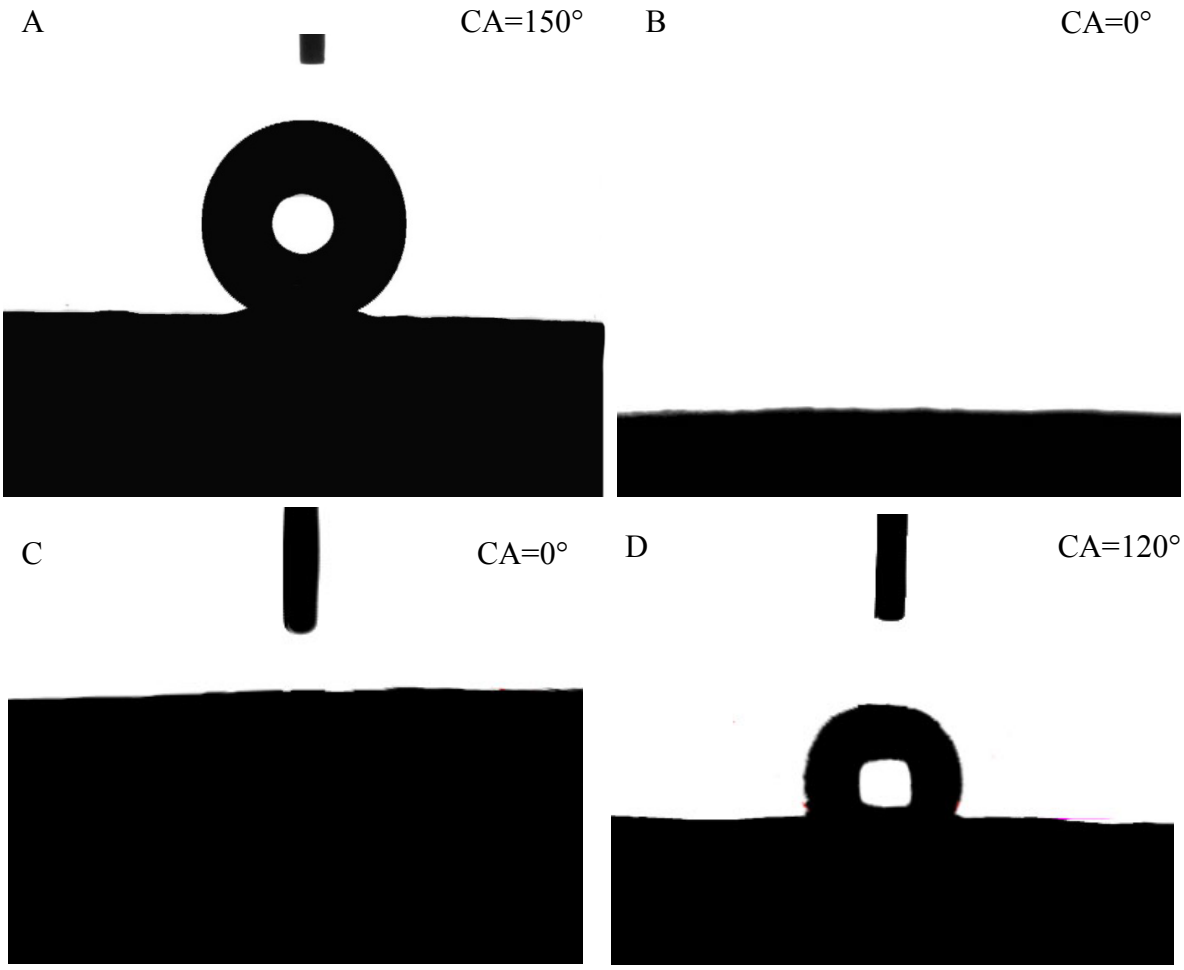

Figure 1.3 Contact angles of (A) water droplet, (B) soybean oil droplet, (C) methanol and (D) glycerin on the surface of *p*-PDVB-SO_3H.

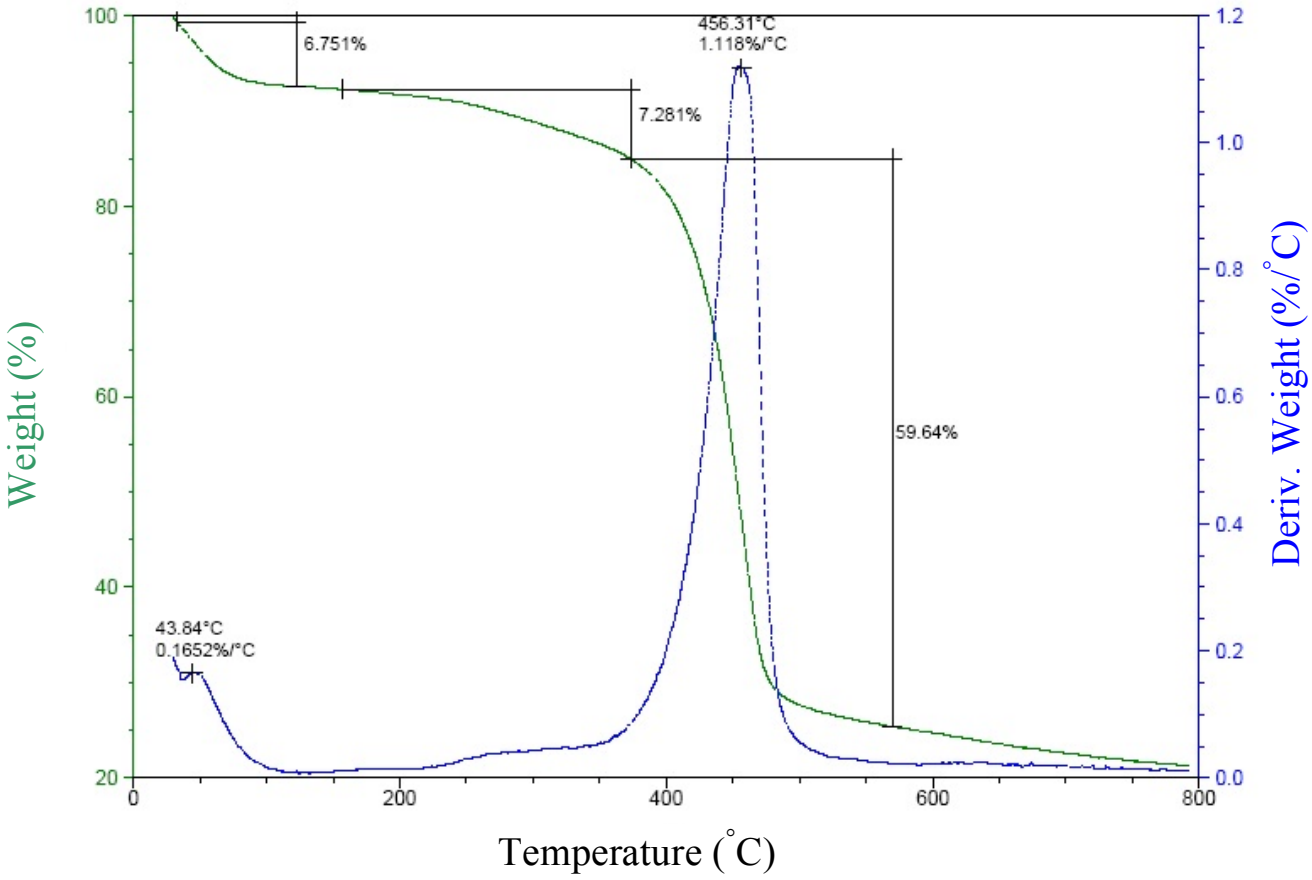

Figure 1.4 TG-DTA curves of *p*-PDVB-SO_3H.

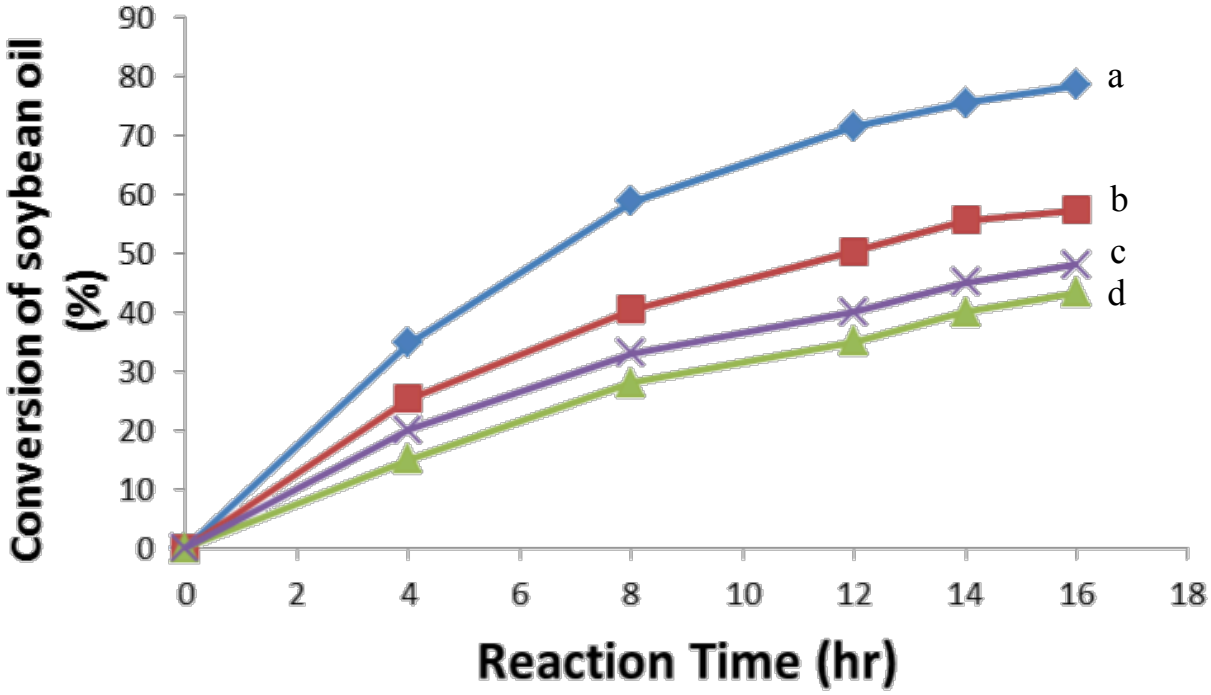

Figure 1.5 Catalytic kinetics curves in the transesterification of soybean oil with methanol over (a) *p*-PDVB-SO_3H, (b) H-form mesoporous ZMS-5 zeolite, (c) Amberlyst 15 and (d) carbon solid acid.

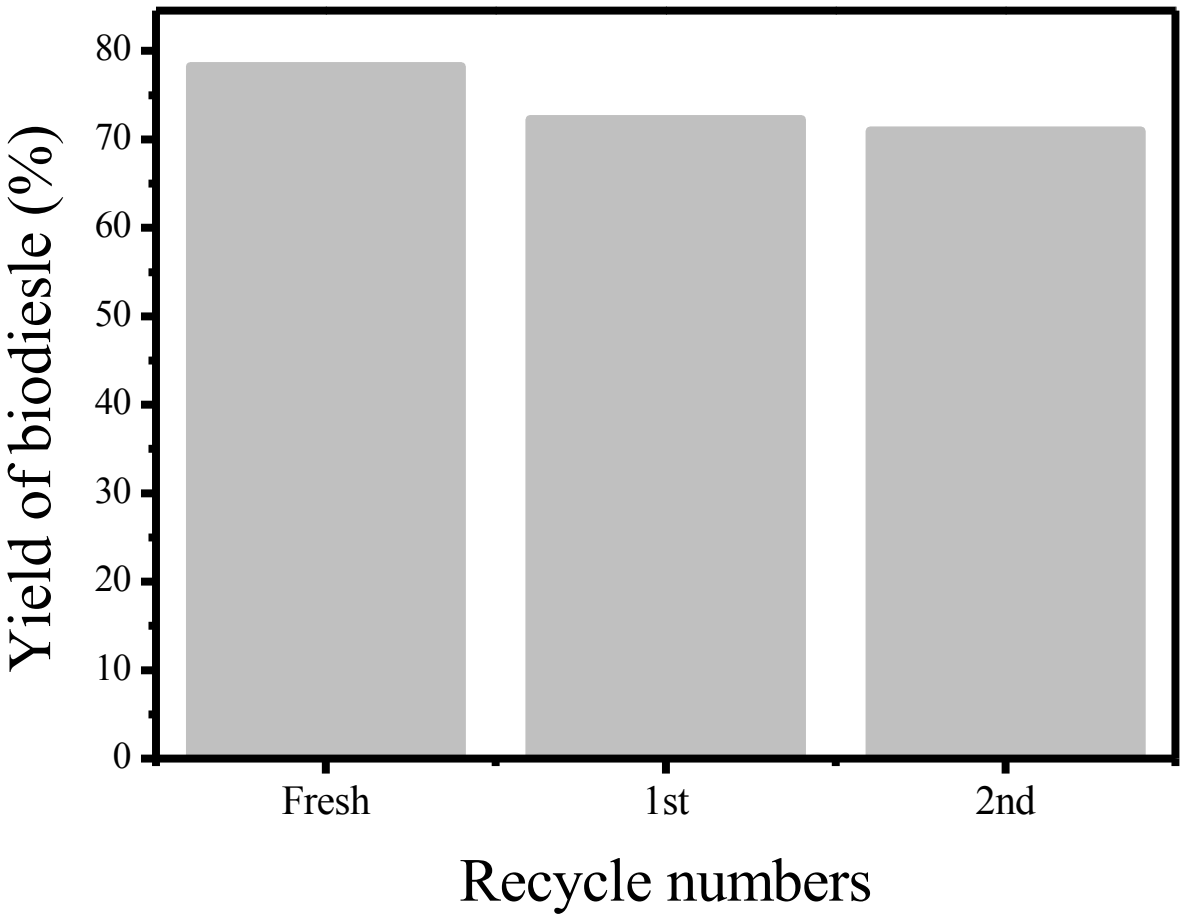

Figure 1.6 *p*-PDVB-SO_3H catalyst recyclability for transesterification of soybean oil with methanol (T=65 °C, time=16 hr)

Chapter1.2 Design and synthesis of hydrophobic and stable mesoporous polymeric solid acid with ultra strong acid strength and excellent catalytic activities for biomass transformation

Introduction

During the last two decades, acid catalysis have received considerable attention because of their wide applications in the areas of oil refining, biomass transformation, green chemical processes and fine chemical industry [1], [2], [3], [4], [5], [6], [7], [8], [9], [10], [11], [12], [13], [14], [15], [16], [17], [18], [19], [20], [21], [22], [23], [24], [25] and [26]. Among various acid catalysts, the fluorine containing acids such as CF_3SO_3H, HF-SbF_5 show very important applications because of their ultra strong acid strength when compared with conventional mineral acids such as H_2SO_4 and HCl [27], [28], [29] and [30], which results from the presence of strong electron withdrawing groups in these acids. The unique strong acid strength results in their extra-ordinary catalytic activities in various reactions such as alkylation, isomerization, oligocondensation reactions of alkanes, Friedel–Crafts, polymerization, Koch carbonylation, cracking and biomass transformation [27] and [31]. However, homogeneous superacids are usually highly toxic, environmentally hazardous, and cannot be easily recovered from the products mixture, which largely constrain their wide applications in industry [31]. The successfully preparation of solid strong acids has basically overcome the problems caused by homogeneous strong acids because of their characters including reductive corrosion, environmentally friendly, superior catalytic activities, good catalytic selectivity and recyclability. Typically solid strong acids such as sulfated metal oxides and heteropolyacids have been widely used in various acid-catalyzed reactions including

esterification, isomerization, transesterification and Friedel–Crafts [32], [33], [34],[35], [36] and [37], which are more active than the solid acids with relatively weak acid strength [32], [33],[34], [35] and [36]. However, the existed drawbacks such as low BET surface areas, partial deactivation of the active sites by the water resulted from the hydrophilic frameworks largely decrease their catalytic activities and lives, which was attributed to the water usually act as a typical byproduct in many acid-catalyzed reactions, further resulting in the opposite reactions and the leaching of active sites [8], [9], [38],[39], [40], [41] and [42].

The presence of Nafion type of acidic resin offers great opportunities for the synthesis of solid strong acids ($pK_a \approx -12$) with hydrophobic polymer network, which was thought to be one of the strongest solid acids [43], [44] and [45], giving excellent thermal stability and good catalytic activities [46], [47] and [48]. However, its very low concentration of acidic site and poor porosity largely constrain it used as efficient solid acid in various acid-catalyzed reactions [43] and [45].

Therefore, synthesis of solid acids with enhanced acid strength, adjustable hydrophobicity and abundant nanoporosity are the crucial problems faced to the scientists working on heterogeneous acid catalysis. However, it is still challenging to synthesize solid acids with large BET surface areas, ultra strong acid strength, adjustable hydrophobic networks, and high contents of acid sites up to now, which would be very important for their wide applications [8], [9], [35], [39], [40], [41], [42], [49], [50], [51], [52], [53] and [54].

We report here the successfully preparation of mesoporous polymeric solid acid (PDVB-SO_3H-SO_2CF_3) with large BET surface areas, good hydrophobicity and oleophilicity, superior thermal stability, and ultra strong acid strength through grafting of strong electron withdrawing group of SO_2CF_3 onto the network of mesoporous solid acid of PDVB-SO_3H, which could be synthesized from sulfonation of superhydrophobic mesoporous PDVB or copolymerization of DVB with sodium *p*-styrene sulfonate. Interestingly, the resulted PDVB-SO_3H-SO_2CF_3 showed much better catalytic activities and recyclability in biomass transformation toward depolymerization of crystalline cellulose to sugars and transesterification to biodiesel, Peckmann reaction of resorcinol with ethyl acetoacetate (PRE) and hydration of propylene oxide with water (HPW) than those of PDVB-SO_3H, Amberlyst 15, sulfonic groups functional mesoporous silica (SBA-15-SO_3H), and solid strong acids of SO_4/ZrO_2 and Nafion NR50. The successfully preparation of PDVB-SO_3H-SO_2CF_3 will open a new way for preparation of efficient and long lived mesoporous polymeric solid strong acid for catalyzing transformation of biomass into biofuels with large scale in industry.

Experimental

Chemicals and regents

All reagents were of analytical grade and used as purchased without further purification. Amberlyst 15, 3-mercaptopropyltrimethoxysilane (3-MPTS), crystalline cellulose of Avicel, tripalmitin, nonionic block copolymer surfactant of poly(ethyleneoxide)–poly(propyleneoxide)–poly(ethyleneoxide) block copolymer (Pluronic 123, molecular weight of about 5800), sodium *p*-styrene sulfonate and trifluoromethanesulfonate were

purchased from Sigma–Aldrich Company, Ltd. (USA). DVB, azobisisobutyronitrile (AIBN), tetrahydrofuran (THF), tetraethyl orthosilicate (TEOS), chlorosulfonic acid, dichlormethane, resorcinol, ethyl acetoacetate, methanol, propylene oxide, and dodecane were obtained from Tianjin Guangfu Chemical Reagent. H-form of Beta zeolite and ultrastable Y zeolite (USY) were supplied by Sinopec Catalyst Co.

Synthesis of samples

Synthesis of superhydrophobic mesoporous PDVB

Superhydrophobic mesoporous PDVB was synthesized by polymerization of DVB under solvothermal condition with starting system of DVB/AIBN/THF/H_2O at molar ratio of 1/0.02/16.1/7.23. As a typical run, 2.0 g of DVB was added into a solution containing of 0.05 g of AIBN and 20 mL of THF, followed by addition of 2 mL of H_2O. After stirring at room temperature for 3 h, the mixture was transferred into an autoclave and treated at 100 °C for 1 day. After evaporation of the solvents at room temperature, the mesoporous PDVB with monolithic morphology and opened mesoporous was obtained.

Synthesis of PDVB-SO_3H

PDVB-SO_3H was synthesized by stirring of PDVB in the mixture of chlorosulfonic acid and CH_2Cl_2. As a typical run, 1.5 g of PDVB was outgassed at 100 °C in a three-necked round flask for 12 h under flowing nitrogen. Then, a mixture containing 40 mL of CH_2Cl_2 and 20 mL of chlorosulfonic acid was quickly added into the flask below 10 °C. After stirring for 24 h under nitrogen atmosphere, the product was obtained from

filtering, washing with large amount of water for removing of residual sulfuric acid, stirring in dioxane, and drying at 80 °C under vacuum.

In the meanwhile, PDVB-SO_3H could also be synthesized from copolymerization of DVB with sodium *p*-styrene sulfonate under solvothermal condition, and the content of sulfonic group could be adjusted by changing of the molar ratio of DVB and sodium *p*-styrene sulfonate. As a typical run, 2.0 g of DVB was added into a solution containing 0.05 g of AIBN and 28 mL of THF, followed by addition of 2.5 mL of H_2O, then 0.64 g of sodium *p*-styrene sulfonate was also introduced. After stirring at room temperature for 3 h to form a homogeneous solution, the mixture was solvothermally treated at 100 °C for 24 h. After evaporation of the solvents at room temperature, the PDVB-SO_3Na sample with monolithic morphology was obtained. To get a PDVB-SO_3H sample, the PDVB-SO_3Na sample was further ion-exchanged using 1 M sulfuric acid. As a typical run, 0.5 g of PDVB-SO_3Na was dispersed into 50 mL of 1 M sulfuric acid. After stirring for 24 h at room temperature, the sample was washed with large amount of water until the filtrate was neutral, drying at 80 °C, PDVB-SO_3H was obtained.

Synthesis of solid strong acid of PDVB-SO_3H-SO_2CF_3

Strong solid acid of PDVB-SO_3H-SO_2CF_3 was synthesized from the treatment of PDVB-SO_3H by using of HSO_3CF_3, which results in grafting of strong electron withdrawing group of -SO_2CF_3 onto the network of PDVB-SO_3H. As a typical run, 1.5 g of PDVB-SO_3H was added into a flask containing 50 mL of toluene, followed by addition of 10 mL of HSO_3CF_3, then the reaction temperature was rapidly increased to 100 °C, after stirring

for another 24 h, PDVB-SO_3H-SO_2CF_3 was obtained from filtration, washing with large amount of CH_2Cl_2, and drying at 80 °C under vacuum.

For comparison, SBA-15-SO_3H with molar ratios of S/Si at 0.1 and SO_4/ZrO_2 were synthesized according to the literature [38] and [55].

Characterizations

Solid ^{31}P NMR characterization

The solid ^{31}P NMR spectra over PDVB-SO_3H and PDVB-SO_3H-SO_2CF_3 were performed as follows: prior to sorption of probe molecules, the sample was placed in a glass tube and then connected to a vacuum line for dehydration. The temperature was gradually increased at a rate of 1 °C/min and the sample was kept at final temperature of 125 °C at a pressure below 10^{-3} Pa over a period of 10 h and then cooled. Detailed procedures involved in introducing the TMPO probe molecule onto the sample can be found elsewhere [56], [57] and [58]. In brief, a known amount of TMPO adsorbate dissolved in anhydrous CH_2Cl_2 was first added into a vessel containing the dehydrated sample in a N_2 glove box, followed by removal of the CH_2Cl_2 solvent by evacuation at room temperature. To ensure a uniform adsorption of adsorbate probe molecules in the pores/channels of the mesoporous adsorbent, the sealed sample vessel was further subjected to a thermal treatment at 100 °C for 12 h. Prior to NMR measurements, the sealed sample tube was opened and the sample was transferred into a NMR rotor with a Kel-F end cap under a dry nitrogen atmosphere in a glove box.

The solid state NMR experiments were performed on a Varian Infinitypuls-400 spectrometer using a Chemagnetic 5 mm double-resonance probe. A Larmor frequency of

400.13, and 161.98 MHz, and a typical $\pi/2$ pulse length of 6.6, and 3.0 μs were adopted for ^{1}H and ^{31}P resonance, respectively. For the single-pulse ^{31}P MAS NMR experiment, an excitation pulse equivalent to ca. $\pi/4$ and are cycle delay of 15 s were used during spectrum acquisition. The chemical shifts for the ^{31}P resonance were referred to $(NH_4)_2HPO_4$ (0.0 ppm) and the experiments were carried out with a MAS frequency of 8 kHz

The acid strength over various samples could be also measured by ammonia sorption and temperature programmed desorption (NH_3–TPD) technique. As a typical run, 0.2 g of catalyst (40–60 mesh) was saturated with NH_3 at 30 °C for 45 min. Then, the sample was exposed to the flowing N_2 for removing of the physically adsorbed ammonia on the surface of the sample. Finally desorption of NH_3 was carried out by heating the sample from 30 to 700 °C. Desorption of NH_3 was analyzed by gas chromatography equipped with a TCD detector.

Nitrogen isotherms were measured using a Micromeritics ASAP 2020M system. The samples were outgassed for 10 h at 120 °C before the measurements. The pore-size distribution for mesopores was calculated using Barrett–Joyner–Halenda (BJH) model. FTIR spectra were recorded by using a Bruker 66V FTIR spectrometer. Differential thermal analysis (DTA) and thermo gravimetric analysis (TG) were performed on a Perkin-Elmer TGA7 and a DTA-1700 in flowing air, respectively. The heating rate was 10 °C/min. TEM images were performed on a JEM-3010 electron microscope (JEOL, Japan) with an acceleration voltage of 300 kV. Contact angles were tested on DSA10MK2G140, Kruss Company, Germany. XPS spectra were performed on a Thermo

ESCALAB 250 with Al Kα radiation at $y = 901$ for the X-ray sources, the binding energies were calibrated using the C_{1s} peak at 284.9 eV.

Catalytic reactions

Preparation of DNS reagent

As a typical run for preparation of DNS solution, 182 g of potassium sodium tartrate was added into 500 mL of hot deionized water at 50 °C, followed by addition of 6.3 g of 3,5-dinitrosalicylic acid (DNS) and 262 mL of 2 M NaOH, after dissolved, 5 g of phenol and 5 g of sodium sulfite were also introduced into the solution under vigorous stirring, after homogeneous solution was formed, the hot solution was cooled to room temperature and diluted with deionized water to 1000 mL to give the DNS reagent.

Depolymerization of crystalline cellulose

As a typical run, 100 mg of crystalline cellulose of Avicel was dissolved into 2.0 g of $[C_4mim]$ Cl ionic liquid at 100 °C for 1 h under stirring condition until a clear solution was formed. Then, 30 mg of PDVB-$[C_4mim][SO_3CF_3]$ was added, further stirring for 5 min to result in good dispersion of catalyst in reaction mixture, followed by addition of 600 μL of water. At different time intervals, samples were withdrawn, weighed, quenched immediately with cold water, and centrifuged at 14,800 rpm for 5 min for removing of catalysts and unreacted cellulose, giving the reaction mixture, which were collected and stored at 0 °C before DNS assay and HPLC analysis. In the meanwhile, the

isolated cellulose was thoroughly washed with water, and recovered by centrifugation. The amount of cellulose isolated was determined by weighing.

Testing total reducing sugar (TRS)

TRS were tested through DNS method [59] and [60]. As a typical run, a mixture containing of 0.5 mL of DNS regent and 0.5 mL of performed reaction mixture was heated for 5 min at 100 °C, after cooled to room temperature, 4 mL of deionized water was added for diluting the mixture. The color intensity of the mixture was measured in a NanoDrop 2000 UV-spectrophotometer at 540 nm. The concentration of total reducing sugars was calculated based on a standard curve obtained with glucose.

The concentrations of glucose and cellobiose in the reaction mixture were measured by HPLC system, in a Water 717plus autosampler (USA) system, in Aminex HPX-87H column and with a refraction index detector. The column's temperature was set to 65 °C. The volume of the injection was 10 μL. The eluent consisted of a previously filtered and degasified solution of sulfuric acid 5 mM at a flow of 0.5 (mL/min).

Results and discussion

Structural characterizations

Fig. 1.7 shows the N_2 sorption isotherms and pore size distribution of PDVB-SO_3H and PDVB-SO_3H-SO_2CF_3. Clearly, both of the samples exhibit typical type-IV isotherms, giving the steep increase at relative pressure between $0.8 < P/P_0 < 0.95$, confirming the formation of obvious mesoporosity in these samples [61] and [62]. Additionally, PDVB-

SO_3H and PDVB-SO_3H-SO_2CF_3 give the BET surface areas of 314 and 376 m^2/g, respectively (Table 1.2), much higher than those of SO_4/ZrO_2 (70 m^2/g, Table 1), Amberlyst 15 (40 m^2/g, Table 1.2) and Nafion NR 50 (0.02 m^2/g, Table 1.2), lower than those of SBA-15-SO_3H and H form zeolites (820–550 m^2/g, Table 1.2). Correspondingly, the pore sizes of PDVB-SO_3H and PDVB-SO_3H-SO_2CF_3 are distributed at 22.9 and 29.3 nm(Fig. 1.7 and Table 1.2), respectively. It should also be noted that after the introduction of -SO_2CF_3 group in PDVB-SO_3H, the BET surface area of PDVB-SO_3H-SO_2CF_3has certain decreasing because of the introduction of SO_2CF_3 group largely increases density of the network and blocks the mesopores of PDVB-SO_3H-SO_2CF_3. Similar result has also been reported previously [8].

Table 1.2 presents the textural parameters of various samples. Notably, PDVB-SO_3H shows the S content at 3.2 mmol/g. After introduction of electron withdrawing groups of -SO_2CF_3 in the sample of PDVB-SO_3H, the corresponding S content was increased up to 5.72 mmol/g, which was much higher than those of Nafion NR50 (0.86 mmol/g, Table 1), SO_4/ZrO_2 (0.72 mmol/g, Table 1.2), SBA-15-SO_3H (1.36 mmol/g, Table 1.2), and Amberlyst 15 (4.3 mmol/g, Table 1.2). The obviously increasing of S content demonstrated that the electron withdrawing group of -SO_2CF_3 has been successfully grafted onto the network of PDVB-SO_3H. It should be also noted that the acid capacity is higher than the amount of S for PDVB-SO_3H, which is attributed to partially oxidation of functional group such as C=C bond in PDVB network, further resulting in Fig. 1.8 shows the transmission electron microscopy (TEM) images of PDVB-SO_3H and PDVB-SO_3H-SO_2CF_3. Clearly, both PDVB-SO_3H and PDVB-SO_3H-SO_2CF_3 have abundant mesoporosity with the pore sizes ranged from 10 to 50 nm, in good agreement with

N_2 sorption isotherms results, the abundant mesoporosity comes from our unique solvothermally synthetic technology [42]. Fig. 1.9 shows the contact angle of PDVB-SO_3H-SO_2CF_3 for water and salad oil. Clearly, PDVB-SO_3H-SO_2CF_3 exhibits the contact angle for the water up to 135° (Fig. 1.9), indicating its excellent hydrophobicity. On the contrary, for the salad oil, PDVB-SO_3H-SO_2CF_3 gives the contact angle nearly 0° (Fig. 1.9), indicating its very good oleophilicity. The superior hydrophobic active site and oleophilic network will be favorable for increasing the exposition degree of active sites for the organic reactants in the processes of various catalytic reactions.

3.3. Active site characterizations

Fig. 1.10 shows the FT-IR spectra of PDVB, PDVB-SO_3H and PDVB-SO_3H-SO_2CF_3. Compared with PDVB, the peak around 1033–1040 cm^{-1} associated with C-S bond can be clearly found in the samples of PDVB-SO_3H and PDVB-SO_3H-SO_2CF_3, suggesting the presence of sulfonic group in these samples [63]. Except for the signal of sulfonic group, a new peak assigned to C-F (1289 cm^{-1}) bond can also be found in PDVB-SO_3H-SO_2CF_3, which confirms the successfully introduction of -SO_2CF_3 group in PDVB-SO_3H [64], in good agreement with element analysis results.

Fig. 1.11 shows the X-ray photoelectron spectroscopy (XPS) measurements of various samples. Clearly, both PDVB-SO_3H and PDVB-SO_3H-SO_2CF_3 show the signals of S, C and O, indicating the presence of sulfonic group in these samples. Except for S, C and O,

a new signal at around 690 eV associated with F_{1s} can also be observed in PDVB-SO_3H-SO_2CF_3, confirming successfully grafting of -SO_2CF_3 onto the network of PDVB-SO_3H. Correspondingly, the high resolved XPS spectrum of C_{1s} shows the signals at around 284.7, 286.2 and 291.4 eV associated with C-C, C-S and C-F bond could be found in PDVB-SO_3H-SO_2CF_3, suggesting the successfully introduction of -SO_2CF_3 in PDVB-SO_3H [64]. Interestingly, compared with PDVB-SO_3H, the signal of S_{2p} in PDVB-SO_3H-SO_2CF_3 shifted from 169.1 to 169.5 eV, attributing to the presence of strong electron withdrawing group of -SO_2CF_3 in PDVB-SO_3H-SO_2CF_3, which plays a key factor for increasing the acid strength of PDVB-SO_3H-SO_2CF_3.

Acid strength

Fig. 1.12 shows the solid-state ^{31}P MAS NMR of adsorbed TMPO over various samples, which is a unique and practical technique for acidity characterization of solid acid catalysts. Such method has been extensively used to investigate the acidity characterization of various solid acids, including zeolites, sulfated mesoporous metal oxides and heteropolyacids [56], [57], [58] and [59]. As verified by our previous investigations that ^{31}P chemical shift of TMPO can serve as the indicator for the Brønsted acid strength of solid catalysts [56]. Fig. 1.12 A-a displays the ^{31}P MAS NMR spectrum of TMPO adsorbed on PDVB-SO_3H, which shows highly overlapped ^{31}P resonance peaks spanning from ca. 70 to 80 ppm. Further analysis by Gaussian simulation reveals that the spectrum may be deconvoluted into two characteristic resonances with ^{31}P chemical shift of 72 and 80 ppm, each corresponding to a relative concentration of 40 and 60%, respectively. According to the range of the ^{31}P chemical shift, these two ^{31}P resonances above are ascribed unambiguously due to TMPO adsorbed on Brønsted acid sites with

various extents of protonation. It is well known that a low-field observed ^{31}P chemical shift value would represent a stronger acidic strength [56], [57], [58] and [59]. After the treatment by using superacid of HSO_3CF_3, the strong electron-withdrawing group of -SO_2CF_3 was grafted onto the network of PDVB-SO_3H, resulting in the sample of PDVB-SO_3H-SO_2CF_3. Correspondingly, the Brønsted acidic strength of PDVB-SO_3H-SO_2CF_3has been significantly enhanced and homogeneously distributed. As shown in Fig. 6 A-b, for PDVB-SO_3H-SO_2CF_3, only one uniform ^{31}P peak with chemical shift at 83 ppm can be observed. It is important to note that the Brønsted acidic proton at 83 ppm is much close to the superacid that a theoretical ^{31}P value of 86 ppm was determined as the threshold for superacidity[56], [57], [58] and [59]. As verified by our previous investigations based on theoretical calculations, a linear correlation between the ^{31}P chemical shift of TMPO and the proton affinity (PA) values, and hence the strengths of Brønsted acid sites [56]. According to the relationship between the PA and ^{31}P chemical shift ($\delta^{31}P = 182.866 - 0.3902 \times DPE$) [56], the proton affinities are ca. 284, 264 and 256 kcal/mol for the Brønsted acidic sites with TMPO ^{31}P chemical shift at 72, 80 and 83 ppm, respectively. It is clear that the treatment by HSO_3CF_3 can dramatically enhance the acidity and make the acid dispersion more uniform in PDVB-SO_3H, which was favorable for promoting its catalytic activities in various reactions, similar results have not been reported previously.

Fig. 1.12 B shows the NH_3-TPD curves of PDVB-SO_3H and PDVB-SO_3H-SO_2CF_3, which is also an effective method for evaluating the acid strength over various solid acids. Interestingly, PDVB-SO_3H-SO_2CF_3 shows a very sharp NH_3 desorption peak centered at 500 C, which was much higher and narrower than that of PDVB-SO_3H

(440 C, a very broaden peak), demonstrating its much stronger acid strength and homogeneous acid distribution than that of PDVB-SO_3H, in good agreement with ^{31}P MAS NMR results.

Thermal stability

Fig. 1.13 shows the TG curves of PDVB-SO_3H-SO_2CF_3 and Nafion NR50 (one of the most stable acidic resins). Clearly, both of the samples exhibited the weight loss between the temperature 290–430 and 430–575 °C, which are associated with the decomposition of functional groups and the destruction of polymeric network, respectively [8]. Notably, the decomposition temperatures of both acidic group (373 °C) and polymeric network (500 °C) in PDVB-SO_3H-SO_2CF_3 are much higher than that of Nafion NR50 (335 and 460 °C), one of the most stable acidic resins, indicating its excellent thermal stability. The superior stability of PDVB-SO_3H-SO_2CF_3 comes from the presence of electron-withdrawing group and highly cross-linked polymeric network in the sample.

Catalytic activities and recyclability

Fig. 1.14 shows the kinetics curves toward depolymerization of crystalline cellulose to sugars catalyzed by PDVB-SO_3H-SO_2CF_3, PDVB-SO_3H and Amberlyst 15, which is one of the most important reactions for production of biofuels, having received extensive attention in recent years [18], [19], [20], [21], [22],[26] and [65]. Clearly, PDVB-SO_3H-SO_2CF_3 exhibits much better catalytic activities and selectivity than those of PDVB-

SO_3H and Amberlyst 15. For example, the yield of total reducing sugars catalyzed by PDVB-SO_3H-SO_2CF_3 was up to 87.1% for 5 h, much higher than those of PDVB-SO_3H (60.7%) and commercial Amberlyst 15 (50.3%). More interestingly, PDVB-SO_3H-SO_2CF_3 shows very good selectivity for glucose (glucose at 66.2% and cellobiose at 9.1%, Table 1.3) as compared with those of PDVB-SO_3H (glucose at 34.0% and cellobiose at 11.2%, Table 1.3) and Amberlyst 15 (glucose at 24.5% and cellobiose at 10.8%, Table 1.3).

PDVB-SO_3H-SO_2CF_3 shows very good recyclability. For the reaction of crystalline cellulose depolymerization, after recycling for five times, PDVB-SO_3H-SO_2CF_3 gave the total reducing sugars up to 84.1%, very close to that of fresh PDVB-SO_3H-SO_2CF_3 (86.7%, Table 1.3, run 3); More importantly, the selectivity for glucose and cellobiose catalyzed by recycled PDVB-SO_3H-SO_2CF_3 were 63.4 and 9.7%, respectively, which were very similar as that of fresh PDVB-SO_3H-SO_2CF_3.

Conclusions

Efficient and stable mesoporous polymeric solid strong acid of PDVB-SO_3H-SO_2CF_3 has been successfully prepared through introduction of strong electron withdrawing group of -SO_2CF_3 onto the network of PDVB-SO_3H, which showed unique characters including large BET surface area, hydrophobic and oleophilic network, enhanced acid strength and homogeneous acid distribution. The above novel characters of PDVB-SO_3H-SO_2CF_3 result in its excellent catalytic activity and good recyclability in biomass transformations of depolymerization of crystalline cellulose to sugars, and

transesterification for production of biodiesel when compared with various conventional solid acids. PDVB-SO_3H-SO_2CF_3 will open new avenues for preparation of porous and stable solid strong acids with abundant mesoporosity, good hydrophobicity and oleophilicity, and excellent catalytic activities and recyclability, which will be potentially important for its wide applications in biomass transformation through green chemical processes in industry.

References

[1] A. Corma, Chemical Reviews 95 (1995) 559.

[2] A. Corma, H. Garcia, Chemical Reviews 103 (2003) 4307.

[3] J.H. Clark, D.J. Macqquarrie, Chemical Society Reviews 25 (1996) 303.

[4] I.V. Kozhevnikov, Chemical Reviews 98 (1998) 171.

[5] R. Sheldon, Chemical Communications 23 (2001) 2399.

[6] M.E. Davis, Nature 417 (2002) 813.

[7] C.W. Jones, K. Tsuji, M.E. Davis, Nature 393 (1998) 52.

[8] F.J. Liu, X.-J. Meng, Y.L. Zhang, L.M. Ren, F. Nawaz, F.-S. Xiao, Journal of Catalysis

271 (2010) 52.

[9] T. Okuhara, Chemical Reviews 102 (2002) 3641.

[10] Y.J. Liu, E. Lotero, J.G. Goodwin Jr., Journal of Catalysis 242 (2006) 278.

[11] Y.J. Xu, W.Q. Gu, D.L. Gin, Journal of the American Chemical Society 126 (2004) 1616.

[12] W. Long, C.W. Jones, ACS Catalysis 1 (2011) 674.

[13] F.J. Liu, T. Willhammar, L. Wang, L.F. Zhu, Q. Sun, X.J. Meng, W. Carrillo-Cabrera,

X.D. Zou, F.-S. Xiao, Journal of the American Chemical Society 134 (2012) 4557.

[14] E. Nikolla, Y. Román-Leshkov, M. Moliner, M.E. Davis, ACS Catalysis 1 (2011)

[15] A. Corma, Chemical Reviews 97 (1997) 2373.

[16] J.H. Clark, Accounts of Chemical Research 35 (2002) 791.

[17] F.J. Liu, L. Wang, Q. Sun, L.F. Zhu, X.J. Meng, F.-S. Xiao, Journal of the American Chemical Society 134 (2012) 16948.

[18] Y. Román-Leshkov, C.J. Barrett, Z.Y. Liu, J. Dumesic, Nature 447 (2007) 982. [19] J.B. Binder, R.T. Raines, Proceedings of the National Academy of Sciences of the United States of America 107 (2010) 4516.

[20] G.W. Huber, J.N. Chheda, C.J. Barrett, J.A. Dumesic, Science 308 (2005) 1446. [21] E. Andrijanto, E.A. Dawson, D.R. Brown, Applied Catalysis B: Environmental

115–116 (2012) 261.

[22] S. Suganuma, K. Nakajima, M. Kitano, D. Yamaguchi, H. Kato, S. Hayashi, M. Hara, Journal of the American Chemical Society 130 (2008) 12787.

[23] D.H. Zuo, J. Lane, D. Culy, M. Schultz, A. Pullar, M. Waxman, Applied Catalysis B: Environmental 129 (2013) 342.

[24] J.B. Binder, R.T. Raines, Journal of the American Chemical Society 131 (2009) 1979.

[25] L.L. Xu, W. Li, J.L. Hu, X. Yang, Y.H. Guo, Applied Catalysis B: Environmental 90 (2009) 587.

[26] H.L.Cai,C.Z.Li,A.Q.Wang,G.L.Xu,T.Zhang,AppliedCatalysisB:Environmental 123–124 (2012) 333.

[27] G.A. Olah, G.K.S. Prakash, J. Sommer, Science 206 (1979) 13.

[28] K. Arata, Applied Catalysis A 146 (1996) 143.

[29] R.J. Gillespie, Accounts of Chemical Research 1 (1968) 202.

[30] R.J. Gillespie, T.E. Peel, Advances in Physical Organic Chemistry 9 (1972) 1. [31] P.Kalita,B.Sathyaseelan,A.Mano,S.M.JavaidZaidi,M.A.Chari,A.Vinu,Chem-istry: A European Journal 16 (2010) 2843.

[32] X. Song, A. Sayari, Catalysis Reviews: Science and Engineering 38 (1996) 329. [33] G.D. Yadav, J.J. Nair, Microporous and Mesoporous Materials 33 (1999) 1.

[34] K. Arata, M. Hino, Materials Chemistry and Physics 26 (1990) 213.

[35] Y.Y.Sun,L.Zhu,H.J.Lu,R.W.Wang,S.Lin,D.Z.Jiang,F.-S.Xiao,AppliedCatalysis A 237 (2002) 21.

[36] J. Macht, R.T. Carr, E. Iglesia, Journal of Catalysis 264 (2009) 54.

[37] Q.H. Yang, J. Liu, J. Yang, M.P. Kapoor, S. Inagaki, C. Li, Journal of Catalysis 228 (2004) 265.

[38] K. Arata, Applied Catalysis A 146 (1996) 3.

[39] Y.C. Du, S. Liu, Y.L. Zhan, C.Y. Yin, Y. Di, F.-S. Xiao, Catalysis Letters 108 (2006)

155.

[40] K. Okuyama, X. Chen, K. Takata, D. Odawara, T. Suzuki, S.I. Nakata, T. Okuhara, Applied Catalysis A 190 (2000) 253.

[41] M. Kimura, T. Nakato, T. Okuhara, Applied Catalysis A 165 (1997) 227.

[42] F.J. Liu, W.P. Kong, C.Z. Qi, L.F. Zhu, F.-S. Xiao, ACS Catalysis 2 (2012) 565.

[43] P. Barbaro, F. Liguori, Chemical Reviews 109 (2009) 515.

[44] A. Heidekum, M.A. Harmer, W.F. Hoelderich, Journal of Catalysis 188 (1999)

230.

[45] M.A. Harmer, Q. Sun, Applied Catalysis A 221 (2001) 45.

[46] E. Lam, E. Majid, A.C.W. Leung, J.H. Chong, K.A. Mahmoud, J.H.T. Luong, Chem-SusChem 4 (2011) 535.

[47] F.Martínez,G.Morales,A.Martín,R.vanGrieken,AppliedCatalysisA347(2008) 169.

[48] M.C. Laufer, H. Hausmann, W.F. Hölderich, Journal of Catalysis 218 (2003) 315.

[49] R. Xing, N. Liu, Y.M. Liu, H.H. Wu, Y.W. Jiang, L. Chen, M.Y. He, P. Wu, Advanced Functional Materials 17 (2007) 2455.

[50] G. Morales, G. Athens, B.F. Chmelka, R. van Grieken, J.A. Melero, Journal of Catalysis 254 (2008) 205.

[51] M.A. Harmer, Q. Sun, W.E. Farneth, Journal of the American Chemical Society 118 (1996) 7708.

[52] M.A. Harmer, Q. Sun, A.J. Vega, W.E. Farneth, A. Heidekum, W.F. Hoelderich, Green Chemistry 6 (2000) 7.

[53] F.J. Liu, S.F. Zuo, W.P. Kong, C.Z. Qi, Green Chemistry 14 (2012) 1342.

[54] I. Jiménez-Morales, J. Santamaría-González, P. Maireles-Torres, A. Jiménez-López, Applied Catalysis B: Environmental 123–124 (2012) 316.

[55] D. Margolese, J.A. Melero, S.C. Christiansen, B.F. Chmelka, G.D. Stucky, Chem-

istry of Materials 12 (2000) 2448.

[56] A. Zheng, H. Zhang, X. Lu, S.B. Liu, F. Deng, Journal of Physical Chemistry B 112 (2008) 4496.

[57] A. Zheng, S. Huang, S.B. Liu, F. Deng, Physical Chemistry Chemical Physics 13 (2011) 14889.

[58] N. Feng, A. Zheng, S.J. Huang, H. Zhang, N. Yu, C.Y. Yang, S.B. Liu, F. Deng, Journal of Physical Chemistry C 114 (2010) 15464.

[59] C. Tagusagawa, A. Takagaki, A. Iguchi, K. Takanabe, J.N. Kondo, K. Ebitani, S. Hayashi, T. Tatsumi, K. Domen, Angewandte Chemie International Edition 49 (2010) 1128.

[60] R. Rinaldi, R. Palkovits, F. Schüth, Angewandte Chemie International Edition 47 (2008) 8047.

[61] D.Y. Zhao, Q.S. Huo, J.L. Feng, B.F. Chmelka, G.D. Stucky, Journal of the American Chemical Society 120 (1998) 6024.

[62] D.Y. Zhao, J.L. Feng, Q.S. Huo, N. Melosh, G.H. Fredrickson, B.F. Chmelka, G.D. Stucky, Science 279 (1998) 548.

[63] J. Scaranto, A.P. Charmet, S. Giorgianni, Journal of Physical Chemistry C 112 (2008) 9443.

[64] C. Koibeck, M. Killian, F. Maier, N. Paape, P. Wasserscheid, H.-P. Steinrück, Langmuir 24 (2008) 9500.

[65] J. Tollefson, Nature 451 (2008) 880.

Table 1.2 The textural and acidic parameters over various samples.

Samples	S content (mmol/g)[a]	Acid sites (mmol/g)[b]	S_{BET} (m^2/g)	V_P (cm^3/g)	D_P [c] (nm)
PDVB	–	–	700	1.34	23.1
PDVB-SO_3H	3.20	3.50	376	0.90	22.5
PDVB-SO_3H-SO_2CF_3	5.72	3.34	314	0.91	29.3
Amberlyst 15	4.30	4.70	45	0.31	40
Nafion NR50	0.86	0.90	0.02	–	–
SO_4/ZrO_2[d]	0.72	–	70	–	–
SBA-15-SO_3H	1.36	1.26	820	1.40	7.3
H-Beta[e]		1.21	550	0.20	0.67
H-USY[f]		2.06	623	0.26	14.7

a) Measured by elemental analysis.
b) Measured by acid–base titration.
c) Pore size distribution estimated from BJH model.
d) SO_4/ZrO_2 synthesized as reference of 24.
e) Si/Al ratio at 12.5.
f) Si/Al ratio at 7.5.

Table 1.3.Yields of sugars and dehydration products in the depolymerization of crystalline cellulose catalyzed by various solid acids.

Run	Samples	Glucose yield (%)[a]	Cellobiose yield (%)[a]	TRS (%)[b]
1	Amberlyst 15	24.5	10.8	50.3
2	PDVB-SO_3H	34.0	11.2	60.7
3	PDVB-SO_3H-SO_2CF_3	66.2	9.1	86.7
4	PDVB-SO_3H-SO_2CF_3[c]	63.4	9.7	84.1

a Monitored by HPLC method.
b Monitored by DNS assay.
c The sample after recycling for five times.

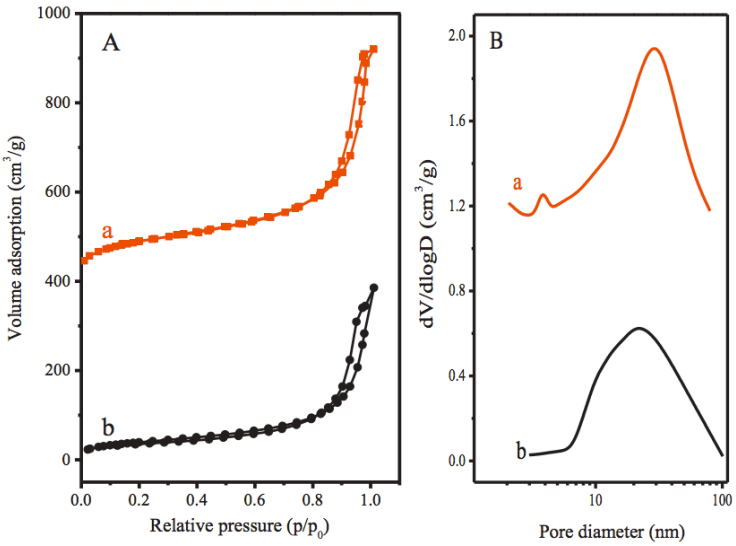

Figure 1.7 (A) N_2 sorption isotherms and the pore size distribution of (a) PDVB-SO_3H, and (b) PDVB-SO_3H-SO_2CF_3. The isotherms for (a) was offset by 400 cm^3/g along with vertical axis for clarity, and pore size distribution for (a) was offset by 1.0 cm^3/g along with vertical axis for clarity, respectively

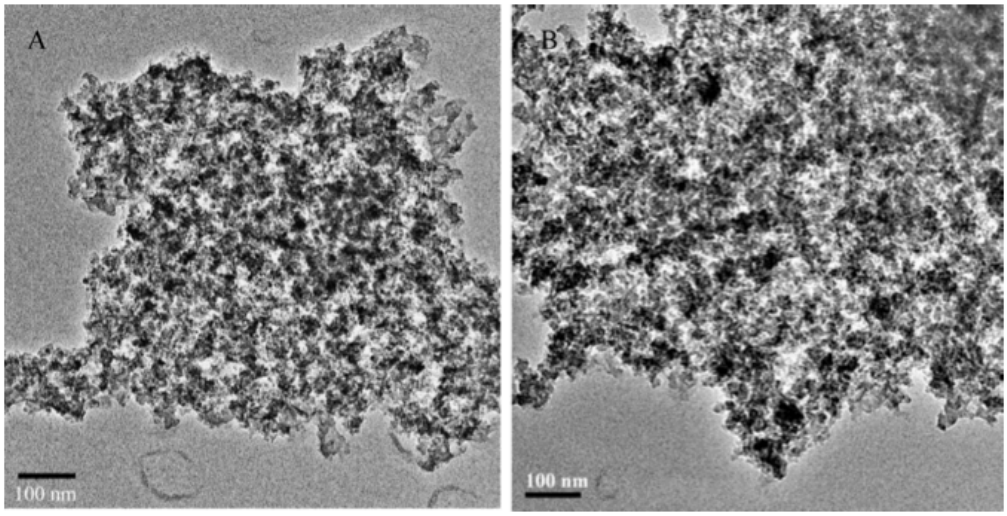

Figure 1.8 Transmission electron microscopy images of (A) PDVB-SO_3H and (B) PDVB-SO_3H-SO_2CF_3.

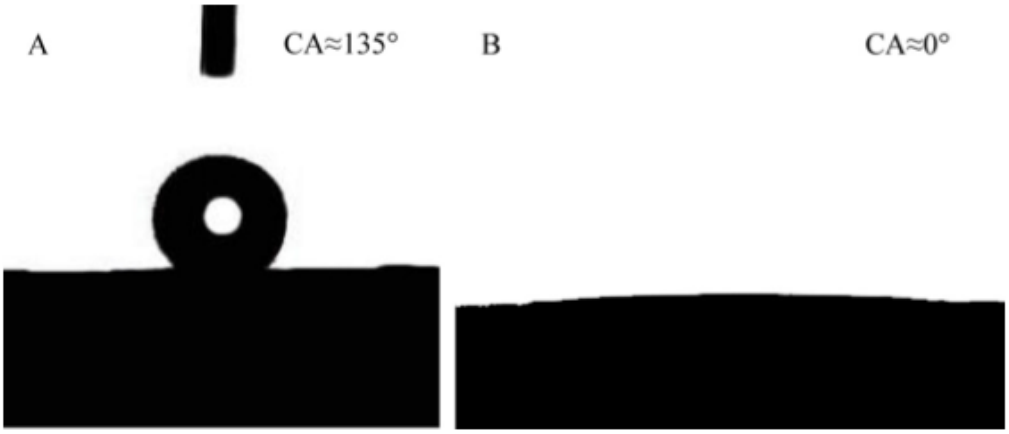

Figure 1.9 Contact angles of (A) water droplet, (B) soybean oil droplet

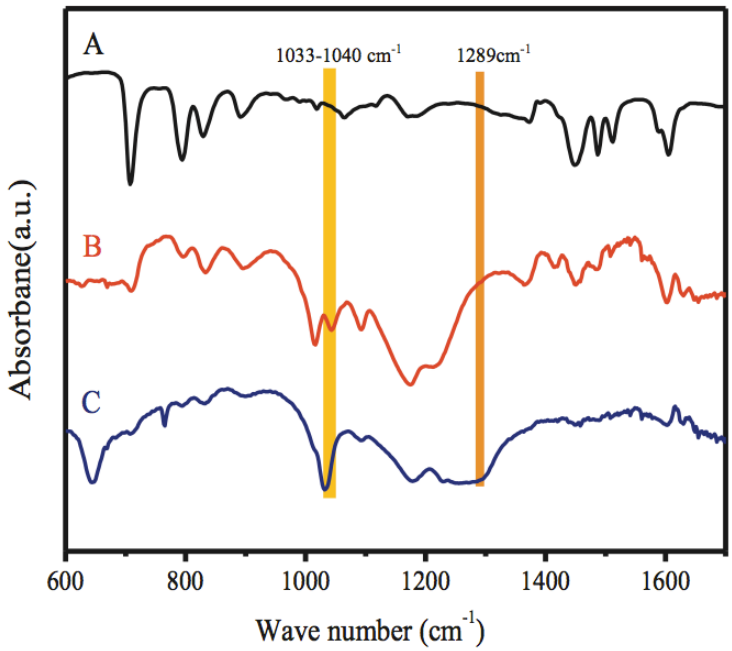

Figure 1.10 FT-IR spectra of (A) PDVB, (B) PDVB-SO_3H and (C) PDVB-SO_3H-SO_2CF_3.

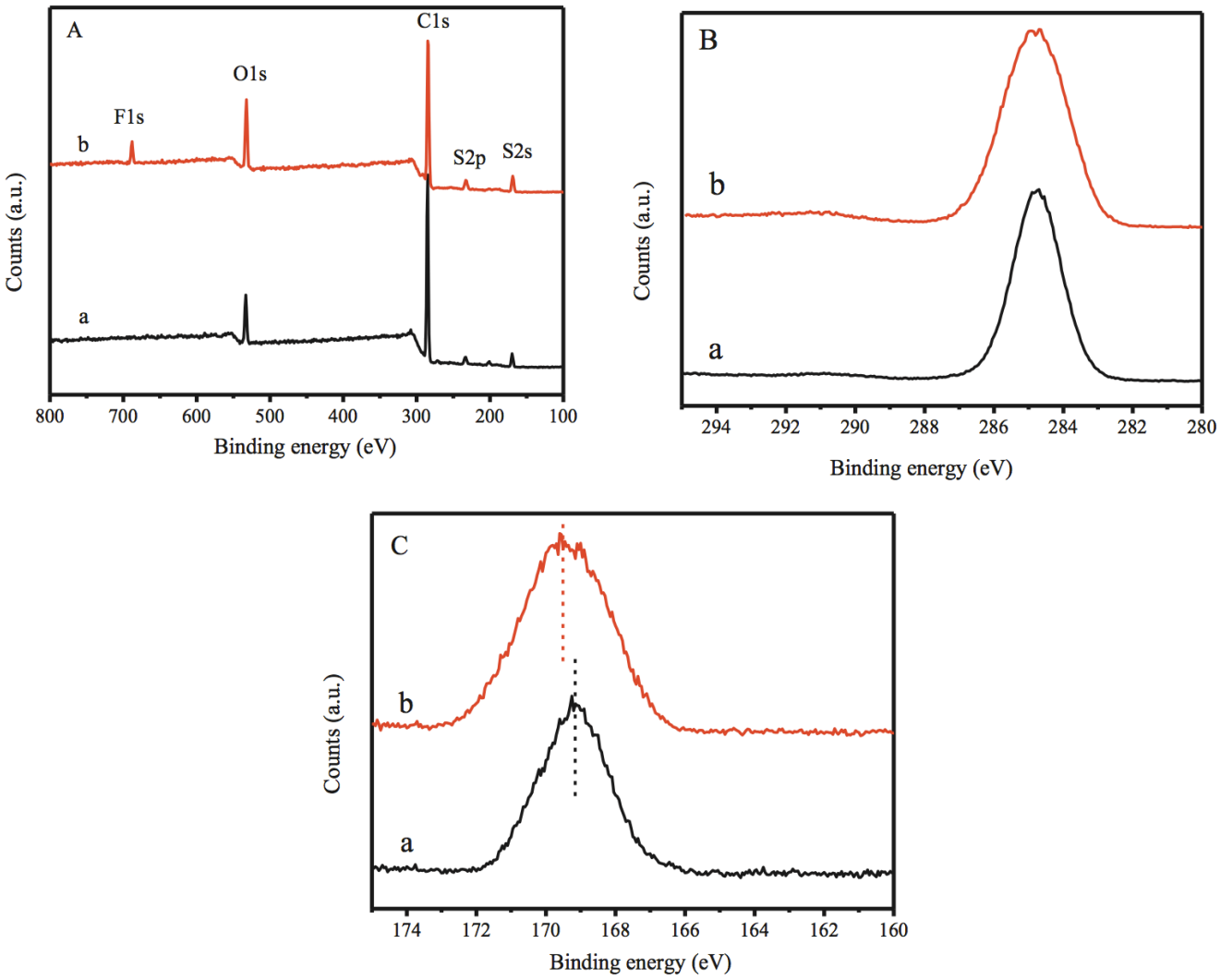

Figure 1.11 X-ray photoelectron spectroscopy measurements of (A) survey, (B) C_{1s}, (C) S_{2p} of (a) PDVB-SO_3H and (b) PDVB-SO_3H-SO_2CF_3.

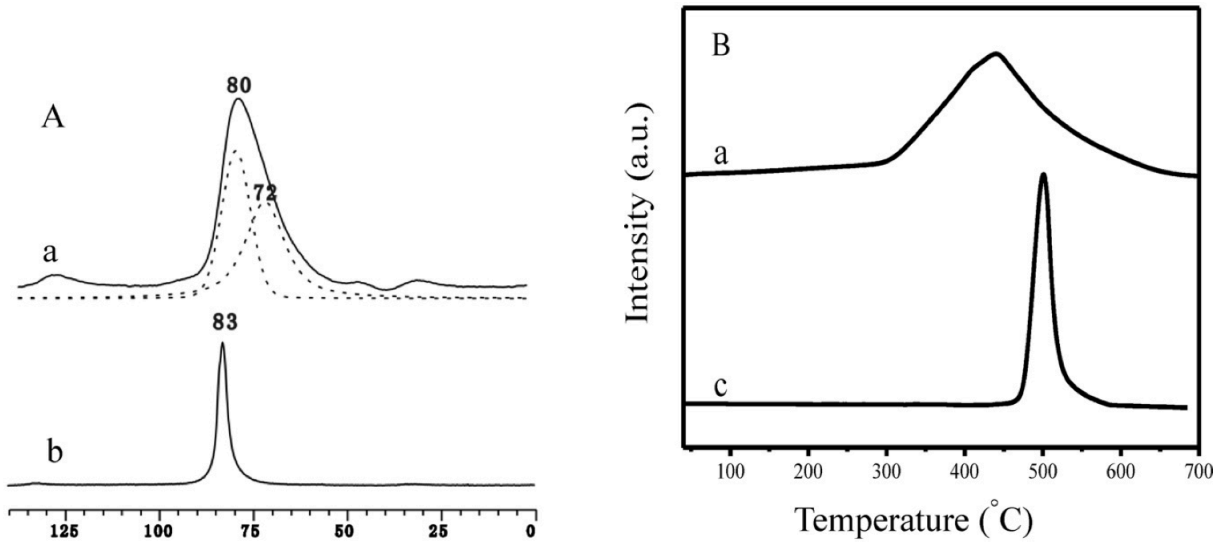

Figure 1.12 (A) Solid-state ^{31}P MAS NMR of adsorbed TMPO and (B) NH_3-TPD curves of (a) PDVB-SO_3H and (b) PDVB-SO_3H-SO_2CF_3.

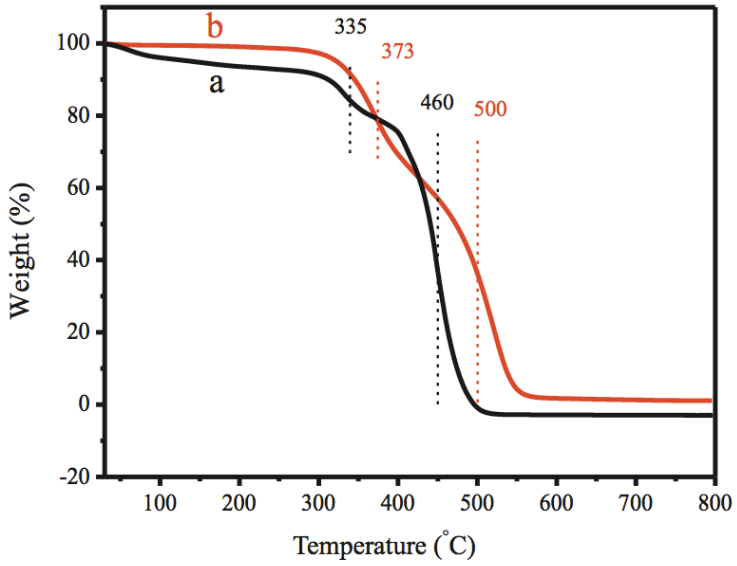

Figure 1.13 TG curves of (a) Nafion NR50 and (b) PDVB-SO_3H-SO_2CF_3.

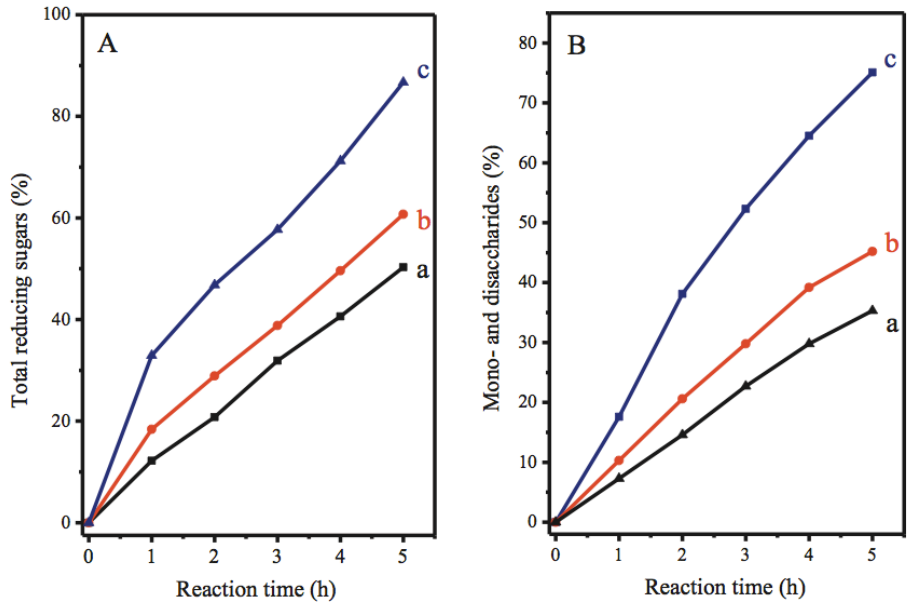

Figure 1.14 Catalytic kinetics curves for depolymerization of crystalline cellulose monitored by (A) DNS assay and (B) HPLC catalyzed by (a) Amberlyst 15, (b) PDVB-SO_3H, and (c) PDVB-SO_3H-SO_2CF_3.

Chapter 2. Acidic ionic liquids grafted nanoporous polymers

Much effort has been made to develop green and cost-effective ways to produce renewable biofuels from cellulosic biomass [1-10]. One of the key challenges in converting biomass into fuels is the recalcitrant nature of the crystalline cellulose, in which densely packed polysaccharide chains are stabilized by an extensive network of hydrogen-bonds and thus resist chemical and enzymatic degradation [11-12]. The depolymerization of cellulose usually requires severe conditions, such as the use of sulfuric acid at high temperatures. Recently, alkylmethylimidazolium ionic liquids (ILs) were found to be good solvents for breaking down the crystalline cellulose into soluble polymer chains, which can be subsequently depolymerized into sugars or other products by using acid catalysts under mild conditions [13-16]. A variety of solid acids such as Amberlyst 15, acidic zeolites or carbon based solid acids have been tested to catalyze the degradation process of cellulose in ILs [15-18]. However, the high cost of ionic liquids and the difficulty in recycling ionic liquids from reaction products on an industrial scale demands new catalysts with extremely high effectiveness. Synthesis of polymeric catalysts containing both the acidic sites and the IL groups may improve the compatibility of the catalysts in IL reaction media and lead to the development of cost-effective catalysts for cellulose depolymerization. Recently, we reported the preparation of strongly acidic ILs functionalized on nanoporous polymers with desired proper- ties such as an adjustable hydrophilic–hydrophobic network, abundant nanoporosity, strong acid strength and the reactant enrichment phenomenon [19]. Herein, we report the synthesis of sponge-like nanoporous polymers functionalized with both the sulfonic group and the ionic liquids group (e.g., PDVB–SO_3H–[C_3vim]- [SO_2CF_3], PDVB:

polydivinylbenzene, vim: 1-vinylimidazolate, SO3H: sodium p-styrene sulfonate, C3: 1,3 propanesultone, SO_2CF_3: HSO_3CF_3 anion-exchanger), which showed excellent catalytic activities for degradation of crystalline cellulose to sugars in comparison with hydrochloric acid, sulfuric acid and acidic resins. The excellent catalytic activity, product selectivity and recyclability found for PDVB–SO3H–[C_3vim][SO_2CF_3] may offer a simple route to depolymerize recalcitrant cellulose into sugars for biofuel productions. Nanoporous polymeric acid catalysts were synthesized by solvothermal copolymerization of divinylbenzene (DVB) with functional monomers of 1-vinylimidazolate (vim) and sodium p-styrenesulfonate at 100 1C, followed by formation of quaternary ammonium salts using 1,3-propanesultone, and finally ion exchanged with HSO_3CF_3, similar to the method we previously reported [19].

Experimental details

Chemicals and reagents.

All reagents were of analytical grade and used as purchased without further purification. Divinylbenzene (DVB), 1-n-butyl-3-methylimidazolium ([C4mim]Cl), 1 ethyl-3-methylimidazolium acetate ([EMIM]Ac), 1-vinylimidazolate (vim), Amberlyst 15 sodium p-styrene sulfonate, nonionic block copolymer surfactant poly(ethyleneoxide) poly(propyleneoxide)-poly(ethyleneoxide) block copolymer (Pluronic 123, molecular weight of about 5800) and Avicel cellulose were purchased from Sigma-Aldrich Co. Azobisisobutyronitrile (AIBN), THF, 1,3-propanesultone, HSO3CF3, H2SO4, HCl, toluene and CH2Cl2 were obtained from Beijing Chemical Agents Company.

Characterization methods.

Nitrogen isotherms were measured using a Micromeritics ASAP 2020M system. The samples were outgassed for 10 h at 150 °C before the measurements. The pore-size distribution was calculated using Barrett-Joyner-Halenda (BJH) model. FTIR spectra were collected by using a Bruker 66V FTIR spectrometer. X-ray powder diffraction (XRD) of samples was recorded on a Rigaku D/max2550 PC powder diffractometer using nickel-filtered CuKα radiation in the range of $10° \leq 2\theta \leq 35°$. SEM images were performed on JEOL 6335F field emission scanning electron microscope (FESEM) attached with a Thermo Noran EDX detector. Transmission electron microscopy (TEM) images were performed on a JEM-3010 electron microscope (JEOL, Japan) with an acceleration voltage of 300 kV. CHNS elemental analysis was performed on a Perkin-Elmer series II CHNS analyzer 2400. XPS spectra were performed on a Thermo ESCALAB 250 with Al Kα radition at y=901 for the X-ray sources, the binding energies were calibrated using the C1s peak at 284.9 eV.

Synthesis of functional nanoporous polymers (PDVB-SO_3Na-vim).

1-vinylimidazolate (vim) and sodium p-styrene sulfonate functionalized nanoporous polymer (PDVB-vim) was hydrothermally synthesized by copolymerization of DVB with vim and sodium p-styrene sulfonate in the starting mixture of DVB/vim/sodium p-styrene sulfonate/AIBN/THF/H_2O at molar ratios of 1/0.5/0.2/0.027/24.1/10.8. In a typical synthesis of PDVB-vim, 2.0 g of DVB, 0.483 g of vim and 0.56 g of sodium p-styrene sulfonate were added into a solution containing 0.07 g of AIBN and 30 mL of THF and 3 mL of water. After stirring at room temperature for 3 h, the mixture was hydrothermally

treated at 100 °C for 24 h, followed by slow evaporation of the solvent at room temperature for 2 days. The product (PDVB-SO_3Na-vim) shows monolith morphology.

Synthesis of ionic liquids and sulfonic group functionalized nanoporous polymers

PDVB-SO_3H-[C_3vim][SO_3CF_3],PDVB-SO_3H [C_3vim][SO_4H] or PDVB-SO_3H-[C_3vim][Cl] (C_3 stands for quaternary ammoniation reagent of 1,3-propanesultone) were synthesized by quaternary ammoniation of PDVB-SO_3Na-vim with 1,3-propanesultone, followed by ion exchanging with HSO_3CF_3, H_2SO_4 or HCl, respectively. In the synthesis of PDVB-SO_3H-[C_3vim][SO_3CF_3], 1.0 g of PDVB-SO_3Na-vim was added into 25 mL of toluene under vigorous stirring, followed by addition of 0.25 g of 1,3-propanesultone. After reacting at 100 °C for 12 h, the product was collected by filtration, washing with a large amount of ethanol and drying at 60 °C. The polymer was then treated with HSO_3CF_3 in toluene solvent for 24 h at room temperature, washed with large amount of CH_2Cl_2 and dried at 80 °C for 8 h, to obtain the final product of PDVB-SO_3H-[C_3vim][SO_3CF_3]. PDVB-SO_3H and PDVB-[C_3vim][SO_3CF_3] were prepared in a similar way for comparison.

Synthesis of homogeneous ionic liquids ([C_3vim][SO_3CF_3]).

2.0 g of vim monomer was added to 20 mL of toluene under vigorous stirring, followed by addition of 0.4 g of 1,3-propanesultone. The reaction was kept at 50 °C for 48 h, to give [C_3vim]. [C_3vim] was then treated by 3-5 mL HSO_3CF_3 in toluene for 24 h, followed by washing with a large amount of CH_2Cl_2. The process was repeated for two times to give [C_3vim][SO_3CF_3].

Preparation of DNS Reagent

182 g of potassium sodium tartrate was added into 500 mL of hot deionized water at 50 °C, followed by addition of 6.3 g of 3, 5-dinitrosalicylic acid (DNS) and 262 mL of 2 M NaOH. 5 g of phenol and 5 g of sodium sulfite were then introduced into the solution under vigorous stirring to obtain homogeneous solution. The solution was cooled to room temperature and diluted with deionized water to 1000 mL to give the DNS reagent.

Depolymerization of Avicel cellulose

100 mg of Avicel cellulose was dissolved into 2.0 g of [C_4mim]Cl ionic liquid at 100 °C for 1 h under vigorous stirring, until a clear solution was obtained. 20 mg of specific catalyst was added, and 600 μL of water was slowly introduced into the reaction mixture and the reaction temperature was kept at 100 °C. At different time intervals, samples were withdrawn, weighed (recorded as M_1), quenched immediately with cold water, and centrifuged at 14,800 rpm for 5 min for removing of catalysts and unreacted cellulose, to give the reaction mixtures for subsequent analysis, the volume was measured and recorded as V_1. Unreacted Avicel was separated, washed and weighted. The contents of mineral acids of H_2SO_4 and HCl used for depolymerization of Avicel cellulose were the same number of catalytic site (H^+) as that in PDVB-SO_3H-[C_3vim][SO_3CF_3].

Depolymerization of Gracilaria

50 mg of Gracilaria was dissolved into 3.0 g of [EMIM]Ac ionic liquid at 110 °C for 12 h under vigorous stirring until a clear solution was obtained, followed by addition of 30 mg of catalysts. 600 μL of water was slowly introduced into the reaction mixture and the

reaction temperature was kept at 110°C. At different time intervals, samples were withdrawn, weighed, quenched immediately with cold water, and centrifuged at 14,800 rpm for 5 min for removing of catalysts and unreacted Gracilaria, to give the reaction mixture for subsequent analysis. Unreacted Gracilaria was separated, washed and weighted. The content of HCl used for depolymerization of Gracilaria cellulose was the same number of catalytic sites (H^+) as that in PDVB-SO_3H-[C_3vim][SO_3CF_3].

Total Reducing Sugar (TRS) tests

TRS was measured by DNS method. 0.5 mL of DNS regent was added into 0.5 mL of the reaction solution and heated at 100 °C for 5 min. The mixture was then cooled to room temperature, and 4 mL of deionized water was added to dilute the solution. The adsorption at 540 nm was measured in a calibrated NanoDrop 2000 UV-spectrophotometer. The yield of TRS was then determined based on a standard curve obtained with glucose.

Measuring the yields of glucose and cellobiose

The concentrations of glucose and cellobiose in the reaction mixture were measured by a Water 717plus high-performance liquid chromatography (HPLC) system, with an Aminex HPX-87H column and a refraction index detector. The temperature of the column was set to 65 °C. The flow rate was 0.5 mL/min. The eluent consisted of a filtered and degasified solution of sulfuric acid (5 mM). The volume of each injection was 10 μL. Pre-measured glucose and cellobiose was used to establish the calibration curves for the HPLC. The concentrations of soluble sugars from the reactions were then

determined from the calibration curves (e.g., Glucose Yield %=carbon mass of glucose/mass of cellulose; Cellobiose Yield %=carbon mass of cellobiose/carbon mass of cellulose).

Results and discussion

Fig. 2.1 shows the XPS spectra of PDVB–SO_3H–[C_3vim][SO_3CF_3]. The peaks associated with the electron binding energy of C1s, S2p, N1s, F1s and O1s were observed, indicating the successful grafting of acidic groups onto the network of PDVB–SO_3H-ILs. C1s peaks were distributed near 284.7, 287.7, 286.8 and 291.4 eV, which were assigned to C–C, C–N, C–S and C–F bonds, respectively. The peaks associated with N1s were centered at 399.6 and 402.0 eV, which were assigned to the C–N bond and the quaternized N of imidazole rings in PDVB–SO_3H–[C_3vim][SO_3CF_3]. The O1s gives two peaks at around 532.5 and 534.1 eV, which correspond to O atoms in –SO_3H and SO_2CF_3 groups. These XPS results indicate that both sulfonic and ionic liquid groups have been successfully incorporated on the surface of PDVB–SO_3H–[C_3vim][SO_3CF_3]. The sample spectrum collected by Fourier transform infrared spectroscopy (FTIR) further confirms the successful synthesis of bifunctionalized polymers (figure 2.2).

Figure 2.3 shows the scanning electron microscopy (SEM) images of PDVB–SO_3H [C_3vim][SO_3CF_3], which have rough surfaces and abundant sponge-like pores (B100 nm in diameter). Under a transmission electron microscope (TEM), PDVB–SO_3H–[C_3vim]-[SO_3CF_3] shows a hierarchical structure with the pore sizes ranging from 30 to 100 nm (Fig. 2.4), in good agreement with the results obtained from N_2 isotherms (Fig 2.5,). The sponge-like nanoporous structure is ideal for facilitating fast diffusion of reactants and

products, and for exposing a high degree of active sites in the reactions.

Fig. 2.6 shows the kinetic behavior of depolymerization of crystalline cellulose catalyzed by different acid catalysts. PDVB– SO_3H [C3vim][SO_3CF_3] exhibited much better catalytic efficiency in the presence of 1-n-butyl-3 methylimidazolium than Amberlyst 15, one of the most efficient commercial acidic resins. PDVB–SO_3H–[C3vim][SO_3CF_3] also showed higher catalytic activity than homogeneous acidic ionic liquids of [C3vim][SO_3CF_3] or the mineral acids, HCl or H_2SO_4. Our study shows that after 5 h of incubation, the yields of total reducing sugars, mono- and disaccharides catalyzed by PDVB–SO_3H–[C3vim][SO_3CF_3] reached almost 100%. We also found that the proportion of glucose in the degradation products was higher when using PDVB– SO_3H–[C3vim][SO_3CF_3] compared with other catalysts (Table 1).

Presumably, the drastic enhancement of the catalytic effectiveness found in PDVB–SO_3H–[C3vim][SO_3CF_3] in cellulose degradation is due to the synergistic effects from the excellent substrate solubility, nanoporosity and the highly acidic strength of the catalyst. To understand this, we synthesized PDVB–SO_3H, PDVB–[C3vim][SO_3CF_3], PDVB–SO_3H–[C3vim][Cl] as control samples and investigated their catalytic performance in depolymerization of Avicel. We found that the samples containing both ionic liquids and sulfonic groups (e.g., PDVB–[C3vim][SO_3CF_3] and PDVB–SO_3H–[C3vim][Cl]) showed the best catalytic activities. The yields of total reducing sugars catalyzed by PDVB–[C3vim][SO_3CF_3] and PDVB–SO_3H–[C3vim][Cl] were up to 98.1 and 96.3%, respectively, much higher than that of PDVB–SO_3H (82.6%, Table 2.1). This result suggests that the grafted ionic groups play an important role either by improving

the compatibility with ILs or by destroying the intermolecular hydrogen bonds of crystalline cellulose, thereby enhancing the catalytic activity for depolymerization. To identify the effect of the grafted ILs on mesoporous polymers, the powder of PDVB–SO_3H [C3vim][SO_3CF_3] was directly mixed with Avicel cellulose without adding any 1-n-butyl-3 methylimidazolium solvent, and heated to 100 1C with stirring. Figure 2.7 shows XRD patterns of Avicel cellulose before and after being treated with only PDVB–SO3H-ILs. Originally, Avicel showed multiple, distinct diffraction peaks as a result of the high crystallinity of the cellulose structure. After 6 hours, the diffraction peaks completely disappeared, indicating the capability of catalytic breakdown of the crystalline cellulose by the grafted ILs on PDVB–SO_3H [C3vim][SO_3CF_3] in the solid phase.

We then expanded our study to test a realistic biomass source of cellulose, a species of Rhodophyta (red algae) called Gracilaria. Gracilaria is a eukaryotic marine seaweed, or macro-algae, characterized by a double cell wall.[20] The outer wall consists primarily of galactose related material and the inner wall consists primarily of cellulose. PDVB–SO_3H–[C3vim][SO_3CF_3] also showed great effectiveness in catalyzing the depolymerization of Gracilaria in comparison to HCl. Table 2 presents a yield of total reducing sugars of up to 83.4% obtained in 5 h by using PDVB–SO_3H–[C3vim]-[SO_3CF_3]. The yields of glucose and cellobiose were 29.2 and 48.6%, respectively, much higher than with HCl (24.3 & 28.5%). When the reaction time was increased to 18 h, the yield of total reducing sugars catalyzed by PDVB–SO_3H–[C3vim][SO_3CF_3] was up to 90.1%, and nearly all the cellobiose was transformed, giving yields of glucose of up to 86.5% (Table 2). In contrast, the yield of TRS catalyzed by HCl was 75.1% at 18 h,

with the yield of glucose and cellobiose at 62.1 and 7.4%, respectively. The excellent catalytic performances of PDVB-SO3H-[C3vim][SO3CF3] should be attributed to its very strong acid strength and supported ionic liquid groups, which would be potentially important for the wide applications of PDVB-SO3H-[C3vim][SO3CF3] in the areas of depolymerization of crystalline cellulose into biofuels for industry.

^{31}P NMR of adsorbed trimethylphosphine (TMP) has been demonstrated to be a sensitive and reliable technique for the determination of the Brønsted and Lewis acid sites in solid catalysts. The adsorption of TMP on the Brønsted acid will give rise to ^{31}P resonances in a rather narrow range (ca. -2 ~ -5 ppm). However, TMP bound to Lewis acid sites, may result in ^{31}P peaks in the range of ca. -20 ~ -60 ppm. As shown in Figure 2.8, using TMP as a probe molecule, the^{31}P resonances at -3.4 ppm was assigned to the protonated adducts, $[(CH_3)_3P\text{-}H]^+$, attributed by the reaction of TMP and the Brønsted acidic protons. It's noteworthy that no resonances were observed in the range of -20 to -60 ppm due to interaction with Lewis acid sites, therefore, it's indicative that no Lewis acid was formed over PDVB-SO3H-[C3vim][SO3CF3]. In order to reveal the interaction strength of P-H bond in the $[(CH_3)_3P–H]^+$ complexes, the NMR experiment without the proton decoupling was done as well. The single ^{31}P resonance (-3.4 ppm) was split into double peaks (at -2.2 and -4.6 ppm) and the JP-H coupling was determined to ca. 500 Hz (see Figure. S5b). This JP-H coupling was very close to the coupling values for $TMPH^+$ inside aqueous HCl solution and related solid catalysts, which is indicative the stronger Brønsted acidity formed in PDVB-SO3H-[C3vim][SO3CF3].

In summary, ILs and sulfonic groups functionalized nano- porous polymers of PDVB-

SO_3H-[C3vim][SO_3CF_3] have been prepared and tested for their effectiveness in cellulose degradation. The polymers exhibit excellent catalytic activities for depolymerization of Avicel cellulose and Algae into sugars. The result may open a new way for applications of heterogeneous catalysts containing both ionic liquids and strong acidic group catalysts for depolymerization of crystalline cellulose into precursors for biofuel production.

References

1 J. B. Binder and R. T. Raines, J. Am. Chem. Soc., 2009, 131, 1979.

2 Y. Roma´n-Leshkov, C. J. Barrett, Z. Y. Liu and J. Dumesic, Nature, 2007, 447, 982.

3 G. W. Huber, J. N. Chheda, C. J. Barrett and J. A. Dumesic, Science,2005, 308, 1446.

4 A. Corma, S. Iborra and A. Velty, Chem. Rev., 2007, 107, 2411.

5 Y. Roma´n-Leshkov, J. N. Chheda and J. A. Dumesic, Science, 2006, 312, 1933.

6 J. Tollefson, Nature, 2008, 451, 880.

7 R. Rinaldi and F. Schu¨th, ChemSusChem, 2009, 2, 1096.

8 E. Nikolla, Y. Roma´n-Leshkov, M. Moliner and M. E. Davis, ACS Catal., 2011, 1, 408.

9 E. I. Gu¨rbu¨z, J. M. R. Gallo, D. M. Alonso, S. G. Wettstein, W. Y. Lim and J. M. Dumesic, Angew. Chem., Int. Ed., 2013, 52, 1270.

10 F. J. Liu, A. M. Zheng, I. Noshadi and F.-S. Xiao, Appl. Catal., B, 2013,136–137, 193–201.

11 M. E. Himmel, S.-Y. Ding, D. K. Johnson, W. S. Adney, M. R. Nimlos, J. W. Brady and T. D. Foust, Science, 2007, 315, 804.

12 M. Jarvis, Nature, 2003, 426, 611.

13 E. Bahcegul, S. Apaydin, N. I. Haykir, E. Tatlic and U. Bakir, Green Chem., 2012, 14, 1896.

14 S. Suganuma, K. Nakajima, M. Kitano, D. Yamaguchi, H. Kato, S. Hayashi and M. Hara, J. Am. Chem. Soc., 2008, 130, 12787.

15 R. Rinaldi, R. Palkovits and F. Schu¨th, Angew. Chem., Int. Ed., 2008,47, 8047.

16 J. B. Binder and R. T. Raines, Proc. Natl. Acad. Sci. U. S. A., 2010, 107, 4516.

17 H. L. Cai, C. Z. Li, A. Q. Wang, G. L. Xu and T. Zhang, Appl. Catal., B,2012, 123–124, 333.

18 S. Suganuma, K. Nakajima, M. Kitano, D. Yamaguchi, H. Kato,S. Hayashi and M. Hara, J. Am. Chem. Soc., 2008, 130, 12787.

19 F. J. Liu, L. Wang, Q. Sun, L. F. Zhu, X. J. Meng and F.-S. Xiao, J. Am. Chem. Soc., 2012, 134, 16948.

20 F. E. Fritsch, The structure and reproduction of the algae, Cambridge Univ. Press, Cambridge, 1945

Table 2.1 Yield of sugars and dehydration products in the depolymerization of Avicel catalyzed by various solid acids and mineral acids

Catalysts	Glucose yield[a] (%)	Cellobiose yield[a] (%)	TRS[b] (%)
Amberlyst 15	25.1	14.8	56.2
HCl	63.4	13.4	94.1
$[C_3vim][SO_3CF_3]$[c]	66.2	12.2	93.8
H_2SO_4	59.6	9.8	86.8
PDVB–SO_3H	56.8	10.2	82.6
PDVB–SO_3H–$[C_3vim][SO_3CF_3]$	77.0	8.2	99.6
PDVB–$[C_3vim][SO_3CF_3]$	75.9	6.8	98.1
PDVB–SO_3H–$[C_3vim][SO_4H]$	76.8	5.6	98.5
PDVB–SO_3H–$[C_3vim][Cl]$	74.1	6.4	96.3

[a] Measured by high-performance liquid chromatography (HPLC) method, the reaction time was 5 h. [b] Total reducing sugar (TRS) was measured using the DNS method. [c] The same number of acidic sites as in PDVB–SO_3H–$[C_3vim][SO_3CF_3]$.

Table 2.2 Yield of sugars and dehydration products in the depolymerization of Gracilaria catalyzed by various solid acids and HCl

Catalysts	Glucose yield[a] (%)	Cellobiose yield[a] (%)	TRS[b] (%)
PDVB–SO_3H–[C_3vim][SO_3CF_3][c]	29.2	48.6	83.4
HCl[c]	24.3	28.5	58.3
PDVB–SO_3H–[C_3vim][SO_3CF_3][d]	86.5	Trace	90.1
HCl[d]	62.1	7.4	75.1

[a] Measured using the HPLC method. [b] Measured using the DNS method. [c] The same number of acidic sites as in PDVB–SO_3H–[C_3vim]-[SO_3CF_3], the reaction time was 5 h. [d] The same number of acidic sites as in PDVB–SO_3H–[C_3vim][SO_3CF_3], the reaction time was 18 h.

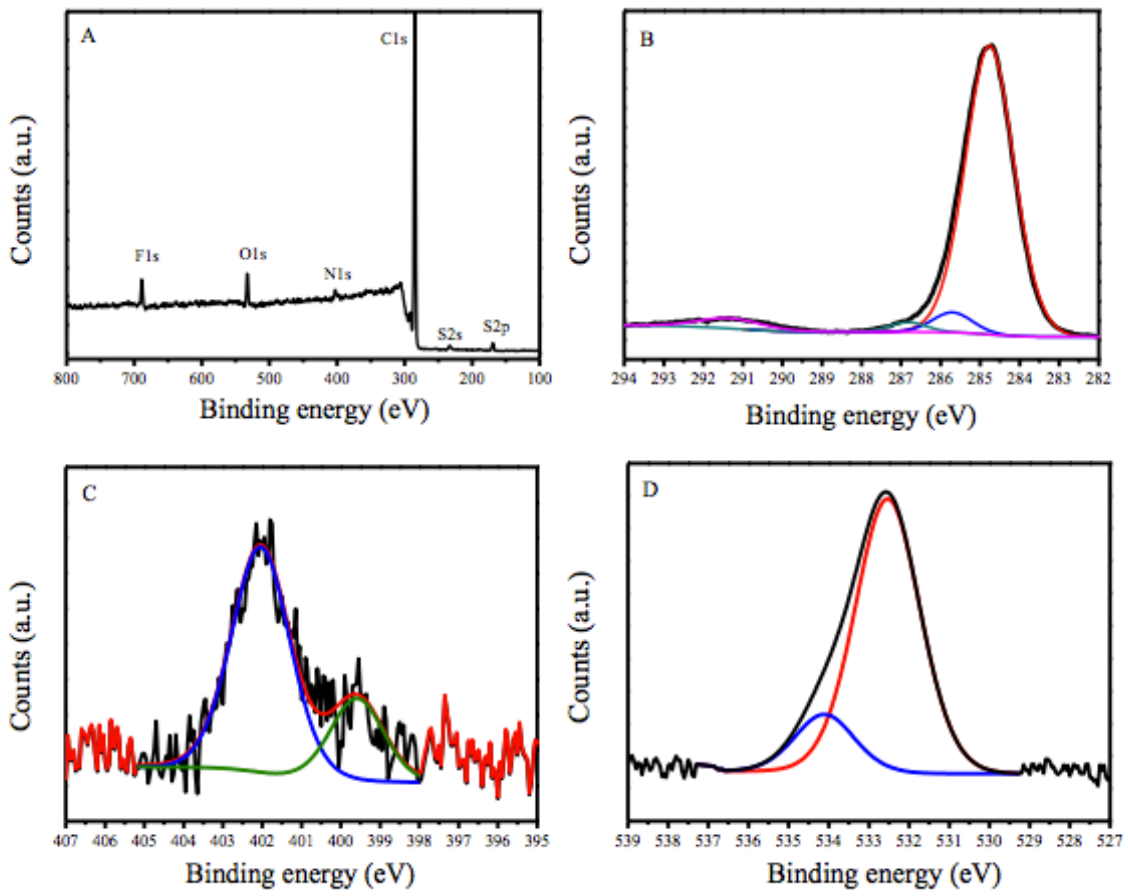

Figure 2.1 XPS spectra of (A) wide-scan survey, (B) C1s, (C) N1s and (D) O1s in PDVB-SO3H-[C3vim][SO3CF3].

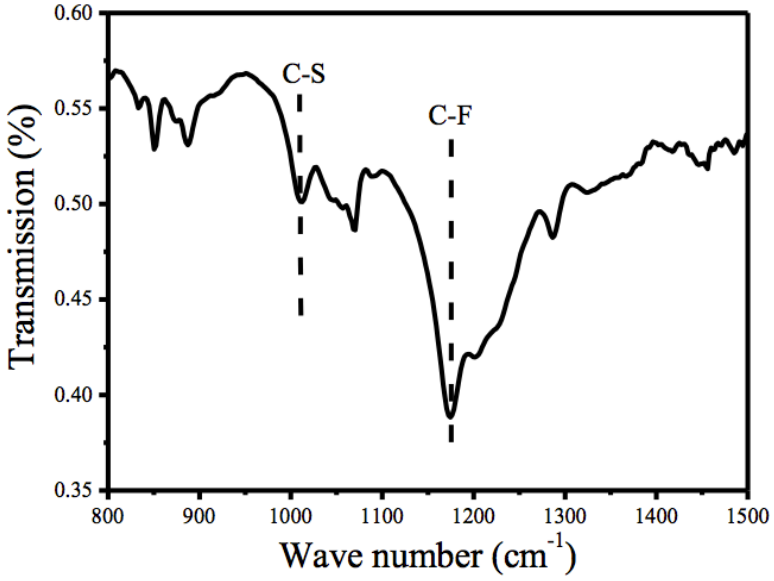

Figure 2.2 FT-IR spectra of PDVB-SO3H-[C3vim][SO3CF3].

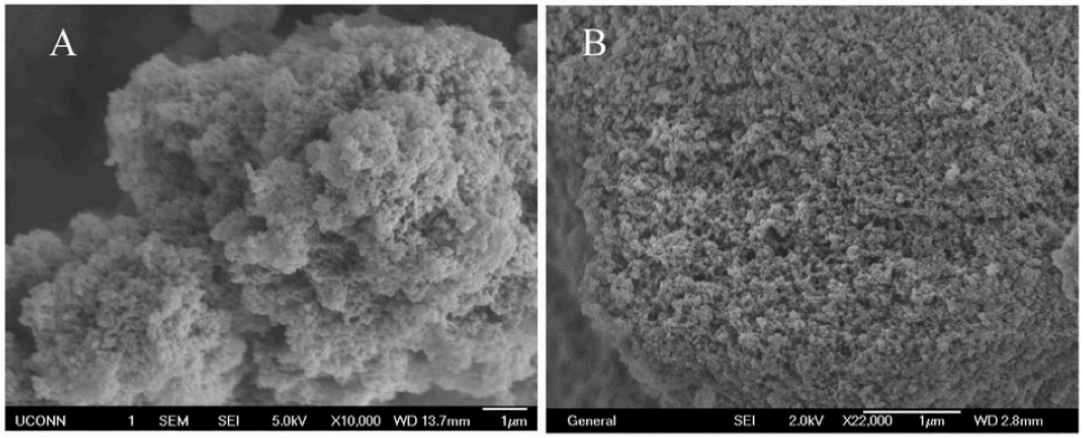

Figure 2.3 SEM images of PDVB–SO3H–[C3vim][SO3CF3].

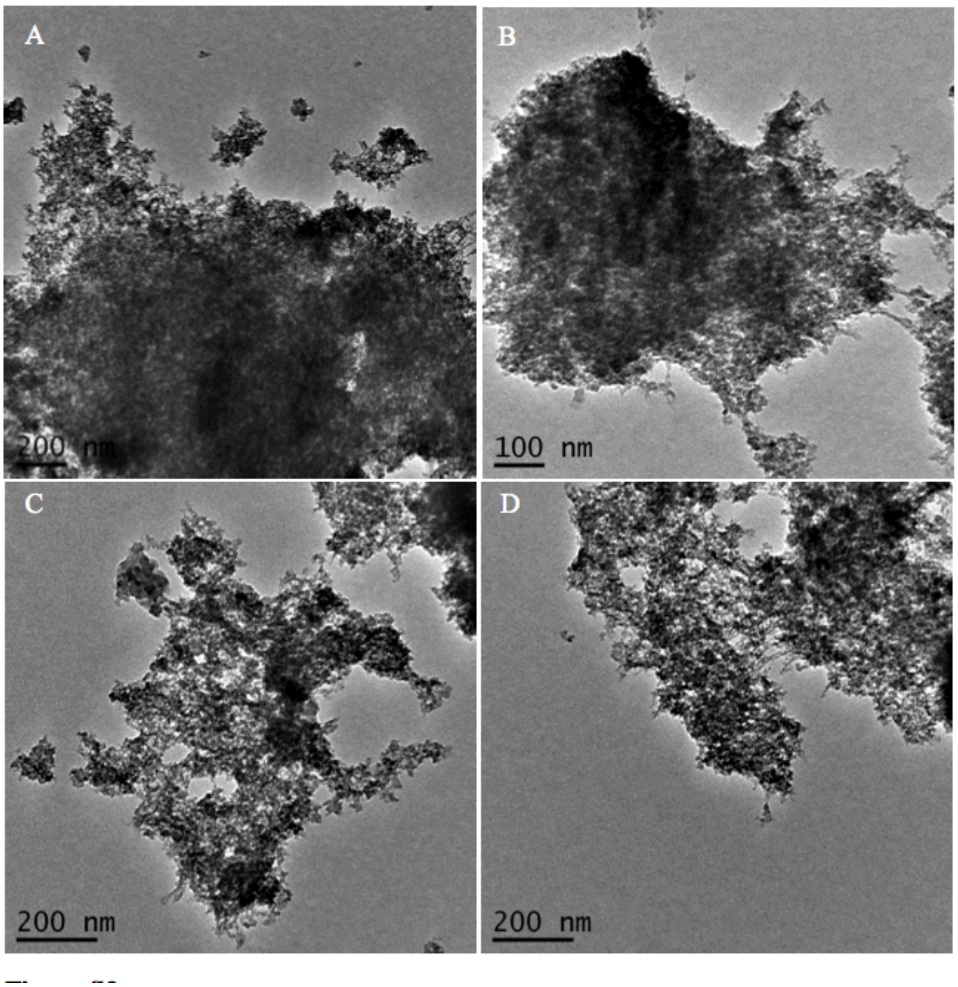

Figure 2.4 TEM images of (A&B) PDVB-SO_3H-[C_3vim][SO_3CF_3] and (C&D) PDVB-SO_3H-[C_3vim][Cl]

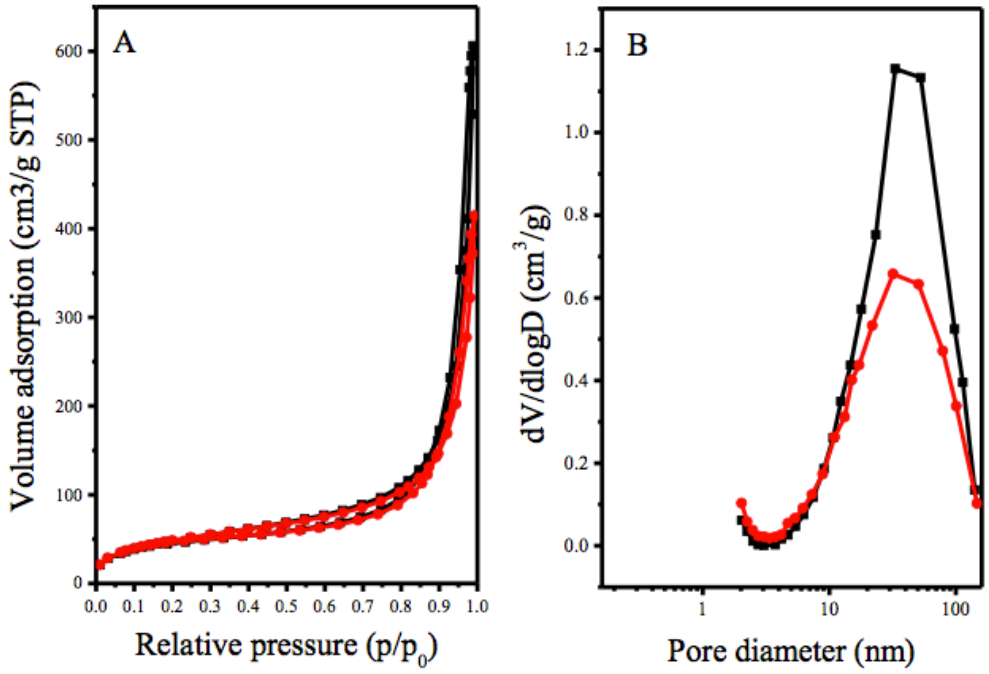

Figure 2.5 N_2 isotherms and pore size distribution of PDVB-SO_3H-[C_3vim][SO_3CF_3] (in red) and PDVB-SO_3H-[C_3vim][Cl] (in black).

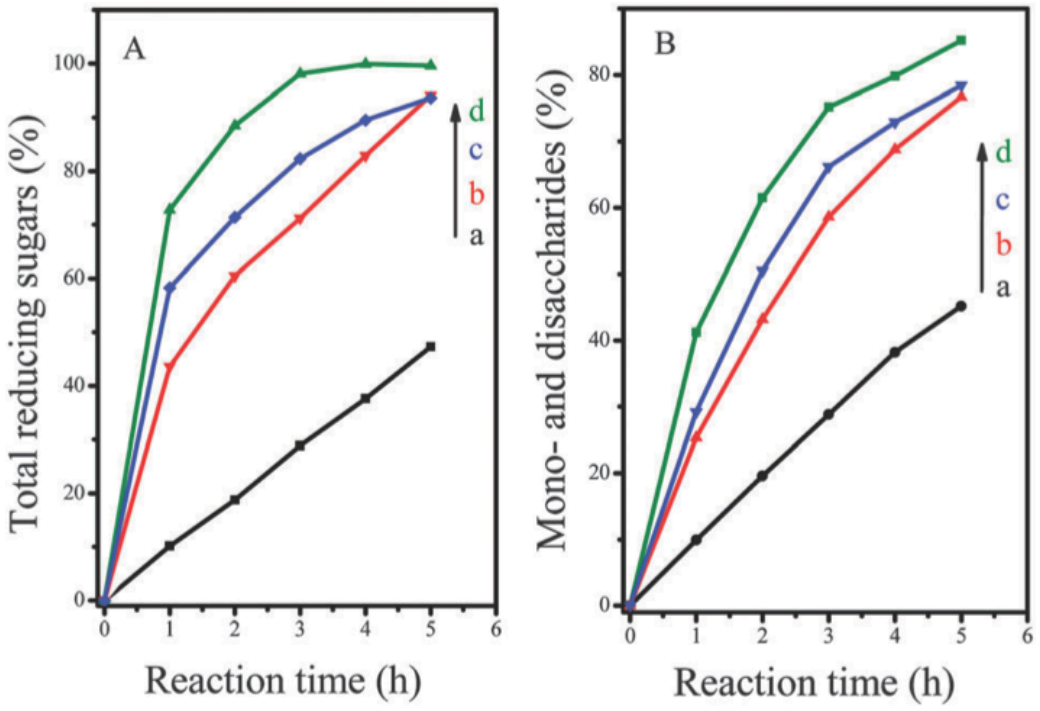

Figure 2.6 Kinetic curves of depolymerization of Avicel monitored by (A) 5-dinitro-salicylic acid (DNS) reagent and (B) HPLC catalyzed by (a) Amberlyst 15, (b) HCl, (c) [C3mim][SO3CF3] and (d) PDVB–SO3H–[C3vim][SO3CF3].

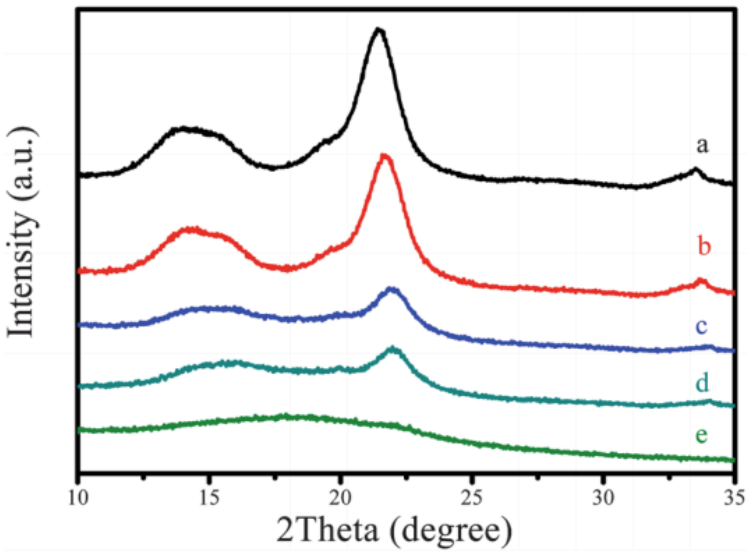

Figure 2.7 XRD patterns of (a) Avicel cellulose, and the Avicel being treated by PDVB–SO3H–[C3vim][SO3CF3] at 100 1C for (b) 0 h, (c) 2 h, (d) 3 h and (e) 6 h

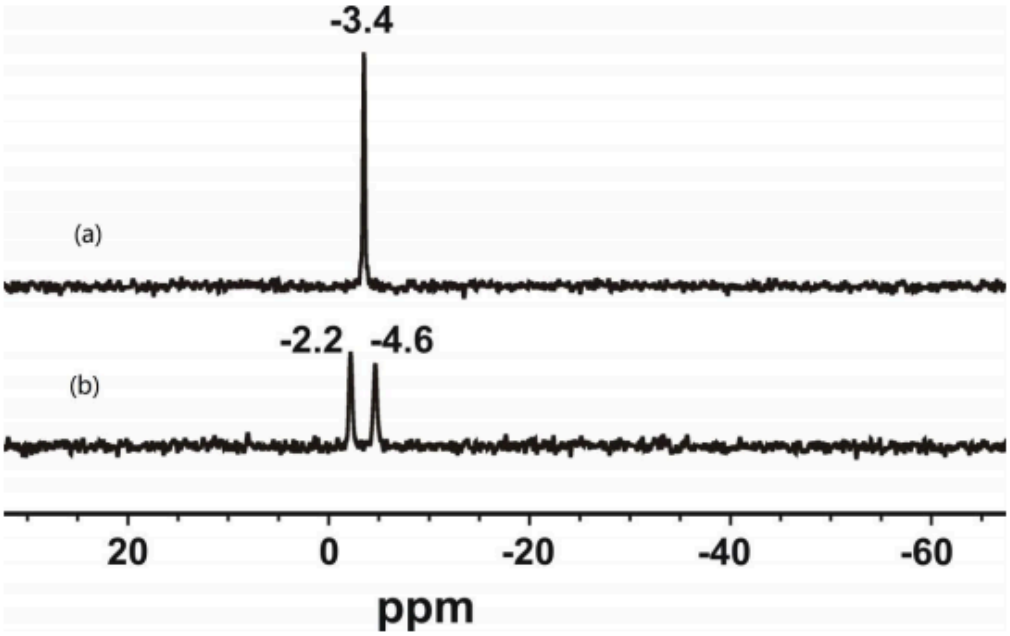

Figure 2.8 Room temperature ^{31}P MAS NMR spectra of TMP acquired (a) with proton decoupling, and (b) without proton decoupling of PDVB-SO3H-[C3vim][SO3CF3].

Chapter 3. Catalyzed production of biodiesel and bio-chemicals from brown grease using Ionic Liquid functionalized ordered mesoporous polymer

Introduction

The issues of environmental degradation and energy security are fundamental challenges of the 21st century. Dependence on conventional fossil fuels is leading to global warming and possible major disruptions in social structures [1]. Therefore, diversification of the energy portfolio with an emphasis on renewable fuels is an imperative policy tool. Of the various forms of renewable energies, biomass based fuels provide several advantages: known production methods, excellent renewability, environmental friendliness and usefulness for both electricity generation and transportation. Biofuels may therefore be the most important feedstock for replacing fossil fuels [2-10].

A typical biomass based fuel is biodiesel, which is typically produced via transesterification of triglycerides or esterification of free fatty acids (FFAs) with short-chain alcohols in the presence of acid or base catalysts [10, 11]. These acid or base catalyzed processes are capable of producing biodiesel from low-quality and low cost feedstock with relatively high FFA content, such as waste cooking oil or renewable plant oils [8, 10, 12, 13]. The production of biodiesel from low cost feedstock rather than from virgin plant or animal oil is important to avoid using food resources to produce fuels. However, large-scale production of biodiesel from low quality feedstock remains a challenge.

Low quality feedstock is often available as waste products, for which industries typically carry high disposal costs. Fuel production and power cogeneration from waste recovery is a sustainable and potentially profitable option that addresses the challenges of economy,

energy independence and waste management. Waste brown grease is one such low-grade and very low-cost potential candidate as a feedstock for the production of biodiesel and other chemicals in such an integrated process. Grease build-up in sewer lines is caused by fats, oils, and greases, which are disposed and accumulate in the sewer system over time. Brown grease is collected in wastewater treatment plants and requires further treatment before disposal and is a mixture of high-value hydrocarbons, such as waste vegetable oil, animal fats and grease. The high level of contamination in brown grease makes it unsuitable for use as animal feed or fertilizer. Brown grease is a significant environmental and health hazard being responsible for about 40% of all sewer overflows, causing back-ups and damage to pipe lines and roughly 20,000,000 illnesses each year in the USA [14]. Its disposal requires special attention and an associated cost.

This work illustrates nearly 100% transformation of brown grease into biodiesel, synthesis gas and bio-oil which can be used for power generation and biofuel production. The experimental study for the conversion of brown grease to energy and energy carriers entails the synthesis and the application of a high activity solid acid catalyst for the esterification of brown grease to biodiesel and the conversion of remnant bio-solids to fuels was investigated by fast pyrolysis.

The difficulties associated with the efficient production of biodiesel from the bio-oil layer of brown grease were mitigated by the use of a solid acid catalyst. The high FFA content of the bio-oil, between 50% and 100%, in addition to non-oil residual components, makes its conversion to biodiesel more difficult and energy intensive, relying primarily on acid catalysis [15-18]. While acid catalysts can simultaneously catalyze esterification of FFA's and transesterification of triglycerides without soap formation [8, 10, 12, 13], the

usage of homogenous acids such as H_2SO_4 and HCl suffer from the disadvantages of non-recyclability and difficult purification. Thus, in order to alleviate such difficulties, we demonstrate the synthesis and application of an efficient super acid catalyst for simultaneous esterification and transesterification of brown grease to biodiesel. An ordered mesoporous resol polymer is synthesized on a template based on the self-assembly of an amphiphilic block copolymer and functionalized by strongly acidic ionic liquids. The solid acid exhibited superior catalytic activity for production of biodiesel than commercial Amberlyst 15 solid acid, and was also superior in catalytic activity to hydrochloric acid.

The brown grease also contains remnant solids that separate from the bio-oil layer. The potential use of the remnant solids was investigated in gasification and pyrolysis experiments. The higher H/C ratio of the brown grease bio-solid, compared to pine and glucose, implies its potential for producing higher aromatic and olefin yields via pyrolysis. Experiments established that almost 99% of the bio-solids are combustible implying the feasibility of producing synthesis gas from the bio-solid through gasification.

Experimental section

Preparation of solid acid

Hydrothermal synthesis of ordered mesoporous resin (OMRs) was carried out at 180 °C from the self-assembly of resol precursors, hexamethylenetetramine (HMTA) cross-linker, and a tri-block copolymer template of Pluronic® F127 (Sigma-Aldrich) (Scheme 3.1) [19]. Pluronic® F-127 has molecular weight approximately 12,500 Da, and consists

of two 96-unit hydrophilic Poly(ethylene oxide) chains surrounding one 69-unit hydrophobic Poly(propylene oxide) chain [20]. Approximately 2.0 g of phenol and 7 mL of a 37 wt% formaldehyde solution were dissolved in 10 mL of a 0.5M NaOH solution, followed by stirring at 80°C for a half hour. This was followed by the addition of a solution containing 2.5 g of F127 and 20 mL of deionized water. As an additional cross-linker, 0.5 g of HMTA was introduced into the mixture.

After an additional 3 hour period of stirring at 80°C, the mixture was further cured in an autoclave for 24h at 180ºC. Following this, a brown solid was observed at the bottom of the autoclave. This solid was filtered and washed with copious amounts of water and dried at 80°C, which finally yielded the OMR-[HMTA] as illustrated in Scheme 3.1.

OMR-[HMTA] with opened mesopores was obtained by calcination of the as-made OMR-[HMTA] at 360°C for 5 h in nitrogen gas containing a small amount (2.5%, v/v) of oxygen. An alternative method is by washing with ethanol for 48 h under reflux.

The treatment of OMR-[HMTA] with 1,4-butanesultone yielded Ordered Mesoporous Ionic Liquid (OMR-ILs), which results in the quaternary ammonium of nitrogen in the network of OMR-[HMTA], followed by ion exchanging with H_2SO_4. As a typical synthesis of OMR-[C_4HMTA][SO_4H], 0.5 g of OMR-[HMTA] was dispersed into 10 mL of toluene, followed by the addition of 0.5 g of 1,4-butanesultone. After that, the temperature was rapidly increased to 100°C and the reaction lasted for 24 h. The sample was then cooled to room temperature, washed with toluene and a large amount of CH_2Cl_2, followed by drying at 80 °C for 6 h to yield OMR-[C_4HMTA]. The final sample was then dispersed into 10 mL of toluene followed by the addition of 4.5 mL of H_2SO_4.

This was further stirred at room temperature for 24 h, following which it was washed with toluene and large amount of CH_2Cl_2 in order to remove the surface adsorbed acids.

Characterization of Solid Catalyst

Nitrogen adsorption isotherms were measured using a Micromeritics ASAP Tristar system at the liquid nitrogen temperature. The samples were outgassed for 10 h at 150°C before the measurements. The pore-size distribution was calculated using the Barrett–Joyner–Halenda (BJH) model. CHNS elemental analysis was performed on a Perkin-Elmer series II CHNS analyser 2400. FTIR spectra were recorded by using a Bruker 66V FTIR spectrometer. Thermogravimetric analyses (TGA) were performed on a PerkinElmer TGA7 in flowing nitrogen gas with a heating rate of 20°C min^{-1}. SEM images were performed on JEOL 6335F field emission scanning electron microscope (FESEM) attached with a Thermo Noran EDX detector and Tecnai T12 transmission electron microscopy.

2.3 Separation of oil from brown grease

The dewatered brown grease from a local wastewater treatment plant was slowly stirred overnight at 35ºC to effect separation of the residual solids and water from the oil. The supernatant oil was collected and the remaining water and solid stirred again at 35ºC for two more times to separate the maximum possible amount of oil. The remaining material was filtered to remove most of the water, and the solid cake was dried at 60ºC for two days to remove remaining water. The residual solids, referred to as bio-solids below, were used for pyrolysis and gasification experiments.

Two step esterification-transesterification of brown grease oil

20g of brown grease oil was heated and centrifuged to remove any solid impurities. In order to avoid any saponification of the free fatty acid (FFA) content, the FFA was esterified with methanol by OMR-[C_4HMTA][SO_4H] . When the FFA content decreased to lower than 1.0%, the sample was centrifuged to separate solid acid (bottom layer) from the esterified oil (middle layer) and methanol (top layer). The esterified brown grease oil was removed by pipette and then washed with water and dried with bubbling air. The treated oil and an appropriate volume of methanol with 5% (w/w) base catalyst (KOH) were placed into a dry reaction flask equipped with reflux condenser and magnetic stirrer. The reaction mixture was blended for 60 min at a temperature of 65 °C. The crude ester layer was separated from the glycerol layer by centrifugation for 2min. To separate methanol, the crude ester phase was washed with distilled water until the wash water was at neutral pH, which usually required three washings. Residual water in the ester product was removed with anhydrous magnesium sulfate.

One step esterification-transesterification of brown grease oil

One step conversion of brown grease oil with methanol was performed as follows: 10g of brown grease oil was added into a three-necked round flask equipped with a reflux condenser and a magnetic stirrer, and then the temperature was increased to 65°C. After the brown grease oil melted, 42 gr of methanol and 0.5g of catalyst were quickly added under strong stirring. The reaction proceeded at 65°C for 5h. The molar ratio of brown grease oil/methanol was approximately 1:40 and the mass ratio of catalyst/brown grease oil was 0.05.

Analysis of Brown Grease Oil and Biodiesel

A basic analysis was conducted to determine the composition and quality of fatty acid methyl ester and brown grease oil. The acid number of the product was obtained using a 0.07 M potassium hydroxide titration using ASTM Method D6751. This acid number was then used to calculate total FFA content and subsequently, conversion. Gas chromatography as per ASTM 6584 method was used to analyze the free and total glycerin content in biodiesel. The derivatized solution was injected (1 μl) into a Hewlett-Packard 5890 Series II Gas Chromatograph equipped with Quadrex Aluminum Clad column with a 1 meter retention gap and employing a flame ionization detector to determine fatty acid methyl-ester (FAME), glycerol and glyceride (tri-, di-,mono-) concentrations. Computer-assisted analysis of resulting chromatograms was performed using Chem-Station software (Hewlett-Packard, now Agilent Technologies).

Gasification and pyrolysis

Preliminary gasification (combustion) and pyrolysis experiments were performed with the bio-solids separated from the brown grease to explore the yields of products that could be expected. The bio-solids were washed 3 times with hexane and dried at 80ºC for 6hr to remove any remaining oil prior to conducting these experiments to avoid skewing the results with residual brown grease oil. Simulated gasification and pyrolysis experiments with the brown grease bio-solids were performed in air and nitrogen, respectively, by thermo gravimetric analysis (TGA) at 10°C/min to 900ºC. Each experiment was held at 120°C for 30 min to remove moisture in the sample.

Production of bio-oil from the bio-solids was subsequently conducted via fast pyrolysis in a quartz reactor heated by a drop tube furnace at 600°C. The fast heating rate was accomplished by sliding the pyrolysis reactor into the hot zone of the furnace. The liquid products were collected on two impingers in a dry-ice bath. The liquid product selectivity was investigated with Gas Chromatography-Mass Spectroscopy (GC-MS). The GC-MS method used for the analysis involves holding the sample at 40°C for 10 min, and then increasing the oven temperature to 280°C at a rate of 5°C/min. Before the GC-MS analysis, the sample was washed and diluted with methanol.

Results and discussion

Characterization of Solid Catalyst

Figure 3.1 shows the pore size distribution and the N_2 BET isotherm of the OMR-[C_4HMTA][SO_4H] prepared in this work, which shows Type-IV curves with a sharp capillary condensation step at p/p0 = 0.6–0.9 with a typical H2-type hysteresis loop. These characteristics are indicative of the presence of mesoscale pore structure [21-25]. The pore size of OMR-[C_4HMTA][SO_4H] was centered near 11.1 nm. Additionally, OMR-[C_4HMTA][SO_4H] has a BET surface area of 406 m^2/g and pore volume of 0.50 cm^3/g. In contrast, Amberlyst 15 has a BET surface area of 45 m^2/g and pore volume of 0.31 cm^3/g [24]. The large surface area and pore volume, with narrowly distributed pore diameters, are favorable for good catalytic activity [21-25]. Previously prepared samples of this catalyst had 1.91 mmol/g acid sites [24].

Fig. 3.2 shows the FT-IR spectra of OMR-[HMTA] after calcination (curve a) and OMR-[C_4HMTA][SO_4H] (curve b). The sharp peaks at 613 and 1066 cm^{-1}, the broad band at 1178 cm^{-1} and the weak peak at 1315 cm^{-1} are the signals for C–S and S=O bonds [26,

27, 28]. The band at 1260 cm^{-1} is the signal for C-N bond. The presence of these bands indicates the successful functionalization of OMR-[HMTA] by the 1,4-butanesultone.

A representative TGA curve of OMR-[C_4HMTA][SO_4H] is shown in Figure 3.3. The decomposition of the acidic groups leading to degradation of the polymeric network accounts for the weight loss exhibited by the sample at temperatures near 349°C and 557°C. This indicates thermal stability of OMR-[C_4HMTA][SO_4H] quite sufficient for the temperature regimes used in typical esterification and transesterification reactions. The good stability of OMR-[C_4HMTA][SO_4H] can be attributed primarily to its high cross link density and presence of strong electron withdrawing groups [26-31].

Figure 3.4 shows the FESEM images of OMR-[C_4HMTA][SO_4H], which exhibited monolithic morphology with rough surface and abundant macroporosity. The unique rough and porous surface was favorable for the enhancement of fast diffusion of bulky substrates during catalytic processes. Figure 3.5 shows a TEM image of the OMR-[C_4HMTA][SO_4H] sample. The microtome sectioning reveals highly ordered mesopores with highly ordered areas corresponding to the cubic symmetry ($Im3^{-}m$) [26].

Oil content of brown grease

Dewatered brown grease obtained from the wastewater treatment plant was heated overnight at a temperature of 35ºC. This separated the water and residual solids from the oil layer, as shown in Figure 3.6 (a) and (b). Figure 3.6(a) shows the brown grease prior to the separation procedure and Fig. 3.6(b) shows the clearly separated layers of the dewatered brown grease after being heat treated at 35ºC for 16 hours. A clear phase separation between the water and solid layer, and the oil layer is evident. The yield of oil was estimated for brown grease samples collected from the same wastewater treatment

facility but at different times of the year and this data is listed in Table 3.1. The average yield of oil from brown grease was 45%. The oil layer was analyzed for FFA and triglyceride content and the FFA varied between 88.3 to 89.2% while the triglyceride content was between 10 and 11%.

Esterification of FFA in brown grease oil with methanol

OMR-[C_4HMTA][SO_4H] was used as a solid acid catalyst for FFA esterification, at a loading of 5 wt% with respect to the weight of oil. A typical run consisted of 20g oil at a methanol/FFA molar ratio of 9:1 and was carried out at 65°C. The ion-exchange resin Amberlyst 15 and HCl were also examined as reference catalysts for the same reaction. Figure 3.7 shows the FFA conversion curves of OMR-[C_4HMTA][SO_4H], Amberlyst 15, and HCl in the esterification reaction. OMR-[C_4HMTA][SO_4H] exhibited higher catalytic activity than either Amberlyst 15 or HCl. When the reaction catalyzed by OMR-[C_4HMTA][SO_4H] was carried out for 1.5 hours, the conversion of FFA to biodiesel was roughly 99.5% and the resultant product passed the ASTM acid number standard for FFA (<0.5%). The slight decline in FFA conversion after 100 minutes is most likely due to the gradual loss of methanol through the reflux condenser on top of the reaction flask. Conversely, with the other two catalysts an FFA conversion of less than 98% was achieved even after 8 hours of reaction and a second esterification step was required to pass the ASTM acid number standard. Previous work with Amberlyst 15 indicates that even under much more aggressive reaction conditions of higher temperature and larger catalyst loading 99% conversion of FFA was not achieved [32]. It may be reasonably suggested that the excellent catalytic activities of OMR-[C_4HMTA][SO_4H] were attributed to its novel properties of a large BET surface area, strong acid strength, and a stable and adjustable hydrophobic polymeric network.

Transesterification of pre-treated brown grease oil with methanol by using homogenous base catalyst

After the FFA content in oil was reduced to less than 0.5 wt% with OMR-[C_4HMTA][SO_4H], the remaining triglycerides in the pre-treated oil were converted to biodiesel using KOH catalyzed transesterification. 0.025 g of KOH was added into pre-treated oil (1.5 g) and methanol (0.4 mL). The reaction mixture was stirred at 65 ºC for 1 h, converting nearly all the triglycerides to biodiesel. Table 3.2 shows the biodiesel specification for two step esterification / transesterification. As shown in table 3.2, the biodiesel obtained using the two step process passed ASTM specifications pertaining to acid number, total and free glycerin.

Simultaneous Esterification and Transesterification

In addition to the successful application of this solid acid for esterification of FFA to biodiesel, the catalyst also demonstrated effectiveness for simultaneous transesterification of triglycerides to biodiesel. There was a rapid conversion of TG to ME observed during the first 60 minutes of reaction using solid acid-catalyzed reaction with methanol, 65% of the TG converted to FAME. After 5 hr, equilibrium was achieved at roughly 75% TG conversion. Commercial Amberlyst 15 achieved a TG conversion of less than 65% after 5hr. The progress of esterification of FFA to FAME was monitored through the decrease in the acid number. An acid number of 0.23 mg of KOH/g oil was achieved in less than 3 h of reaction time, as shown in Figure 3.8. Both reactions, esterification and transesterification, took place simultaneously by converting the FFA and reducing the glyceride content, as shown in Figure 8. These results are significant as the quality of the

biodiesel product obtained was very close to passing ASTM D 6751 specifications, which limit the triglyceride content to a maximum value of 0.24 mass% and an acid number of 0.5 mg of KOH/g.

Table 3.2 shows the specification of biodiesel obtained from both one and two step processes. The biodiesel obtained using the two-step process passed ASTM specifications pertaining to acid number, total and free glycerin. The solid acid plays an important part in the conversion of FFA while the two-step process employs KOH as the catalyst for the transesterification of the triglycerides to FAME and glycerol. The simultaneous esterification - transesterification process employs only the solid acid for both the reactions.

These results in effective conversion of FFA to FAME but the solid acid is not as effective as the KOH to convert the TG to FAME. Thus, although the free glycerin passes the requirements, some unreacted di, tri and mono glyceride esters remain contributing to the total glycerin content being a little above the allowed ASTM specifications.

Typical chromatograms obtained for samples of brown grease oil and brown grease biodiesel as per ASTM D6584 are shown in Figures 3.9 (a-b), respectively. In Fig 3.9b, the biodiesel, the several large peaks observed in the chromatogram from 9-16 minutes are due to the FAMEs of various chain lengths, and containing 1, 2, or 3 double bonds. Mono-glycerides elute in the 17-19 minute time period and the di- and triglycerides elute between 19 and 25 minutes. Also, three specific peaks are identified, glycerin (4.2 min), 1,2,4-butanetriol (6.4 min, internal standard 1) and tricaprin (19.8 min, internal standard 2). Peak identification for each compound or compound class is made using the relative retention times in the ASTM method. In Fig 3.9a, the brown grease oil, the FAME

region is almost exactly replaced by the FFA region from 9-17 minutes. Thus, differentiating FFA from FAME in samples of intermediate conversion is very difficult. Conversion was computed in Fig 3.7 in terms of FFA by considering the acid number and in Fig. 3.8 for the triglycerides by considering peaks from 20-25 minutes in the GC. Although interpretation of oil and biodiesel GC data is complicated significant literature exists to permit reliable data analysis [4, 29]. Figure 3.10 shows the biodiesel composition analyzed with GC-MS.

The recyclability of OMR-[C_4HMTA][SO_4H] in esterification of brown grease oil with methanol is shown in figure 3.11. There is a loss of roughly 3% in activity after five cycles, which indicates that there is little leaching or deactivation of the functional groups. After each cycle, the catalyst was washed with CH_2Cl_2 to prepare for the next cycle, but no attempt to regenerate the catalyst was made. Additional experiments using a larger number of cycles and in a continuous reactor configuration are required to establish operational limits with this catalyst.

Gasification and pyrolysis results

The concept of using brown grease bio-solids in gasification originated from an elemental analysis of the material. A comparison of the hydrogen-to-carbon and oxygen-to-carbon ratios (Table 3.3) to those of lignocellulosic biomass (pine sawdust) and glucose appeared quite favorable. The elemental analysis (H/C, O/C and H/C_{eff} in Table 3.3) shows that the brown grease bio-solids compose a hydrogen rich feedstock, which implies its potential for gasification. The feasibility of pyrolyzing feedstocks with high H/C_{eff} ratios, such as brown grease bio-solids, was articulated by Zhang et al. [30], where the aromatic and olefin yield (desired pyrolysis products) was studied. They found that

increasing H/C_{eff} ratio from 0 (glucose) to 2 (methanol) results in increasing the aromatic and olefin yields from 27% to 80%, respectively. Moreover, they found an inflection point at H/C_{eff} ratio of 1.2, after which the aromatic and olefin yield did not increase rapidly.

As shown in Table 3.3, all the materials analyzed in this study have $0 < H/C_{eff} < 1.2$, which means the aromatic and olefin yield is expected to change significantly among these feedstocks. The brown grease bio-solid has a much greater H/C_{eff} than pine and glucose, which implies its potential for producing higher aromatic and olefin yields via pyrolysis.

As shown in Figure 3.12, simulated gasification and pyrolysis of the brown grease bio-solids were performed in (a) air and (b) nitrogen, respectively, in TGA at 10°C/min to 900°C. In Figure 3.12 (a), multiple peaks appear in the DTG analysis of the combustion of bio-solids, with the first peak in the 200-400°C range and the second in the 400-500°C range. By comparing the combustion (Figure 3.12(a)) and pyrolysis (Figure 3.12(b)) experiments, the first DTG peak is attributed to thermal decomposition of the bio-solids and the second DTG peak represents the oxidation of bio-solid chars [33].

As shown in the pyrolysis TGA experiment, about 10% char residue is left after the pyrolysis. In the combustion experiment less than 1% residue remained in the TGA crucible. This result indicates that about 9% of the total residue after (slow) pyrolysis is char, which cannot be further pyrolyzed in inert gas atmosphere, but it is combustible. The 1% residue after combustion should include mostly inorganic compounds (ash). Figure 3.12a indicates that almost the entirety (99%) of the bio-solids is combustible,

which also implies the feasibility of producing synthesis gas from the bio-solid through gasification.

Fast pyrolysis experiments with the biosolids and glucose were conducted at 600^{o}C. As shown in Table 3.4 and figure 3.13, the liquid products of the fast pyrolysis of bio-solids are mostly long-chain hydrocarbons. As a comparison, the liquid products from the fast pyrolysis of glucose (a lignocellulosic biomass model compound) at 600°C are also listed in Table 3.4, and contain many small oxygenates, such as furan compounds. Production of oxygenates from pyrolysis of lignocellulosic biomass is often reported in the literature [33–39]. These preliminary pyrolysis experiments of bio-solids indicate they may be advantageous as compared to other commonly studied biomass sources. Future studies will focus on reactor conditions that optimize the production of high quality bio-fuel from the brown grease bio-solids.

Sulfur content in Biodiesel from Brown Grease and its removal

Fossil fuels are known to contain sulfur as an impurity. When sulfur-containing fuels are burned, the sulfur is oxidized to sulfur dioxide considered an air pollutant responsible for acid rain. Additionally, it is a respiratory hazard. In petrochemical processes, the presence of sulfur is considered as a catalyst poison for catalytic reformation processes. A concern for environment has formulated regulations and standards for the removal of sulfur to low levels in fuels as well as exhaust gases [40]. Various such regulations are applicable for gasoline, diesel and biodiesel for the removal of heteroatom containing molecules [40]. In petrochemical refineries, the process of sulfur removal is well established by the process of hydrodesulfurization. The reaction is called hydrogenolysis which cleaves a C-X

heteroatom bond and converts it into a C-H and H-X bond. Thus the hydrodesulfurization results in the formation of H_2S. Industrial processes include facilities for the capture of the H2S and its conversion into either sulfuric acid or elemental sulfur. Further developments in sulfur removal from diesel oil or naphtha has been in the form of activated charcoal [41, 42] and zeolite adsorbents [43] with limited cost advantage.

Biodiesel, on the other hand is produced from feedstocks which contain sulfur in a wide variety of forms, including mercaptans, organic sulfonates and sulfur containing proteins. The sulfur containing molecules may have high molecular weight and complex structures which arise from animal protein degradation.

Biocatalytic sulfur removal from petroleum fuels has been explored, with the identification of microbial biocatalysts that can transform selectively remove sulfur from dibenzothiophene heterocyclic compounds [44].

Mercaptan scavengers used for sweetening natural gas have had limited success in sulfur removal of complex compounds present in biodiesel feedstock. They are successful in removing simple low molecular weight sulfur species.

Vacuum distillation has been used to remove sulfur. The methyl esters are separated from the sulfur species, but the technique is only applicable for low molecular weight species which can be flashed out of the liquid phase. However, the heavy and high molecular weight sulfur residue remains behind with the biodiesel phase.

Usage of adsorbents such as silicas and clays has been tried to limited efficacy. Only absorbents acting as catalytic sites for hydrogenation of mercaptan like molecules have been explored with some success [45]. The catalytic sites are prone to poisoning by sulfur and other heteroatomic species. Hydrotreating of waste cooking oil has been explored to

remove heteroatomic species including sulfur. However it requires unit operation at temperatures in excess of 350^0C [46]. There have been some studies in using ionic liquids to remove sulfur compounds from fuels but they have been limited to rather low molecular weight sulfur compounds and have not been used for treating biodiesel with high molecular weight sulfur containing fractions [47].

A comparative analysis of the effect of catalyst on the sulfur levels was carried out by estimating the remnant sulfur levels in biodiesel produced from brown grease, post a two-step esterification and transesterification process.

Typically, concentrated sulfuric acid is used to sulfonate vegetable oils and FFA [48]. The reaction of sulfonation usually takes place via addition to the C=C double bonds in vegetable oils and FFA [49]. The concentration of sulfuric acid used in these experiments mentioned below was far lower. However it is possible that it might may lead to some amount of sulfonation of C=C double bond in oils and fats. The leaching of SO3H groups of the OMR solid acid catalyst into the FAME may add to the sulfur content reading.

The samples of biodiesel produced from esterification using either solid acid or HCl or H_2SO_4 were analyzed for sulfur content according to the details above at two different locations: Center for Environmental Sciences and Engineering (CESE), University of Connecticut and AmSpec Sevices, LLC, MA. The results are shown in Table 3.4 below.

The brown grease samples which were used to produce the biodiesel were collected from two separate locations: Black Gold Inc. and Torrington water treatment plant. As shown

in the table, the sulfur content with HCl esterified samples from Torrington water treatment plant, but tested in two different labs, showed a lower value (32 – 35mg/kg) than that made using H_2SO_4 as the esterification catalyst (148 mg/kg). However, no repeat testing results were obtained on H_2SO_4 esterified biodiesel produced from Torrington water treatment plant's brown grease.

It may be hypothesized that the use of H_2SO_4 causes a small amount of sulfonation of various groups in the bio oil consisting of high molecular weight macro structures, which do not get washed away with water and remain behind in the oil layer. This may lead to an increase in overall sulfur content.

The results on biodiesel produced from brown grease obtained from Black Gold Inc were not tested for repeatability. The sulfur content with OMR solid acid catalyzed biodiesel, tested at AmSpec showed sulfur content of 109.97 mg/kg. Leaching of SO_3H groups is possible even with solid acids. The hypothesis of sulfonation of high molecular weight molecules, such as proteins, holds true in the case of OMR type solid acids too.

With the non-repeatability of results, it is difficult to compare the levels of possible sulfonation facilitated by the homogenous H_2SO_4 versus the heterogeneous OMR catalyst.

These are the initial results on the sulfur content tested at two separate locations using materials of different origins. The sulfur content may vary due to the original sulfur and other heteroatom and heavy metal content in the brown grease samples. Additionally, experimental procedures and accuracy introduce errors in determination. The third factor is indeed the possible leaching of sulfur bearing groups from the homogenous or heterogeneous catalysts and subsequent sulfonation. However, it must be noted that

sulfonation of only those fractions that stay behind in the FAME layer are accounted for. It is expected that thorough washing of biodiesel gets rid of all low molecular weight sulfur containing fractions.

The Sulfur content of OMR resin is 1.64 millimole/gram. A quantity of 0.5g of the OMR resin was used for 5ml brown grease esterification. From the data on activity reduction of OMR catalyst, it may be recounted that the catalyst loses around 0.4% activity after 1 cycle. Even if 0.4% activity loss is assumed after a single cycle of brown grease esterification and attributed solely to the loss of sulfonate groups leading to sulfonation of water insoluble FAME fractions, the maximum possible addition to the sulfur content in biodiesel can be ~23 ppm. The assumption of this calculation is that the loss in activity has a linear relationship with the loss of sulfonate groups. This estimation additionally assumes that the entire sulfur coming from the OMR catalyst stays back as water insoluble fraction in the biodiesel layer. The calculation also assumes that these sulfur-containing molecules are sulfonated methyl esters.

The results of Virgin Oil conversion to biodiesel using H_2SO_4 as esterification catalyst are shown in Table 3.4. Interestingly H_2SO_4 contributes 3.5ppm sulfur to virgin oil with zero starting sulfur concentration.

Since no error bars or standard deviation for the results can be estimated with just one data point for each sample, the future research presents opportunities for more research to determine the repeatability and reproducibility of these results.

The certificate of analysis from AmSpec Services. LLC are attached as an annexure.

Sulfur Removal

For Sulfur removal, 20ml of HCl treated biodiesel and 4 g of 50% Raney Nickel dispersion in water were mixed together and stirred at 140C for eight hours and at 500 stirrer RPM. After 8 hours, the mixture was centrifuged to separate the hydrophobic biodiesel layer.

The biodiesel was analyzed for sulfur content by Gas Chromatography (SCD column). The Sulfur content analyses were carried out by AmSpec Services. LLC, Everett, MA by ASTM D5453 method.

The sulfur content in biodiesel produced using HCl catalyst was seen to reduce from 32mg/kg to 8.83 mg/kg using this method of removal. The ASTM standard for sulfur content in biodiesel is 15mg/kg (max). Thus the biodiesel, after treatment with Raney Nickel was seen to satisfy the ASTM requirements for Sulfur Content.

Conclusions

The possibility of 100% utilization of the brown grease waste for producing biofuels was explored. The brown grease oil layer was transformed into biodiesel with a mesoporous solid acid catalyst. The catalyst was synthesized from a polymeric base using a templating method that led to an ordered pore structure with narrow pore size distribution and high surface area. Acid functionalization was controlled to yield a hydrophobic material with superior catalyst properties compared to homogenous catalysts and commercial heterogeneous catalysts. Esterification of the FFA in the brown grease oil with the solid acid catalyst, followed by conventional transesterification of the

triglycerides produced biodiesel that passed the critical ASTM quality tests of acid number and free and total glycerin.

The bio-solids separated from the aqueous layer of the brown grease were analyzed and found to have a H/C_{eff} ratio greater than wood, implying excellent potential for producing higher aromatic and olefin yields via pyrolysis. When pyrolyzed at 600^{o}C, the bio-solids yielded liquid products that were mostly long-chain hydrocarbons according to GC/MS analysis. Almost 99% of the bio-solids were combustible implying the feasibility of producing synthesis gas from the bio-solids through gasification. These results establish the feasibility of converting ~100% of the raw brown grease to valuable energy products.

References

[1] Aslani A, Wong KFV. Analysis of renewable energy development to power generation in the United States. Renewable Energy 2014; 63: 153–161.

[2] Noshadi I, Amin NAS, Parnas RS. Continuous production of biodiesel from waste cooking oil in a reactive distillation column catalyzed by solid heteropolyacid: optimization using response surface methodology (RSM). Fuel 2012; 94: 156-164.

[3] Talebian-Kiakalaieh A, Amin NAS, Zarei A, Noshadi I. Transesterification of waste cooking oil by heteropoly acid (HPA) catalyst: Optimization and kinetic model. Applied Energy 2013; 102 : 283-292.

[4] Knothe GH. A technical evaluation of biodiesel from vegetable oils vs. algae. Will algae-derived biodiesel perform? Green Chemistry. 2011; 13: 3048-3065.

[5] Boucher MB, Weed C, Leadbeater NE, Wilhite BA, Stuart JD, Parnas RS. Pilot scale two-phase continuous flow biodiesel production via novel laminar flow reactor−separator. Energy and Fuels 2009; 23: 2750-2756.

[6] Unker SA, Boucher MB, Hawley KR, Midgette AA, Stuart JD, Parnas RS. Investigation into the relationship between the gravity vector and the flow vector to improve performance in two-phase continuous flow biodiesel reactor. Bioresource Technology 2010; 101 (19): 7389-7396.

[7] Talebian-Kiakalaieh A, Amin NAS, Mazaheri H. A review on novel processes of biodiesel production from waste cooking oil. Applied Energy 2013; 104: 683–710.

[8] Liu F, Wang L, Sun Q, Zhu L, Meng X, Xiao FS. Transesterification Catalyzed by Ionic Liquids on Superhydrophobic Mesoporous Polymers: Heterogeneous Catalysts That Are Faster than Homogeneous Catalysts. J. Am. Chem. Soc. 2012; 134; 16948−16950

[9] Corma A. From Microporous to Mesoporous Molecular Sieve Materials and Their Use in Catalysis. Chemical Reviews 1997; 97: 2373-2420.

[10] De Vos DE, Dams M, Sels BF, Jacobs PA. Ordered Mesoporous and Microporous Molecular Sieves Functionalized withTransition Metal Complexes as Catalysts for Selective Organic Transformations. Chemical Reviews 2002; 102: 3615-3640.

[11] Dioumaev VK, Bullock RM, Recyclable Catalyst that Precipitates at the End of the Reaction. Nature 2003; 424: 530-532.

[12] Melero JA, Grieken RV, Morales G. Advances in the Synthesis and Catalytic Applications of Organosulfonic-Functionalized Mesostructured Materials. Chemical Reviews 2006; 106: 3790-3812.

[13] Leung DYC, Wu X, Leung MKH. A review on biodiesel production using catalyzed transesterification. Applied Energy 2010; 87(4): 1083–1095.

[14] Fats, Oils and Grease, Environmental Assistance Office Newsletter, UNC Charlotte, 2011.

[15] Davis ME. Ordered porous materials for emerging applications. Nature 2002; 417: 813–821.

[16] Chai F, Cao FH, Zhai FY, Chen Y, Wang XH, Su ZM, Transesterification of Vegetable Oil to Biodiesel using a Heteropolyacid Solid Catalyst. Advanced Synthesis and Catalysis 2007; 349: 1057-1065.

[17] Wan Y, Zhao DY, On the Controllable Soft-Templating Approach to Mesoporous Silicates. Chemical Reviews 2007; 107: 2821-2860.

[18] Xing R, Liu N, Liu YM, Wu HH, Jiang YW, Chen L, He MY, Wu P. Novel Solid Acid Catalysts: Sulfonic Acid Group-Functionalized Mesostructured Polymers. Advanced Functional Materials 200; 17: 2455.

[19] Liu FJ, Li CJ, Ren LM, Meng XJ, Zhang H, Xiao F-S. Hydrothermal Synthesis of Ordered Mesoporous Silicas with Extraordinarily Ultra-low Dielectric Constants. Journal of Materials Chemistry 2009; 19(42): 7921-7928.

[20] Schmolka IR, Lundsted IG. The Synthesis and Properties of Block Copolymer Polyol Surfactants, Block and Graft Copolymerization New York: Wiley; 1986.

[21] Liu F, Kamat RK , Noshadi I, Peck D, Parnas RS , Zheng A, Qi J, Lin Y. Depolymerization of Crystalline Cellulose Catalyzed by Acidic Ionic Liquids Grafted on Sponge-Like Nanoporous Polymers. Chem. Commun. 2013; 49: 8456-8458.

[22] Miao S and Shanks BH, Esterification of biomass pyrolysis model acids over sulfonic acid-functionalized mesoporous silicas. Appl. Catal. A 2009; 359: 113-120.

[23] Tucker MH, Crisci AJ, Wigington BN, Phadke N, Alamillo R, Zhang JP, Scott SL, Dumesic JA. Acid-functionalized SBA-15-type periodic mesoporous organosilicas and their use in the continuous production of 5-hydroxymethylfurfural. ACS Catalysis 2012; 2: 1865-1876.

[24] Liu F, Zuo S, Kong W, Qi C. High-temperature synthesis of strong acidic ionic liquids functionalized, ordered and stable mesoporous polymers with excellent catalytic activities. Green Chem 2012; 14: 1342-1349.

[25] Noshadi I, Kumar RK, Kanjilal B, Parnas R, Liu H, Li J, Liu F. Transesterification Catalyzed by Superhydrophobic–Oleophilic Mesoporous Polymeric Solid Acids: An Efficient Route for Production of Biodiesel. Catalysis Letters 2013 ; 143: 792-797.

[26] Zhang F, Meng Y, Gu D, Yan Y, Yu C, Tu B, Zhao D. A Facile Aqueous Route to Synthesize Highly Ordered Mesoporous Polymers and Carbon Frameworks with Ia$\bar{3}$d Bicontinuous Cubic Structure J. AM. CHEM. SOC 2005; 127: 13508-13509

[27] Fukuhar K, Nakajima K, Kitano M, Hayashic S, Hara M, Synthesis and acid catalysis of zeolite-templated microporous carbons with SO3H groups. Phys. Chem. Chem. Phys. 2013; 15: 9343—9350.

[28] Iliev I, Yordanova H, Petrenko P, Novakov P. Reaction of Phenol-Formaldehyde Novolac Resin and Hexamethylenetetramine in OH–Containing Solvents as Medium. Journal of the University of Chemical Technology and Metallurgy. 2006 ; 41: 29-34

[29] Baig A, Flora T, Ng T. A Single-Step Solid Acid-Catalyzed Process for the Production of Biodiesel from High Free Fatty Acid Feedstocks. Energy Fuels 2010; 24(9): 4712–4720.

[30] Zhang H,Cheng YT, Vispute TP, Xiao R, Huber GW. Catalytic Conversion of Biomass-derived Feedstocks into Olefins and Aromatics with ZSM-5: The Hydrogen to Carbon Effective Ratio. Energy & Environmental Science 2011; 4: 2297-2307.

[31] Cheng G, He PW, Xiao B, Hu ZQ, Liu SM, Zhang LG, Cai L. Gasification of biomass micron fuel with oxygen-enriched air: Thermogravimetric analysis and gasification in a cyclone furnace. Energy 2012; 43: 329-333.

[32] Park JY, Kim DK, Lee JS, Esterification of free fatty acids using water-tolerable Amberlyst as a heterogeneous catalyst. Bioresource Technol. 2010; 101: S62-S65.

[33] Patwardhan PR, Satrio JA, Brown RC, Shanks BH, Product distribution from fast pyrolysis of glucose-based carbohydrates. Journal of Analytical and Applied Pyrolysis 2009; 86: 323-330.

[34] Mullen CA, Boateng AA. Chemical composition of bio-oils produced by fast pyrolysis of two energy crops. , Energy & Fuels 2008; 22: 2104-2109.

[35] Branca C, Giudicianni P, Di Blasi C. GC/MS characterization of liquids generated from low-temperature pyrolysis of wood. Ind. Eng. Chem. Res 2003; 42(14): 3190-3202.

[36] Olazar M, Aguado R, Bilbao J, Barona A, Pyrolysis of sawdust in a conical spouted-bed reactor with a HZSM-5 catalyst. AIChE Journal 2000; 46: 1025-1033.

[38] Carlson TR, Tompsett GA, Conner WC, Huber GW, Aromatic Production from Catalytic Fast Pyrolysis of Biomass-derived Feedstocks. Topics in Catalysis 2009; 52: 241-252.

[39] Du S, Valla JA, Bollas GM. Characteristics and origin of char and coke from fast and slow, catalytic and thermal pyrolysis of biomass and relevant model compounds. Green Chemistry 2013; 15: 3214-3229.

[40] Yosuke S, Kazuom S, Ki-Hyouk C, Yozo K, Isao M.Two- step adsorption process for deep desulphurization of diesel oil. Fuel, 2005; 84, 7-8, 903-910.

[41] Gamil MHR, Nasser MM. Desulphurization of Um Al Nar refinery straight run kerosene and gas oil using pal fruit kernel activated charcoal: a locally made adsorbent. Adsorption science and technology. 1997; 15, 311-321

[42] Abu baker Salem SH. Naphtha desulphurization by adsorption. Ind. Eng. Chem. Res, 1994; 33, 336-340.

[43] Toida Y. Adsorption desulphurization agent for desulphurizing petroleum fraction and desulphurization method using the same. USA Patent, 2005; 20050173297.

[44] McFarland BL, Boron DJ, Deever W, Meyer JA, Johnson AR, Atlas RM. Biocatalytic Sulfur Removal from Fuels: Applicability for Producing Low Sulfur Gasoline, Critical Reviews in Microbiology 1998; 24, 2 , 99-147,

[45] Ma XL, Sprague M, Song C. Deep desulphurization of gasoline by selective adsorption over Nickel-based adsorbent for fuel cell application. Ind. Eng. Chem. Res, 2005; 44, 15, 5768-5775.

[46] Bezergianni S, Dimitriadis A, Kalogianni A, Pilavachi PA.Hydrotreating of waste cooking oil for biodiesel production. Part I: Effect of temperature on product yields and heteroatom removal, Bioresource Technology, 2010; 101, 17, 6651-6656

[47] Zhang S, Zhang ZC. Novel properties of ionic liquids in selective sulfur removal from fuels at room temperature, Green Chem 2002; 4, 376-379

[48] Frank C. Vilbrandt , Paul E. Chapman , Jerome M. Crockin. Sulfonation of Tall Oil. Ind. Eng. Chem., 1941 ;33 (2) 197–200

[49] Vincent J. Nowlan , Thomas T. Tidwell. Structural effects on the acid-catalyzed hydration of alkenes. Acc. Chem. Res., 1977; 10 (7), 252–258

Table 3.1 yield and composition of oil layer from dewatered brown grease

Sample No.	Initial volume of brown grease	Oil layer	Yield (%)	FFA %	glycerides %
1 (Mid Jan)	2L	1L	50	88.32	11
2 (Early Feb)	1.8 L	0.8 L	44.4	88.76	11
3 (Late Feb)	2 L	0.8 L	40	89.23	10

Table 3.2 Biodiesel specification

	Acid Number (ASTM limit: <0.5)	Free glycerin (ASTM limit <0.02)	Total glycerin (ASTM limit <0.24)
Two-step Process	0.46	0.02	0.18
Simultaneous esterification-Transesterification	0.23	0.01	0.36

Table 3.3 Elemental analysis of bio-solid, pine and glucose (mol%, dry basis)

Feedstock	N	C	H	O*	H/C	O/C	H/C_{eff}
Bio-solid	1.19	33.80	54.64	10.37	1.62	0.31	1.00
Pine	0.20	34.52	46.33	18.95	1.34	0.55	0.25
Glucose	0.00	25.00	50.00	25.00	2.00	1.00	0.00

* Oxygen content was calculated by difference

Table 3.4 Sulphur Content in Biodiesel

Sample Name	**Sulphur Content**	**Testing Lab**
Raw Material : Brown Grease from Black Gold Inc.		
OMR Esterified	109.97mg/kg	AmSpec Services. LLC
Raw Material : Brown Grease from Torrington water treatment plant.		
HCl Esterified	32 mg/kg	AmSpec Services. LLC
HCl Esterified	35.5mg/kg	CESE, University of Connecticut
H_2SO_4 Esterified	148.3 mg/kg	CESE, University of Connecticut
Raw Material : Virgin Oil		
H_2SO_4 Esterified	3.5 mg/kg	CESE, University of Connecticut

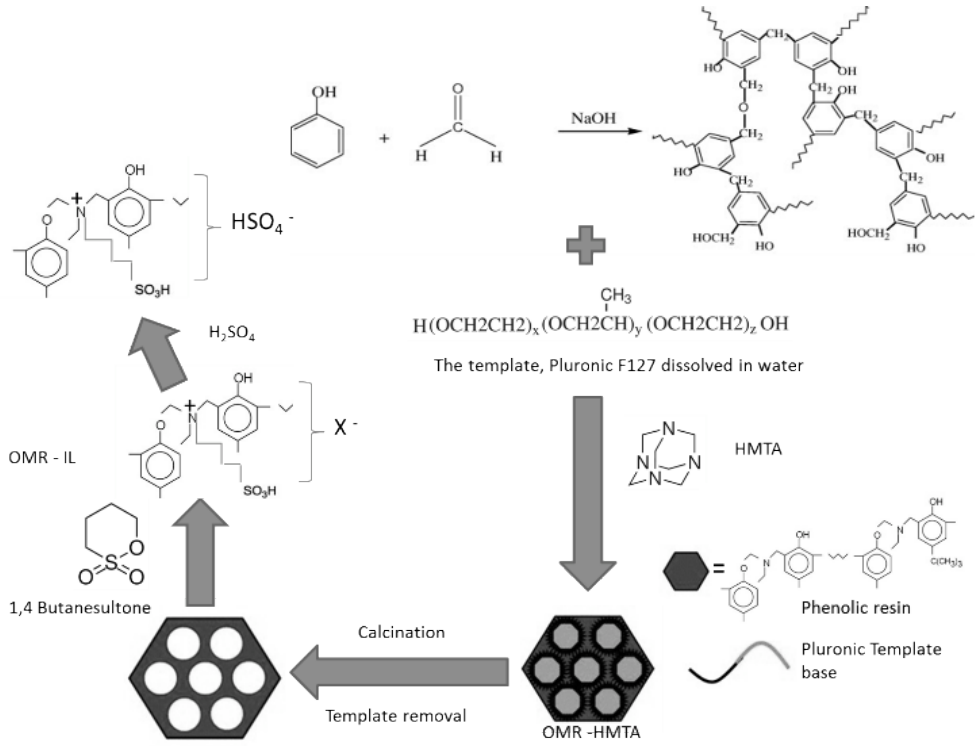

Scheme 3.1. Synthesis of OMR-[C_4HMTA][SO_4H]

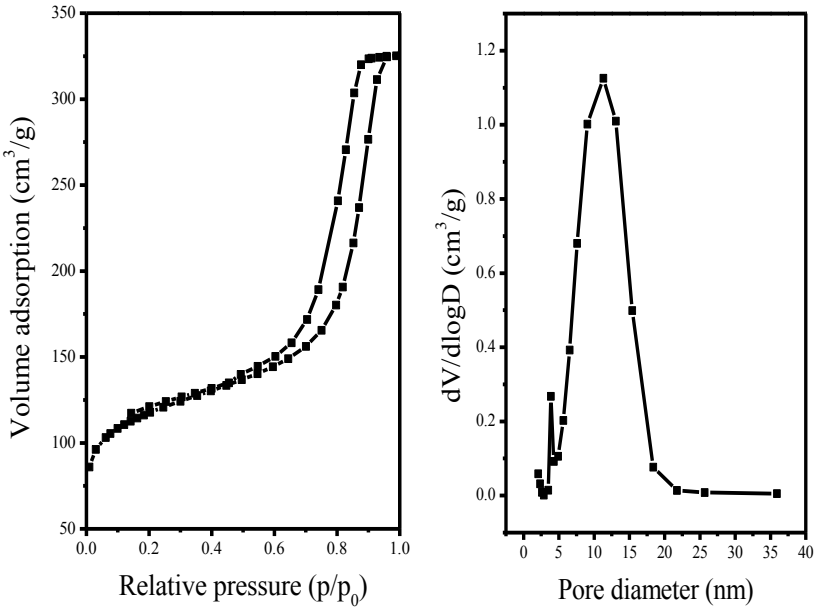

Fig 3.1 N_2 isotherm and pore size distribution of OMR-[C_4HMTA][SO_4H].

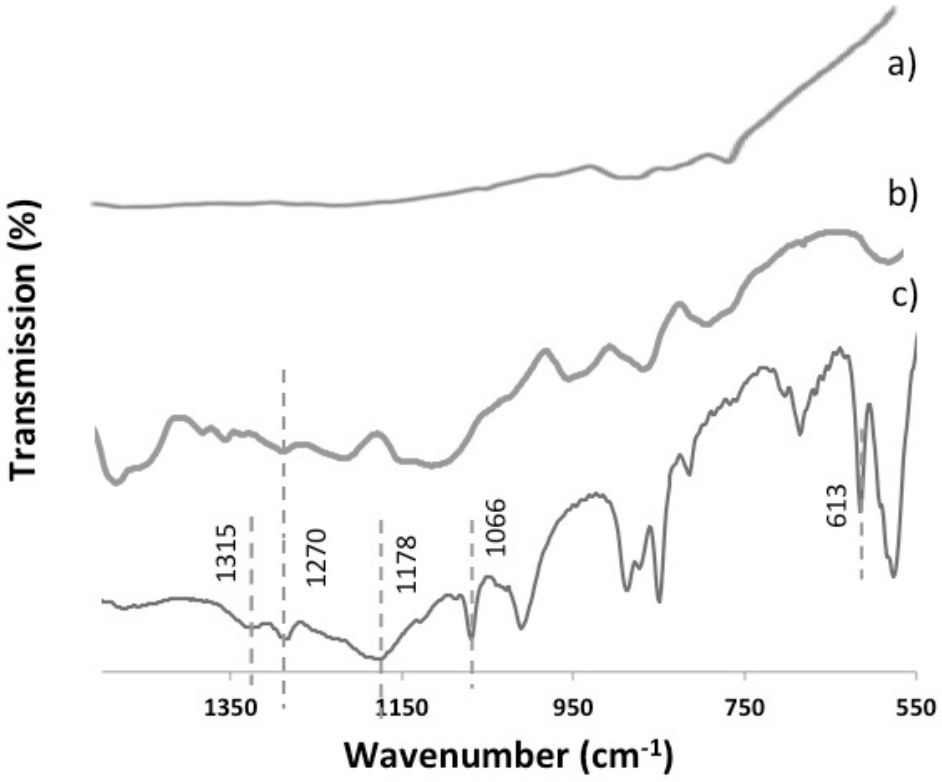

Fig 3.2 FT-IR spectra of a) OMR-[HMTA] b) OMR-[C_4HMTA][SO_4H]. The peaks marked at 613, 1066, 1178, 1250 and 1315 cm^{-1} are the signals for C–S , S=O and C-N bonds, indicating successful functionalization.

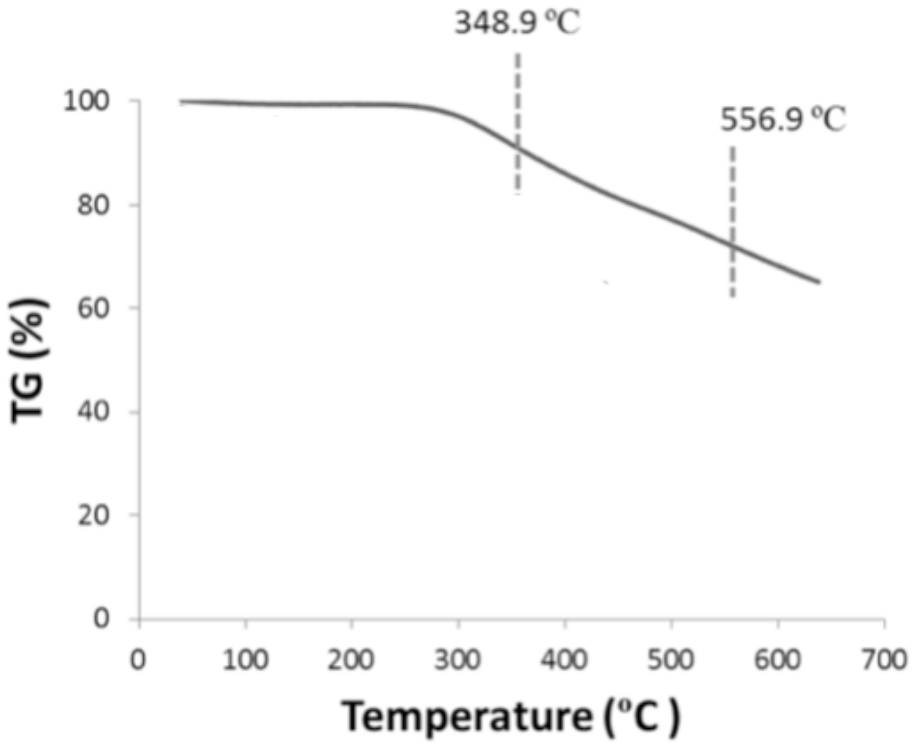

Figure 3.3 TGA in N_2 of OMR-[C_4HMTA][SO_4H] illustrating that thermal degradation begins at temperatures above 250 ^oC, with minor peaks at 349 ^oC and 557 ^oC.

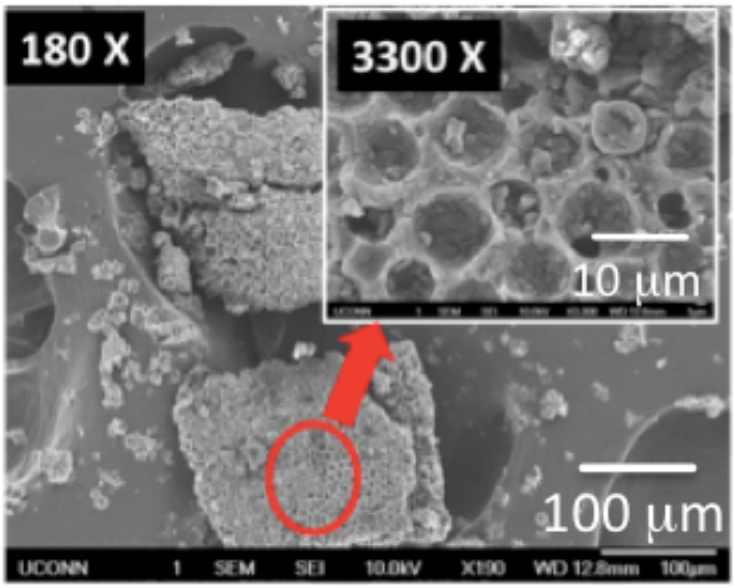

Figure 3.4 FESEM image of an OMR-[C_4HMTA][SO_4H] solid particle on carbon tape at a magnification of 180X. Inset: same particle magnified to 3300X showing the highly porous nature of the catalyst.

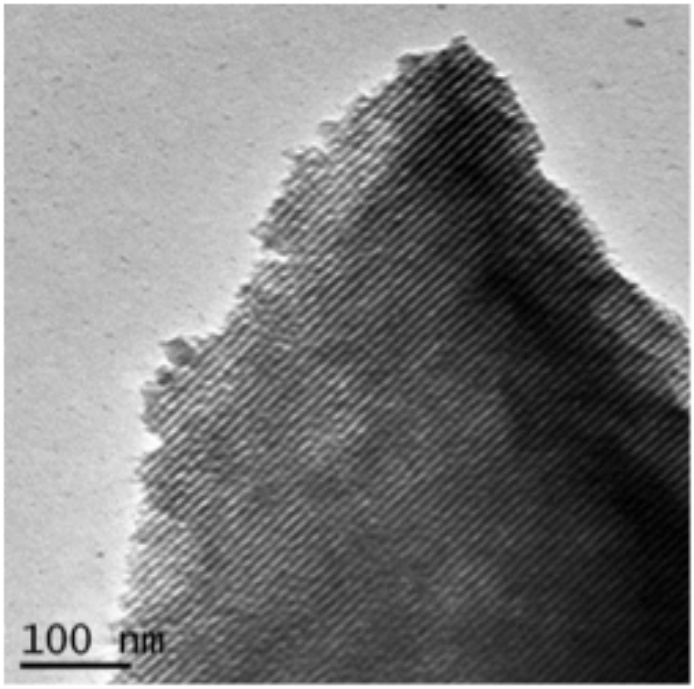

Figure 3.5 TEM image of OMR-[C_4HMTA][SO_4H]

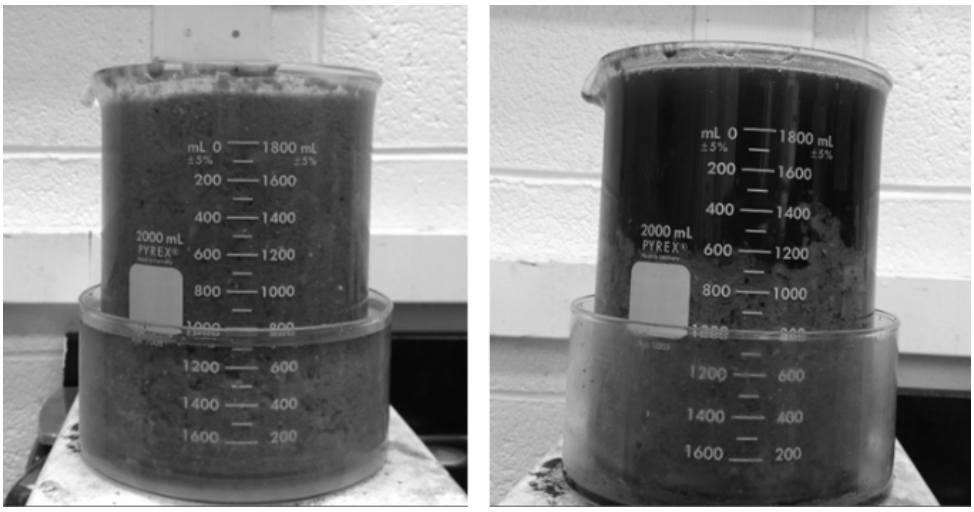

Figure 3.6 Oil separation from dewatered brown grease: (a) brown grease prior to separation; (b): separated layers of brown grease oil (top) and aqueous layer (bottom) after being heat treated at 35ºC for 16 hours.

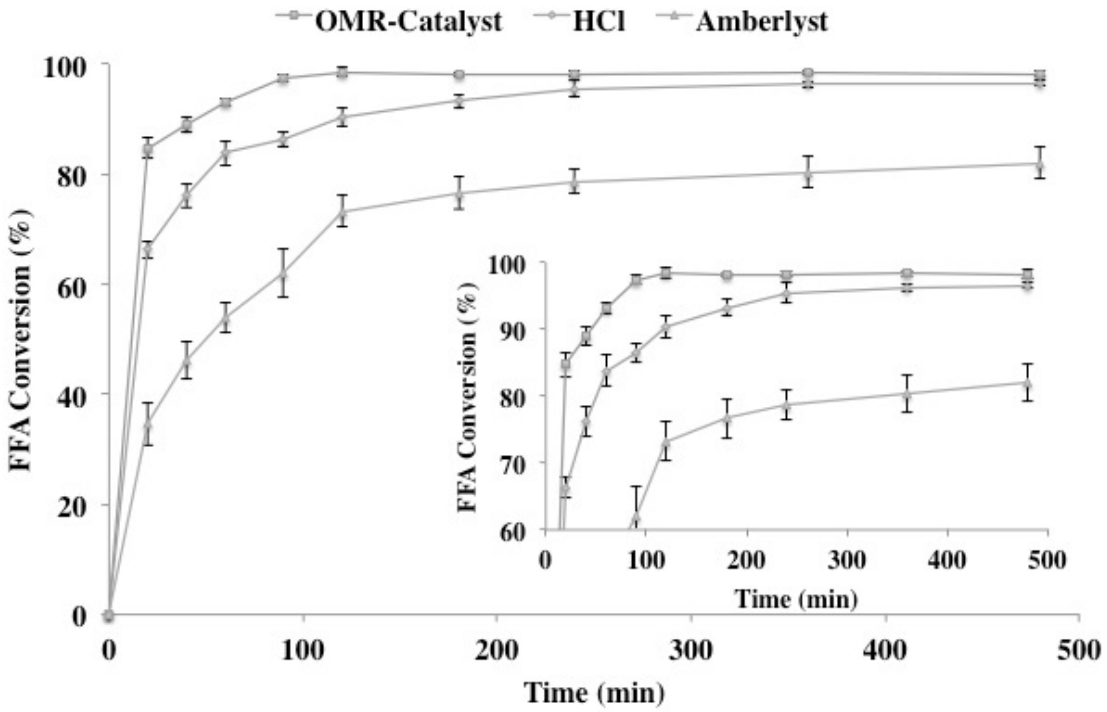

Figure 3.7 FFA conversion during esterification of brown grease with homogenous and heterogeneous catalysts. Oil/methanol molar ratio, 1:9; Temperature, 65°C; catalyst, 5 wt % of the brown grease. Inset – detailed view of conversion above 80% illustrating run-to-run reproducibility.

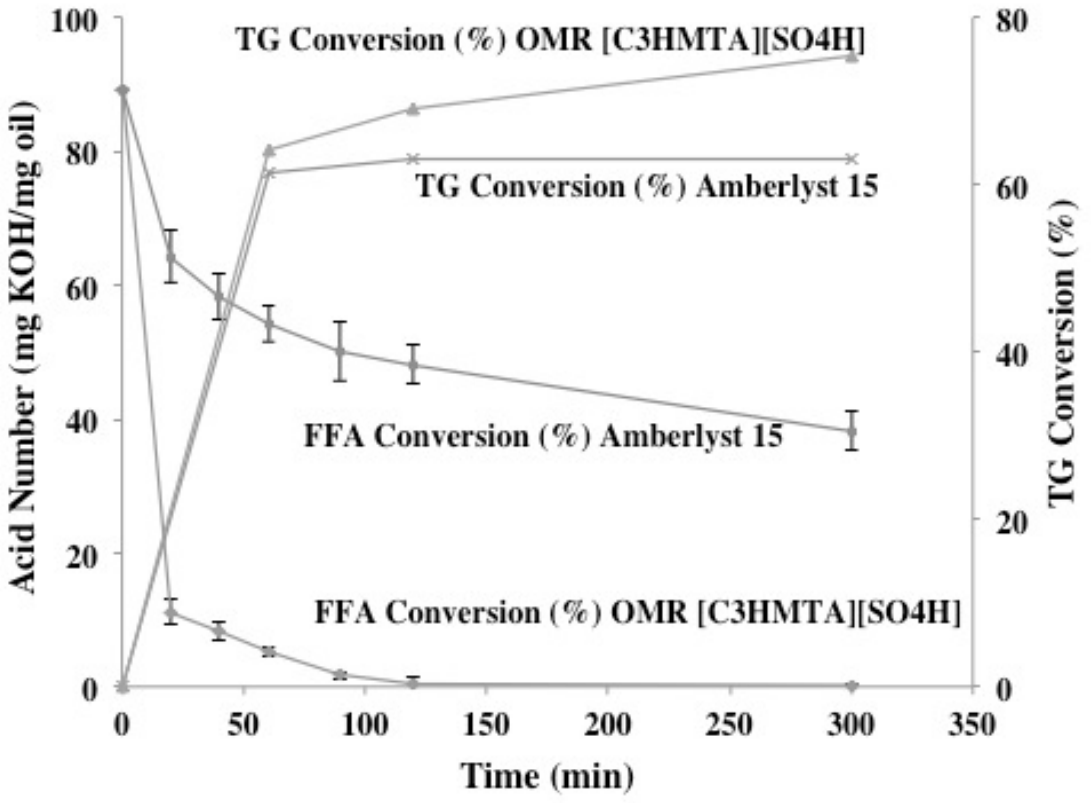

Figure 3.8. Acid Number and triglyceride (TG) conversion vs. time for the simultaneous esterification and transesterification of brown grease oil containing 90 wt % FFA with OMR-[CH_4MTA][SO_4H] and Amberlyst 15. Reaction conditions: Temperature, 65^{o}C; molar ratio of oil/alcohol, 1:40; catalyst, 5 wt % (Catalyst/oil)

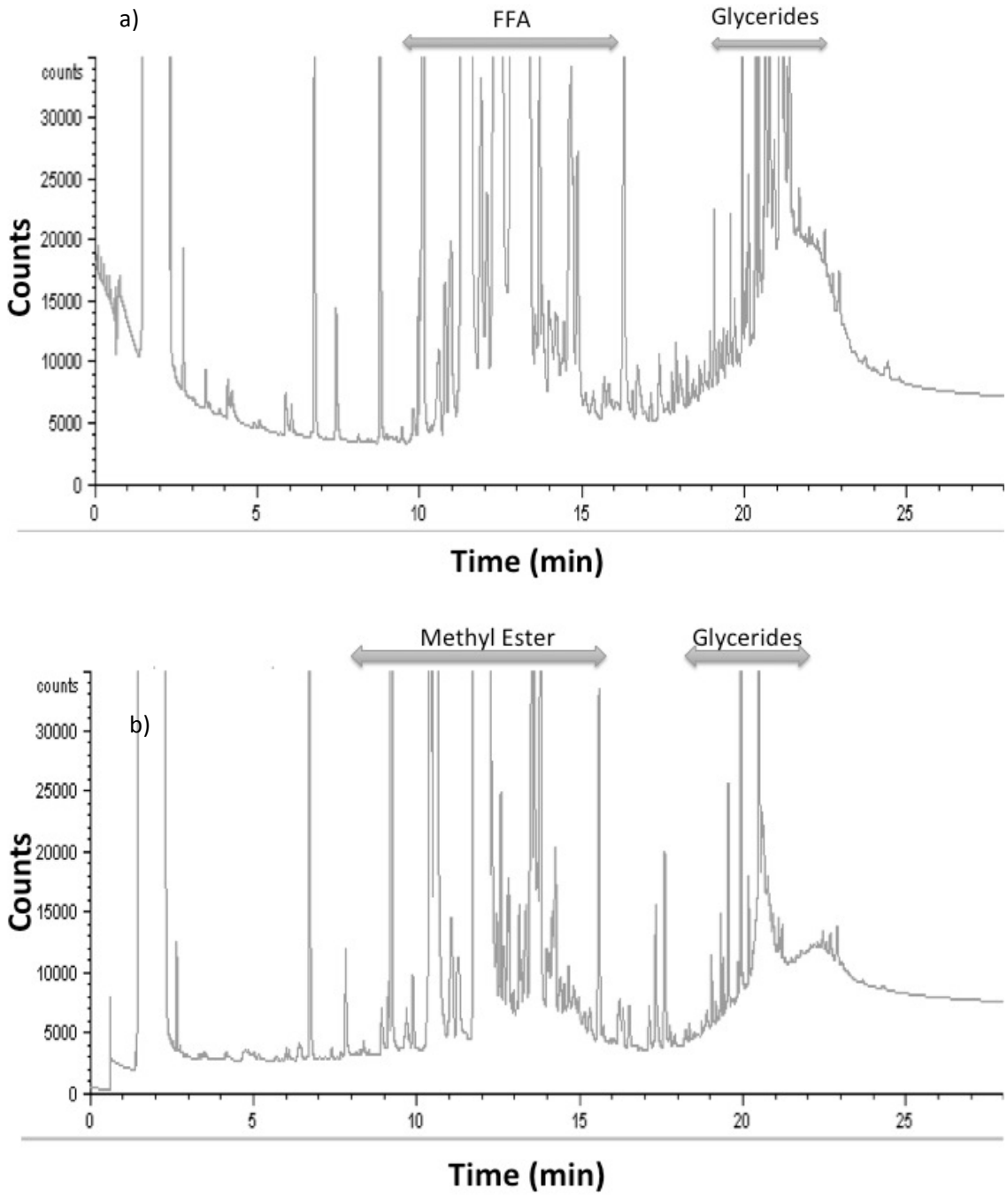

Figure 3.9 GC chromatograms of a) brown grease oil b) biodiesel from brown grease oil.

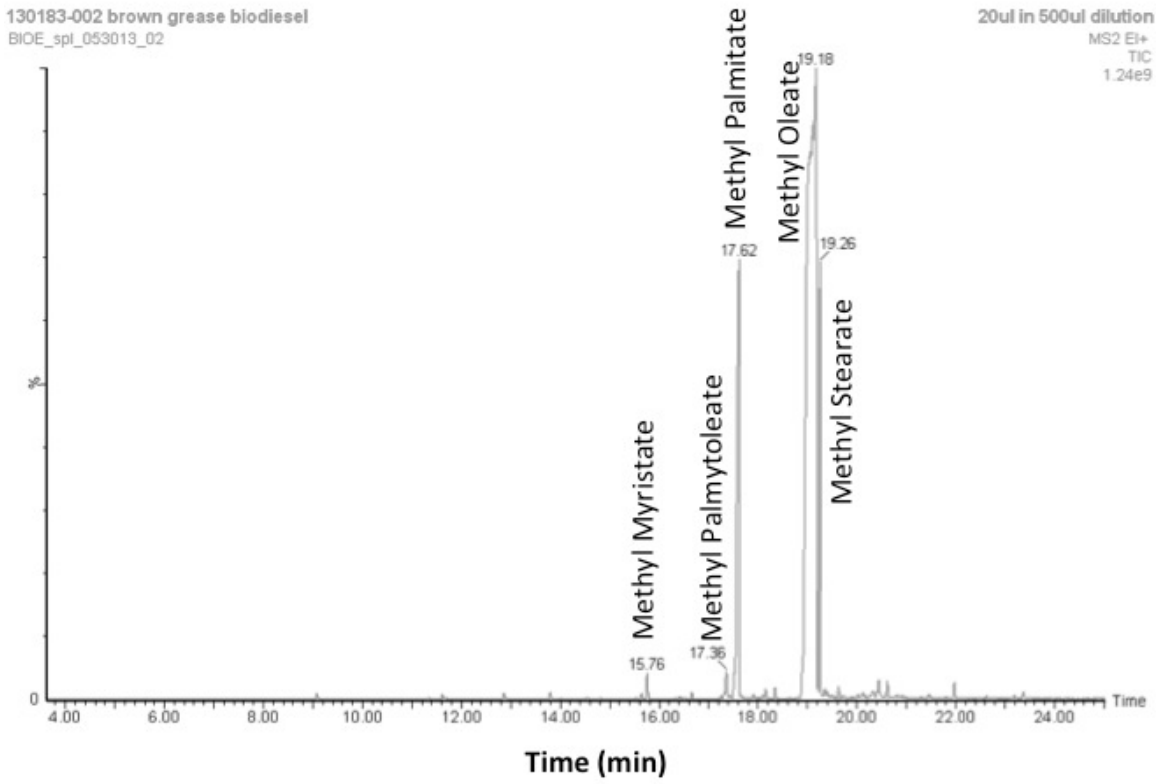

Figure 3.10 Biodiesel composition

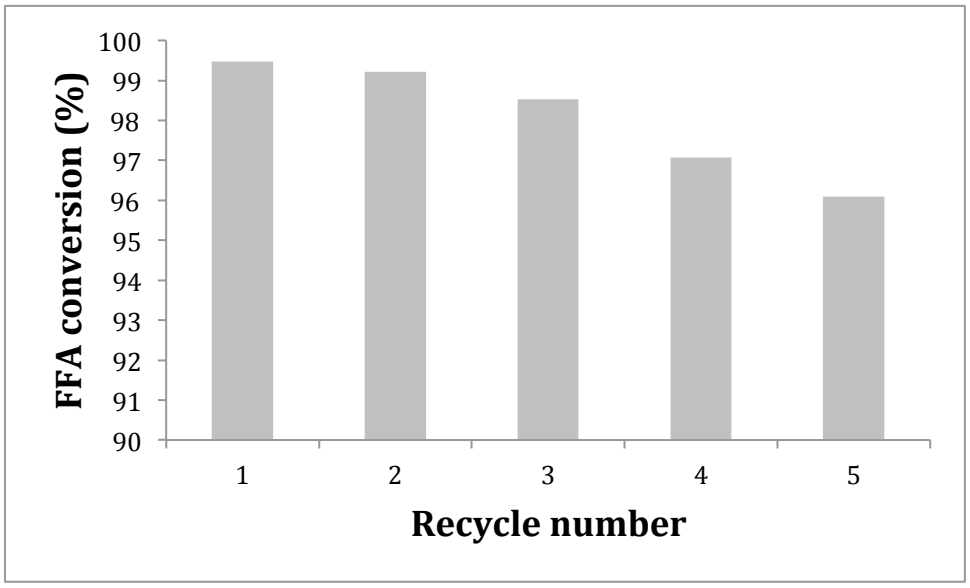

Figure 3.11 OMR-[CH_4MTA][SO_4H] catalyst recyclability for esterification of brown grease with methanol (T=65 °C, time=2 hr).

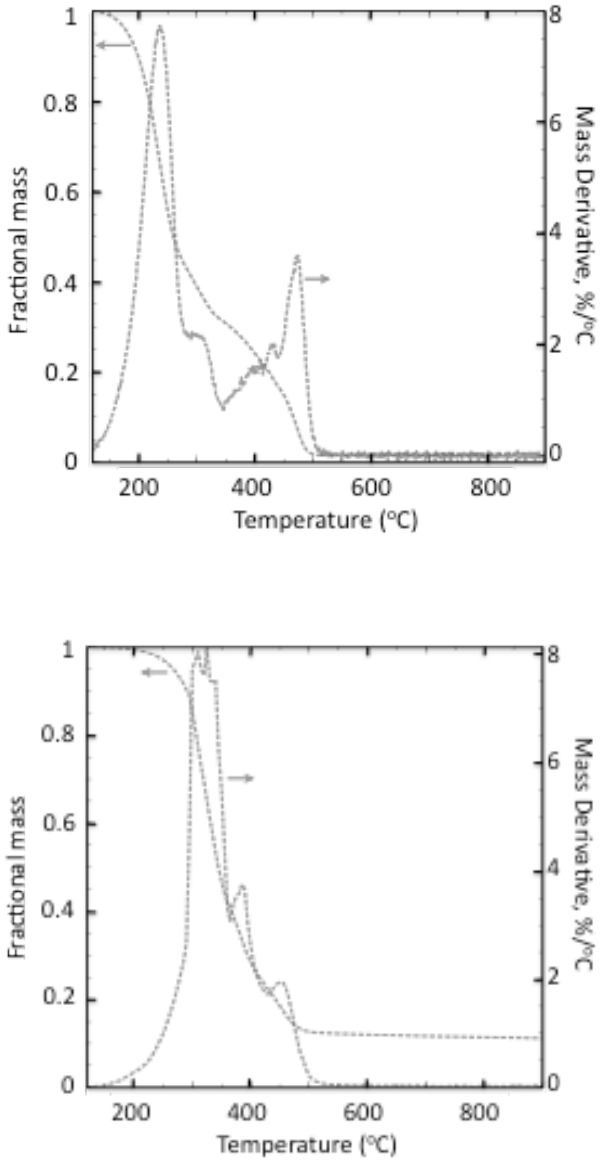

Figure 3.12 Thermogravimetric analysis (TGA) of biosolid in (a) air and (b) nitrogen

Fig

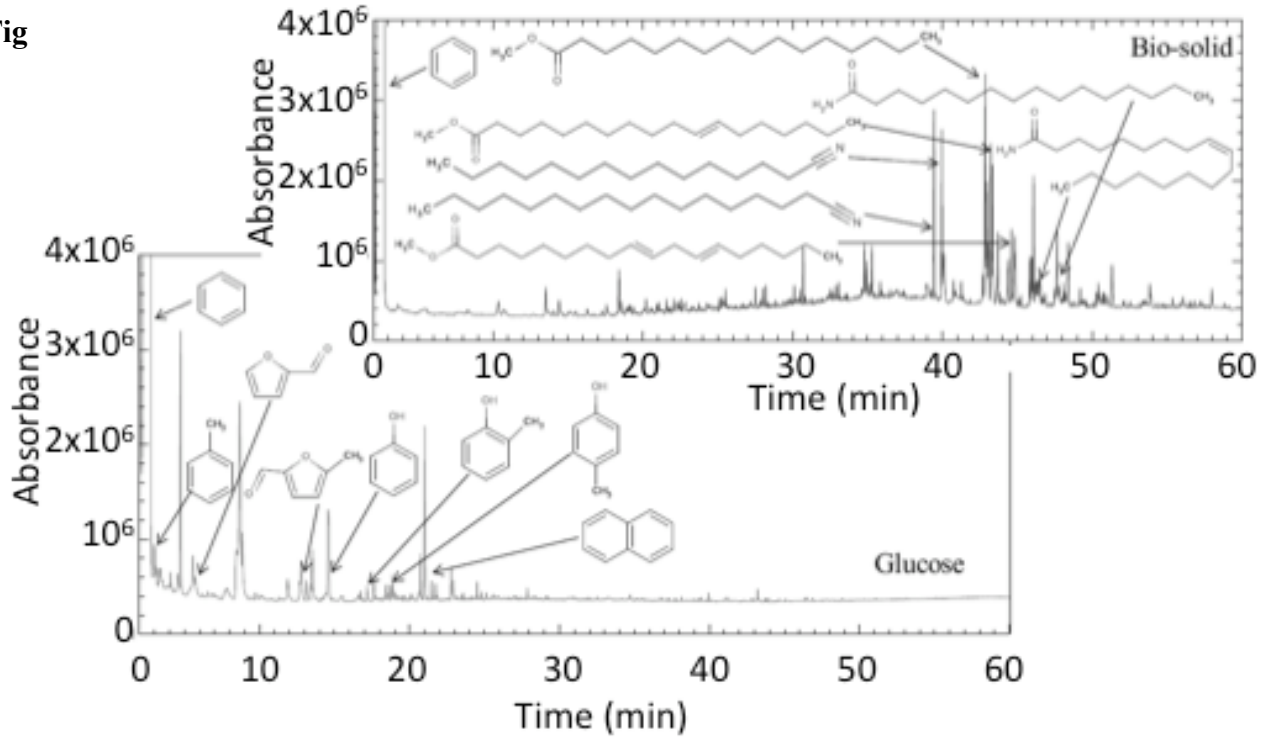

Figure 3.13 GC chromatograms of glucose and biosolid pyrolysis. MS analysis of peaks shown in Table 4.

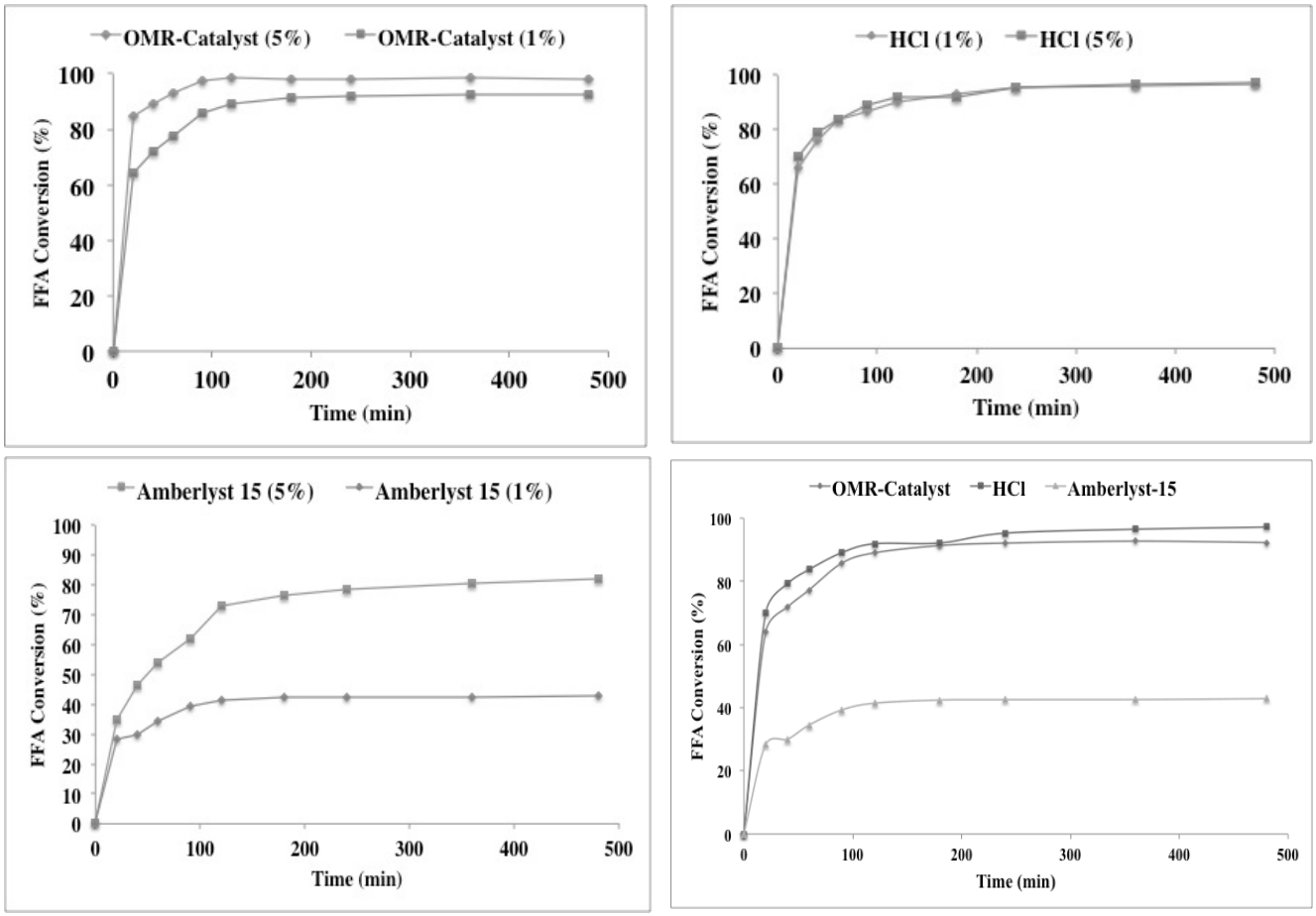

Figure 3.14 FFA conversion during esterification of brown grease with homogenous and heterogeneous catalysts. Oil/methanol molar ratio, 1:9; Temperature, 65°C; catalyst, 1 wt % of the brown grease. a) OMR-Catalyst b) HCl c) Amberlyst-15 d)

Chapter 4. Complete use of acidulated bone waste with crystalline mesoporous ɣ-Al_2O_3-K_2O solid base catalyst coupled with fast pyrolysis

Introduction

Hydrocarbon-based biofuels derived from renewable, non-food carbon sources serve as a promising alternative to petroleum-derived fuels and are capable of mitigating greenhouse gas emissions. A sustainable biofuel strategy should utilize easily renewable biomass feedstocks, especially wastes, for which industries carry the high cost of disposal. Fuel production and power cogeneration from waste recovery is a sustainable and potentially profitable means of addressing economic challenges of energy costs and waste management [1]. An interesting candidate in this scenario is the organic fraction of acidulated bone. Acidulated bone is waste ground bone or bone meal treated with sulfuric acid. After acidulation, the inorganic fraction is normally used to make Gelatin. The organic fraction is a process waste and it consist of hydrocarbons [2].

The use of animal fats as animal feed has been discontinued due to the possibility of disease, and such fats present a more abundant raw material source than frying oils for making biodiesel, in addition to being a recourse for recycling such wastes [3]. Various animal fats such as pork lard, beef tallow and chicken fat, in addition to vegetable based yellow grease, have been used for the production of biodiesel [3]. Lard has also been used to make biodiesel by base catalyzed transesterification [4]. The high free fatty acid (FFA) content in most animal fat feedstock is a problem in base-catalyzed transesterification. The FFA reacts with the basic catalyst resulting in soaps. This reduces catalyst efficiency and makes the process of biodiesel manufacture more costly [5-6]. The FFA can be converted to biodiesel by an esterification pretreatment step using acid

catalyst, which is then followed by a base catalyzed transesterification of the triglycerides.

Biodiesel from renewable sources is a topic of current interest due to the increasing demand for energy and concerns for the environment [7-16]. Acid and base catalyzed transesterification of triglycerides with short chain alcohols is an important route for producing biodiesel. Conventional acid and base homogenous catalysts such as H_2SO_4, NaOH and KOH, while proffering good catalytic activities also have disadvantages related to waste, corrosion and difficult recyclability which adversely affect their application. Solid catalysts such as sulfated zirconia or supported heteropolyacids, have limitations in their catalytic activity for industrial applications arising from low active site exposure and leaching [15]. But, at the same time, they are advantageous with respect to catalyst recycling and a high stability towards CO_2 - a catalyst poison - in air [7-16].

While base catalysts are more active and less expensive than acid catalysts, homogenous base catalysts also have disadvantages with respect to the environment and difficulty in catalyst regeneration which limit their applications. While solid bases show similar catalytic activities as those of homogenous base catalysts, they are prone to poisoning by H_2O, CO_2, and fatty acids (FFAs). Their surface texture, wettability and subsequent adsorption properties also affect their catalytic performance [7-16].

Efficient and superhydrophobic mesoporous polymeric solid acid catalysts have been prepared from copolymerization of divinylbenzene (DVB) with 4-vinylbenzenesulfonate

(SVBS) (H-PDVB-SO_3H-*x*s, where *x* stands for the molar ratio of sodium *p*-styrene sulfonate to DVB) under solvothermal conditions. Catalytic tests confirmed that H-PDVB-*x*-SO_3H exhibited better catalytic performance for esterification of FFA than ZSM-5 zeolite, carbon solid acid and Amberlyst 15, making them a better catalyst choice for large scale application in biodiesel production [17].

In this work, poly-4-vinylpyridine (P4VP) is used as a template for the high temperature hydrothermal synthesis of crystalline mesoporous ɣ-Al_2O_3 solid base catalyst by self-assembly of the ɣ-Al_2O_3 with the template P4VP. The high synthesis temperature (180°C) results in highly crystalline catalysts with good stability when compared with the samples synthesized at relatively low temperature (100°C). Following the self-assembly, treatment with KF solution and calcination at 550°C leads to the final catalyst, a solid super base sometimes abbreviated as ɣ-Al_2O_3-K_2O with large BET surface area, good stability and ultra-strong base strength [18]. Notably, the resulting mesoporous solid super base exhibits excellent catalytic activities and good recyclability in transesterification when compared with conventional solid base such as layer doubled hydroxides (LDHs), CaO, nonporous ɣ-Al_2O_3 supported super base, and a porous ɣ-Al_2O_3 supported super base prepared by another method [19-24]. Response surface methodology (RSM) was used to optimize the processing conditions with the solid base catalyst for transesterification of food grade canola oil.

The main goal of this project is to explore the possibility of transforming 100% of acidulated bone into biodiesel and synthesis gas that can be used for power generation.

Thus, the two catalysts discussed above were used for the first time to convert acidulated bone oil to biodiesel. To convert the remaining acidulated bone solid residue to useful energy products, preliminary experiments were conducted to determine the feasibility of either pyrolysis or gasification.

Experimental Section

Catalyst Preparation

Preparation of mesoporous H-PDVB-SO_3H

Sodium 4-vinylbenzenesulfonate (SVBS) was copolymerized with DVB by using AIBN initiator in an autoclave at 100°C. 2.0 g of DVB was added to 0.5 g of SVBS. This monomer mixture was added to a mixture of 0.065 g AIBN, 25 ml THF and 2.5 ml distilled water and stirred for 2 hours at room temperature, followed by reaction in an autoclave at 100°C for 1 day. The solid powder was dried by evaporating the solvents. Then, the sample was ion exchanged with sulfuric acid as follows: 1.0 g of this solid was added into a mixture of 30 ml distilled water, 10 ml ethanol and 5 ml sulfuric acid (96%) , vigorously stirred for 24 hours and filtered. The residue on the filter paper was washed thoroughly with water and dried at 80°C for 6 hours prior to use, giving the sample of H-PDVB-SO_3H. For comparison, zeolites such as ZSM-5 are typically prepared at high temperature and pressure [25].

Preparation of mesoporous ɣ-Al_2O_3 supported K_2O

4.0 g of 4-vinylpyridine was polymerized using 0.1 g AIBN by refluxing at 80ºC in 20 ml ethanol solvent. The mixture was cooled and to it 1 g of Aluminum isopropoxide was added and stirred for 12 hours. The mixture was kept at room temperature for 24 hours under stirring until all solvent evaporated. The solid obtained was autoclaved at 180 ºC

for 48 hours. The autoclaved solid was calcined at 550ºC for 5 hours to obtain the mesoporous Aluminum oxide. To 0.5 g of this mesoporous Al oxide, 2 molar KF solution was added dropwise until the solid appeared to absorb no more of the KF solution. The sample was dried for 6 hours at 100ºC and kept at 180ºC for 12 hours. This was then followed by calcination at 550ºC for 3 hours.

Catalyst Characterization

Nitrogen adsorption isotherms were measured using a Micromeritics ASAP Tristar system at the liquid nitrogen temperature. The samples were outgassed for 10 h at 150°C before the measurements. The pore-size distribution was calculated using the Barrett–Joyner–Halenda (BJH) model. FTIR spectra were recorded by using a Bruker 66V FTIR spectrometer. X-ray powder diffraction (XRD) of samples was recorded on a Rigaku D/max2550 PC powder diffractometer using nickel-filtered CuKα radiation. Electron microscopy images were obtained on a JEOL 6335F field emission scanning electron microscope (FESEM) with a Thermo Noran EDX detector and a Tecnai T12 transmission electron microscope. CHNS elemental analysis was performed on a Perkin-Elmer series II CHNS analyzer 2400. Thermogravimetric analyses (TGA) were performed on a PerkinElmer TGA7 in flowing nitrogen gas and air (60 ml/min) with a heating rate of 20°C min^{-1}.

Separation of bio-oil from bio-solid

The organic fraction of the acidulated bone was obtained from a bone processor. Slow stirring of this material at 35ºC, over a period of 16 hours, effected the separation of

residual solids and additional water from the oil. After separating the supernatant oil, the water and remaining material was similarly treated with overnight stirring two more times, at 35ºC, to separate additional oil from the mixture. The solid material that remained behind was filtered to rid it of excess water. The resultant solid cake was dried at 60ºC for two days to remove remaining water and the residual solid was used for pyrolysis.

Esterification of oleic acid

Esterification of oleic acid was carried out with the solid acid catalyst at 65°C in a 25ml three-neck round bottom flask fitted with a water-cooled reflux condenser for control purposes as a comparison to other acid catalysts and as a comparison to the experiments with the acidulated bone oil. The methanol to oleic acid molar ratio was kept at 9:1. All the catalysts were used at the same mass concentration, 5% (w/w) with respect to the oleic acid. The samples withdrawn periodically were centrifuged at 3500RPM (RCF = 2060 g's) for 2min to form two layers, the upper layer being methanol and water, and the lower layer being methyl esters of oleic acid. The lower layer was titrated to determine the amount of remaining oleic acid and therefore the free fatty acid conversion.

Transesterification of food grade canola oil

The solid base catalyst was used for transesterification of food grade canola oil for control experiments according to a statistical design of experiments. A careful

experimental protocol was undertaken in this section of the work to explore this new catalyst for transesterification of triglyceride oils. The reactions were carried out in a 25 mL three-neck round bottom flask, provided with thermometer, mechanical stirring and condenser. The flask with cooking oil was preheated to 65ºC, then the methanol was added. The amount of methanol was calculated to give a molar ratio of 10:1 methanol:oil, assuming a molecular weight of canola oil equal to 880 g/mol [5]. The reaction was catalyzed using the solid base catalyst, which was added after the methanol had been added. Samples were withdrawn and centrifuged at 3500RPM for 2min to form two phases. The upper phase consisted of methyl esters and the lower phase contained glycerin. The methyl ester layer was washed with water and dried using sodium sulfate and analyzed by GC.

The statistical design of these experiments followed the response surface methodology (RSM). RSM was utilized to design experiments and model conversion of oil as a response. A Box-Behnken design with three factors was utilized to determine the effect of variables on oil conversion. The three factors investigated were reaction temperature (T), reaction time (t) and catalyst concentration (C). Seventeen experiments, including five replications at design center, were carried out randomly to estimate errors. Design-Expert 7.1 software was used in this study to plot response surface and analyze the experimental data [6].

Two-step esterification-transesterification of acidulated bone oil

Acidulated bone oil was converted to biodiesel via solid catalysts for the first time. 20 ml of acidulated bone oil were heated and centrifuged to remove any remaining solid

impurities. In order to avoid saponification reaction in the high free fatty acid (FFA) content oil, the FFA was esterified with methanol by either H_2SO_4 or H-PDVB-SO_3H solid acid catalyst. When the FFA content was lower than 0.5%, the samples were centrifuged to separate acid catalyst from esterified oil and methanol. The treated oil and an appropriate volume of methanol with either KOH or super base solid catalyst (5.5 w/w%) were placed into a dry reaction flask equipped with reflux condenser and magnetic stirrer. The reaction mixture was blended for 60 min at a temperature of 65°C. The crude ester layer was separated from the glycerol layer by 2min centrifugation. To separate methanol, the crude ester phase was washed three times with distilled water, until the washings were neutral. The ester layer was dried by using anhydrous magnesium sulfate and filtered.

Gasification and pyrolysis

Thermogravimetric analysis (TGA) in air was used to carry out the gasification of bio-solids. The experiment aimed at exploring the extent of gasifiability. Pyrolysis of the bio-solids was studied by both TGA and in a fixed bed reactor. Gas chromatography with a Mass Spectrophotometric detector was employed to analyze the composition of the pyrolysis liquid products. The gasification and pyrolysis of the bio solids was performed in (a) air and (b) nitrogen, respectively, employing a heating rate of 10°C/min to 900ºC. Each experiment was held at 120°C for 30 min to remove moisture in the sample.

Fast pyrolysis was carried out in a quartz reactor [Figure S1 Supporting information] heated by a drop tube furnace at 600C to produce bio oil from the bio solids. The fast

heating rate was attained by sliding the pyrolysis reactor into the hot zone of the furnace. The liquid products, collected using two impingers in dry-ice bath, were analyzed for product selectivity with Gas Chromatography - Mass Spectroscopy (GC-MS). The column temperature was held at 40°C for 10 min and then increased to 280°C at a rate of 5°C/min. Before the GC-MS analysis, the sample was washed and diluted with methanol.

Analysis of Acidulated bone oil and Biodiesel

The composition and quality of the biodiesel obtained from acidulated bone oil as the feedstock was analyzed in several ways. The acid number of the product was determined, as per ASTM D7651, by titration with 0.07 M potassium hydroxide solution and the FFA content and the conversion were computed subsequently. Gas chromatography as per ASTM 6584 was used to analyze the free and total glycerin content in biodiesel. The derivatized solution was injected (1 μl) into a Hewlett-Packard 5890 Series II Gas Chromatograph equipped with Quadrex Aluminum Clad column with a 1 meter retention gap and employing a flame ionization detector to determine fatty acid methyl-ester (FAME), glycerol and glyceride (tri-, di-,mono-) concentrations. The resulting chromatograms were analyzed by computer-assisted programs using Chem-Station software (Hewlett-Packard, now Agilent Technologies).

Results and Discussion

Catalyst Characterization

Characterization of solid acid H-PDVB-SO_3H

Figure 4.1 shows the N_2 isotherms and pore size distribution of H-PDVB-SO_3H. H-PDVB-SO_3H shows a type-IV curve with a sharp capillary condensation step at P/P0=0.8-0.95, indicating the formation of mesopores in the sample [17]. A BET surface area of 171 m^2/g was obtained, which is larger than Amberlyst 15 and smaller than H-ZSM-5 (Table 1). The obtained pore volume of 0.52 cm^3/g is significantly higher than both Amberlyst 15 and H-ZSM-5 (Table 4.1). The H-PDVB-SO_3H shows very uniform pore size centered at 21.2 nm, in good agreement with previous results for this family of catalysts [19]. Additionally, the S content and H concentration of H-PDVB-SO_3H were 1.3 and 1.8 mmol/g respectively, higher than those of H-ZSM-5, and lower than those of Amberlyst 15. In general, increasing the concentration of active sites usually results in decreasing the BET surface areas of the samples [20-26]

Figure 4.2 shows the FT-IR spectrum of H-PDVB-SO_3H. Notably, the peaks near 620 and 1092 cm^{-1} associated with S-O, and S=O bond are clearly seen. Also, the weak peak at 1042 cm^{-1} assigned to the formation of C-S bond is also observed. Above results confirmed that the sulfonic group has been successfully introduced into H-PDVB-SO_3H.

Characterization of mesoporous ɣ-Al_2O_3 supported K_2O

Figure 4.3 shows the XRD patterns of crystalline mesoporous ɣ-Al_2O_3 before and after treatment with solution. The peaks can be indexed to the cubic structure of ɣ-Al_2O_3 as shown by the structural indices noted on curve (a) in Figure 4.3, which are in good agreement with the literature results [22]. After treatment with KF, and a second calcination, a weak peak near $2\theta = 42.7^o$ was observed, which is assigned to the presence of K_2O, indicating the transformation of KF to K_2O during the calcination process

[23,24]. The above results demonstrate that the K_2O active site has been successfully loaded in the sample of crystalline mesoporous ɣ-Al_2O_3.

Figure 4.4 shows the N_2 isotherms and pore size distribution of crystalline mesoporous γ-Al_2O_3 and ɣ-Al_2O_3-K_2O. Both of the samples show type IV isotherms, giving a sharp capillary condensation step at relative pressure (P/P0) ranging from 0.70 to 0.95, indicating the presence of mesoporous structure in these samples [17, 19].

Correspondingly, the pore sizes of ɣ-Al_2O_3-K_2O are centered at 13.8 nm, lower than that of ɣ-Al_2O_3, which should be attributed to the introduction of K_2O active site, partially blocking the mesopores in ɣ-Al_2O_3. It should be noted here that the BET surface areas, pore sizes and pore volumes of ɣ-Al_2O_3-K_2O decrease when compared with that of crystalline mesoporous γ-Al_2O_3. For example, crystalline mesoporous γ-Al_2O_3 has the BET surface area, pore size and pore volume at 185 (m^2/g), 23 nm and 1.0 (cm^3/g), respectively. After loading of 10 wt% of KF, the sample of ɣ-Al_2O_3-K_2O gives the BET surface area, pore size and pore volume at 173 (m^2/g), 13.8 nm and 0.48 (cm^3/g) (Figure 4). The decreased surface areas, pore sizes and pore volumes for ɣ-Al_2O_3-K_2O were mainly attributed to the introduction of KF, and similar results have been reported previously [14]. Figure 4.5 shows the SEM images of ɣ-Al_2O_3-K_2O, which exhibits the monolith morphology with rough surface, giving abundant nanoporosity, the porous structure was favorable for good catalytic performance.

Oil content of Acidulated bone

Dewatered acidulated bone was heated overnight at a temperature of 35ºC. This separated the water and residual solids from the oil layer, as shown in Figure 4.6. Figure 4.6 (a)

shows the acidulated bone prior to the separation procedure and Figure 4.6 (b) shows the clearly separated layers of the dewatered acidulated bone after being heat treated at 35ºC for 16 hours. A clear phase separation between the water and solid layer, and the oil layer is evident. The average yield of oil from acidulated bone was 40%. The oil layer was found to be approximately 11.3% FFA and roughly 89% triglycerides.

Catalytic activity of H-PDVB-SO_3H.

The esterification of oleic acid catalyzed by H-PDVB-SO_3H, Amberlyst 15, ZSM-5 zeolite and H_2SO_4 is shown in Figure 7 with all catalysts at 5% (w/w) with respect to the oleic acid. The conversions increase steadily, reach the maximum values (ca. 97.1%) after a reaction time of 5h and plateau afterwards. Clearly, H-PDVB-SO_3H samples showed much higher catalytic activities in esterification than did the solid acids of Amberlyst 15 and ZSM-5 zeolite. In some cases, the activities of H-PDVB-SO_3H samples were comparable with those of H_2SO_4.

Catalytic activity of ɣ-Al_2O_3- K_2O **and effect of different variables on oil conversion**

The relationship between canola oil conversion and three independent variables, reaction temperature, reaction time and catalyst concentration, were studied. The experimental design listed in Table 2 provides the conversion of canola oil for each experimental run.

Regression model and statistical analysis

The responses obtained are detailed in Table 4.2. Three independent variables were correlated with the response using a polynomial. Least squares regression was used to fit the obtained data to the polynomial and the best fit model obtained was Eq. (1):

$$\text{Conversion}(\%) = +98.15 + 6.42t + 26.63C + 8.15Tt - 8.44tC - 9.25t^2 - 21.21C^2 \quad (1)$$

Where T is Temperature, t is time, and C is catalyst concentration.

Table 4.3 shows the Analysis of Variance (ANOVA) of this model. The results indicate that this model describes the experiments well [6]. The correctness of the fit between the suggested model and experimental data were evaluated in terms of the F-value, R^2, R^2_{adj}, and p-value [6].

Table 4.3 gives the statistical parameters and it can be seen that the F-value was 35.58 and p-value was less than 0.0001 which indicates that the quadratic model was significant. Moreover, each term in the model was also tested for significance. A p-value smaller than 0.05 implies that the corresponding model term is significant. The significance of the linear terms for reaction time (t) and catalyst concentration (C) on the conversion is apparent as shown in Table 4.3 in the corresponding high F values. The low p-values (<0.0001) also indicate the insignificant chance (0.01%) of the F value being due to noise in the experiment

Figure 4.8a plots the studentized residuals versus predicted FAME yield [6]. The random scatter nature of the plot indicates that the variations in the original observations are unrelated to the value of the response [6]. The random scatter of the residuals also underscores the appropriateness of the suggested model as a description of the process.

Figure 4.8b plots the actual and predicted oil conversion taking actual values for each specific run from Table 4.2 while the predicted values are produced by the model, Eq.(1). R^2 calculates the variation around the mean described by the model. If there exist extraneous terms in a model, large values of R^2 can be misleading [6]. Additional factors in a given model inflate the value of R^2 irrespective of their significance. The data in figure 8a lead to values of R^2 and R^2_{adj} of 0.9786 and 0.9511, respectively. The significance of the model is underscored by the high value of the adjusted determination coefficient.

Influence of catalyst concentration (C), reaction time (t) and reaction temperature (T) on canola oil conversion. The catalyst concentration was identified statistically as the most important variable in the response analysis. Table 3 shows that the catalyst concentration has a large positive effect on the oil conversion response.

A response surface plot for oil conversion in Figure 4.9 depicts the change of oil conversion with varying catalyst concentration and reaction time, plotted for the case where reaction temperature is 60ºC. The maximum oil conversion of 99.07% was obtained at 5.5 % catalyst concentration. Reaction time has a positive effect on the oil conversion. The maximum oil conversion of 99.07% was achieved when the reaction time is 50 min.

Figure 4.10 shows the influence of catalyst concentration and reaction temperature on oil conversion for the case where the reaction time is 50 min. The reaction temperature has a positive effect on the oil conversion response. By increasing reaction temperature, oil conversion increased. The maximum oil conversion of 99.07% was achieved when the reaction temperature is 70C. However, the temperature did not appear alone as a significant variable in the regression model due to the narrow range of temperatures tested.

Two-step biodiesel production from acidulated bone oil with heterogeneous catalysts

H-PDVB-SO_3H was used as a solid acid catalyst for FFA esterification, at a loading of 5 wt% with respect to the weight of acidulated bone oil. A typical run consisted of 10g acidulated bone oil at a methanol:FFA molar ratio of 9:1 and was carried out at 65°C. The progress of esterification of FFA to ME was monitored through the decrease in the acid number. An acid number of 0.23 mg of KOH/g oil was achieved in less than 3h of reaction time, as shown in Figure 4.11.

After the FFA content in acidulated bone oil was reduced to less than 0.5 wt% with H-PDVB-SO_3H, the pre-treated acidulated bone oil was used for the subsequent biodiesel production using ɣ-Al_2O_3-K_2O catalyzed transesterification. 0.025 g of ɣ-Al_2O_3- K_2O was added into pre-treated acidulated bone oil (1.5 g) and methanol (0.4 mL).

The reaction mixture was stirred at 65 ºC. There was a rapid conversion of TG to ME observed during the first 30 minutes of reaction using solid based-catalyzed reaction with methanol, 95% of the TG converted to ME. After 60min, equilibrium was achieved at about 99.5% TG conversion. Table 4 shows the specification of biodiesel obtained from

acidulated bone oil. As shown in table 4.4, the biodiesel passed ASTM specifications pertaining to acid number, total and free glycerin.

A comparison of the results for acidulated bone oil with the control experiments indicate close correspondence between the observed reaction rates. The esterification of the FFA in the bone oil transpired at a roughly equal rate to that in the oleic acid. In both cases, approximately 3 hours were required to achieve high FFA conversion to methyl esters. The transesterification of TG to methyl esters may have occurred slightly slower in the bone oil than in the canola oil. Very high conversion of TG was achieved in roughly 50 minutes in the canola oil but 60 minutes was required with the acidulated bone oil.

Reusability experiments

The recyclability of solid base ɣ-Al_2O_3-K_2O has been checked by determining the performance of the recycled catalysts without any reactivation using food grade canola oil. Figure 4.12 shows the recycling experiments carried out under the most active conditions. There is a loss of roughly 20% in activity after five cycles. More work is required to determine if this activity loss is acceptable in a designed process that includes regeneration. The recyclability results are comparable with a previously reported study for ɣ-Al_2O_3-K_2O catalyzed transesterification of pure triglycerides, where the catalyst was prepared with a more difficult procedure with sol gel method [24]. Verziu et al [24] used ɣ-Al_2O_3-K_2O solid base for transesterification of sunflower oil and with microwave heating. The oil conversion decreases from 98% to 57% after 6 runs at a temperature of 75°C and 120min reaction time. With the new catalyst reported here, the oil conversion

decreases from 99% to 75% after 6 runs at a reaction temperature of 60°C and reaction time of 60min.

Gasification of heavy product

The concept of utilizing acidulated bone bio-solids in gasification was driven by the comparison of the hydrogen-to-carbon and oxygen-to-carbon ratios, as well as the hydrogen-to-carbon effective ratio (Table 4.5), with those of lignocellulose biomass (pine sawdust) and glucose. The elemental analysis (H/C, O/C and H/C_{eff} in Table 4.5) shows that the acidulated bone bio-solids compose a hydrogen rich feedstock, which implies its potential for gasification. The feasibility of pyrolyzing feedstocks of high H/C_{eff} ratios was articulated by Zhang et al. [27], where the aromatic and olefin yield (desired pyrolysis products) as a function of H/C_{eff} was studied. They found that increasing H/C_{eff} ratio from 0 (glucose) to 2 (methanol) results in increasing the aromatic and olefin yields (from 27% to 80%, respectively). Moreover, there is an inflection point at H/C_{eff} ratio of 1.2, after which the aromatic and olefin yield does not increase rapidly. As shown in Table 4.5, all the materials analyzed in this study have the H/C_{eff} less than 1.2, which means the aromatic and olefin yield are expected to change significantly among these feedstocks as the H/C_{eff} varies. The acidulated bone bio-solid has a much greater H/C_{eff} than pine and glucose, which implies its potential to producing higher aromatic and olefin yields via pyrolysis.

As shown in Figure 4.13, gasification and pyrolysis of the bio-solid were simulated in (a) air and (b) nitrogen, respectively, in TGA at 10ºC/min to 900 ºC. In Figure 4.13 (a), multiple peaks appear in the DTG analysis of the combustion of bio-solids, with the first in the 200ºC-400ºC range and the second in the 400ºC-600ºC range. By comparing the

combustion (Figure 4.13 (a)) and pyrolysis (Figure 4.13 (b)) experiments, the first DTG peak is attributed to thermal decomposition of the bio-solids and the second DTG peak represents the oxidation of bio-solid chars [27]. As shown in the pyrolysis TGA experiment, about 18% char residue was left after the pyrolysis. In the combustion experiment less than 1% residue remained in the TGA crucible. This result indicates that about 17% of the total residue after (slow) pyrolysis is char, which cannot be further pyrolyzed in inert gas atmosphere, but it is combustible. The 1% residue after combustion should include mostly inorganic compounds (ash). Further analysis of the residue and its environmental impact will be discussed in the future. The above analysis indicates that almost the entirety (99%) of the bio-solids is combustible, which also implies the feasibility of producing synthesis gas from the bio-solid through gasification.

As shown in Table 4.6 and figure 4.14, the liquid products of pyrolysis of bio-solids are mostly long-chain hydrocarbons. This preliminary result appears to not follow the trend observed by Zheng et al.[27] since the aromatic and olefin yield are low. As a comparison, the liquid products from the fast pyrolysis of glucose (a lignocellulose biomass model compound) at 600°C are also listed in Table 6, and contain many small oxygenates, such as furan compounds. Production of oxygenates from pyrolysis of lignocellulose biomass is often reported in the literature [27-35]. In that respect, pyrolysis of bio-solids is advantageous as compared to other commonly studied biomass sources. Future studies will focus on reactor conditions that optimize the production of high quality bio-oil from the brown grease bio-solids.

Conclusions

The possibility of 100% utilization of the acidulated bone waste for producing biofuels was studied. An efficient mesoporous polymeric solid acid catalyst (H-PDVB-SO_3H) with superhydrophobic properties was used as a catalyst for pretreatment of acidulated bone oil. Crystalline mesoporous ɣ- Al_2O_3 based solid base (ɣ- Al_2O_3- K_2O) with large BET surface area, stable framework and ultra-strong base strength was synthesized for transesterification reaction. The resulting mesoporous solid super base of ɣ- Al_2O_3- K_2O exhibits excellent catalytic activity and good recyclability in transesterification when compared with conventional solid base such as LDH, CaO, and nonporous ɣ-Al_2O_3 supported K_2O super base. The biodiesel passed ASTM specifications pertaining to acid number, total and free glycerin.

The bio-solids separated from the aqueous layer of the acidulated bone were analyzed and found to have a H/C_{eff} ratio greater than wood, implying excellent potential for producing higher aromatic and olefin yields via pyrolysis. When pyrolyzed at 600°C, the bio-solids yielded liquid products that were mostly long-chain hydrocarbons according to GC/MS analysis. Almost 99% of the bio-solids were combustible implying the feasibility of producing synthesis gas from the bio-solids through gasification. These results establish the feasibility of converting ~100% of the raw acidulated bone to valuable energy products.

References

[1] Toda M, Takagaki A, Okamura M, Kondo JN, Hayashi S, Domen K, Hara M. Green chemistry: Biodiesel made with sugar catalyst. Nature 2005; 438:178.

[2] Damschroder RE, Kantiman ME. Method of preparing gelatin. US patent, 1946, No. 646,211

[3] Dias JM, Alvim-Ferraz MCM, Almeida MF. Mixtures of vegetable oils and animal fat for biodiesel production: influence on product composition and quality. Energ. Fuel 2008; 22: 3889–3893.

[4] Berrios M, Gutiérrez MC, Martín MA, Martín A. Application of the factorial design of experiments to biodiesel production from lard. Fuel Process. Technol. 2009; 90: 1447–1451.

[5] Singh A, He B, Thompson J, Van Gerpen J. Process optimization of biodiesel production using alkaline catalysts. Applied Engineering in Agriculture. 2005; 22 (4): 597-600.

[6] Noshadi I, Amin NAS, Parnas RS. Continuous production of biodiesel from waste cooking oil in a reactive distillation column catalyzed by solid heteropolyacid: optimization using response surface methodology (RSM). Fuel 2012; 94:156-164.

[7] Talebian-Kiakalaieh A, Amin NAS, Zarei A, Noshadi I. Transesterification of waste cooking oil by heteropoly acid (HPA) catalyst: Optimization and kinetic model. Applied Energy 2013;102: 283-292.

[8] Knothe GH. A technical evaluation of biodiesel from vegetable oils vs. algae. Will algae-derived biodiesel perform?. Green Chemistry 2011;13:3048-3065.

[9] Noshadi I, Kanjilal B, Du S, Bollas GM, Suib SL, Provatas A, Liu F, Parnas RS. Catalyzed production of biodiesel and bio-chemicals from brown grease using Ionic Liquid functionalized ordered mesoporous polymer. Applied Energy 2014;129:Pages 112–122

[10] Unker SA, Boucher MB, Hawley KR, Midgette AA, Stuart JD, Parnas RS. Investigation into the relationship between the gravity vector and the flow vector to improve performance in two-phase continuous flow biodiesel reactor. Bioresource Technology 2010;101(19):7389-7396.

[11] Talebian-Kiakalaieh A, Amin NAS, Mazaheri H, A review on novel processes of biodiesel production from waste cooking oil. Applied Energy 2013;104: 683–710

[12] Corma A. Inorganic Solid Acids and Their Use in Acid-Catalyzed Hydrocarbon Reactions. Chemical Reviews 1995;95: 559-614.

[13] Jaliliannosrati H, Amin NAS, Talebian-Kiakalaieh A, Noshadi I. Microwave assisted biodiesel production from Jatropha curcas L. seed by two-step in situ process: Optimization using response surface methodology. Bioresource Technology 2013;136: 565–573.

[14] De Vos DE, Dams M, Sels BF, Jacobs PA. Ordered Mesoporous and Microporous Molecular Sieves Functionalized withTransition Metal Complexes as Catalysts for Selective Organic Transformations. Chemical Reviews 2002;102: 3615-3640.

[15] Sivasamy A, Cheah KY, Fornasiero P, Kemausuor F, Zinoviev S, Miertus S. Catalytic Applications in the Production of Biodiesel from Vegetable Oils. ChemSusChem 2009;2: 278 – 300.

[16] Melero JA, Van Grieken RV, Morales G. Advances in the Synthesis and Catalytic Applications of Organosulfonic-Functionalized Mesostructured Materials. Chemical Reviews 2006; 106: 3790-3812.

[17] Noshadi I, Kumar RK, Kanjilal B, Parnas R, Liu H, Li J, Liu F. Transesterification Catalyzed by Superhydrophobic–Oleophilic Mesoporous Polymeric Solid Acids: An Efficient Route for Production of Biodiesel. Catalysis Letters 2013; 1-6.

[18] Blass BE. KF/Al2O3 Mediated organic synthesis. Tetrahedron. 2002; 58 (11): 9301–9320

[19] Liu F, Kamat RK, Noshadi I, Peck D, Parnas RS, Zheng A, Qi C, Lin Y. Depolymerization of crystalline cellulose catalyzed by acidic ionic liquids grafted onto sponge-like nanoporous polymers. Chem. Commun. 2013;49: 8456.

[20] Roggenbuck J, Sch¨afer H, Tsoncheva T, Minchev C, Hanss J, Tiemann M. Mesoporous CeO2: Synthesis by Nanocasting, Characterisation and Catalytic Properties. Microporous Mesoporous Mater. 2007; 101: 335.

[21] Yang HF, Zhao DY. Synthesis of replica mesostructures by the nanocasting strategy. J. Mater. Chem. 2005;15: 1217.

[22] Powder Diffraction Files (Joint Committee on Powder Diffraction Standards, Philadelphia, 1967) card 29-0063 (γ-Al2O3), now called The International Ceter for Diffraction Data

[23] Liu F, Zuo S, Xia X, Sun J, Zou Y, Wang, L, Li C, Qi C. Generalized and high temperature synthesis of a series of crystalline mesoporous metal oxides based nanocomposites with enhanced catalytic activities for benzene combustion. Journal of Materials Chemistry A. 2013;28: 4089-4096.

[24] Verziua M, Floreaa M, Simon S, Simon V, Filip P, Parvulescu VI, Hardacre C. Transesterification of vegetable oils on basic large mesoporous alumina supported

alkaline fluorides—Evidences of the nature of the active site and catalytic performances. Journal of Catalysis 2009;263: 56–66.

[25] Liu F, Wang L, Sun Q , Zhu L, Meng X, Xiao FS. ZSM-5 Zeolite Single Crystals with b-Axis-Aligned Mesoporous Channels as an Efficient Catalyst for Conversion of Bulky Organic Molecules. J. Am. Chem. Soc. 2012;134 (10): 4557–4560

[26] Lowell S, Shields JE, Thomas MA, Thommes M. Characterisation of Porous Solid and Powders: Surface Area, Pore Size and Density, Kluwer Academic Publischers, 2004.

[27] Zhang H,Cheng YT, Vispute TP, Xiao R, Huber GW. Catalytic Conversion of Biomass-derived Feedstocks into Olefins and Aromatics with ZSM-5: The Hydrogen to Carbon Effective Ratio. Energy & Environmental Science 2011; 4: 2297-2307.

[28] Cheng G, He PW, Xiao B, Hu ZQ, Liu SM, Zhang LG, Cai L. Gasification of biomass micron fuel with oxygen-enriched air: Thermogravimetric analysis and gasification in a cyclone furnace. Energy 2012; 43: 329-333.

13

[29] Park JY, Kim DK, Lee JS, Esterification of free fatty acids using water-tolerable Amberlyst as a heterogeneous catalyst. Bioresource Technol. 2010; 101: S62-S65.

[30] Patwardhan PR, Satrio JA, Brown RC, Shanks BH, Product distribution from fast pyrolysis of glucose-based carbohydrates. Journal of Analytical and Applied Pyrolysis 2009; 86: 323-330.

[31] Mullen CA, Boateng AA. Chemical composition of bio-oils produced by fast pyrolysis of two energy crops. Energy & Fuels 2008; 22: 2104-2109.

[32] Branca C, Giudicianni P, Di Blasi C. GC/MS characterization of liquids generated from low- temperature pyrolysis of wood. Ind. Eng. Chem. Res 2003; 42(14): 3190-3202.

[33] Olazar M, Aguado R, Bilbao J, Barona A. Pyrolysis of sawdust in a conical spouted-bed reactor with a HZSM-5 catalyst. AIChE Journal 2000; 46: 1025-1033.

[34] Carlson TR, Tompsett GA, Conner WC, Huber GW, Aromatic Production from Catalytic Fast Pyrolysis of Biomass-derived Feedstocks. Topics in Catalysis 2009; 52: 241-252.

[35] Du S, Valla JA, Bollas GM. Characteristics and origin of char and coke from fast and slow, catalytic and thermal pyrolysis of biomass and relevant model compounds. Green Chemistry 2013; 15: 3214-3229

Table 4.1 The textural and acidic parameters of various solid acid catalysts

Samples	S content (mmol/g)[a]	Acid sites (mmol/g) [b]	S_{BET} (m^2/g)	V_p (cm^3/g)	D_p (nm) [c]
H-PDVB-SO_3H	1.3	1.8	171	0.52	21.5
Amberlyst 15	4.30	4.70	45	0.31	40
H-ZSM-5	-	0.92	368	0.31	14.5
H_2SO_4	10.2	20.4	-	-	-

[a] Measured by elemental analysis
[b] Measured by acid-base titration
[c] Pore size distribution estimated from BJH model

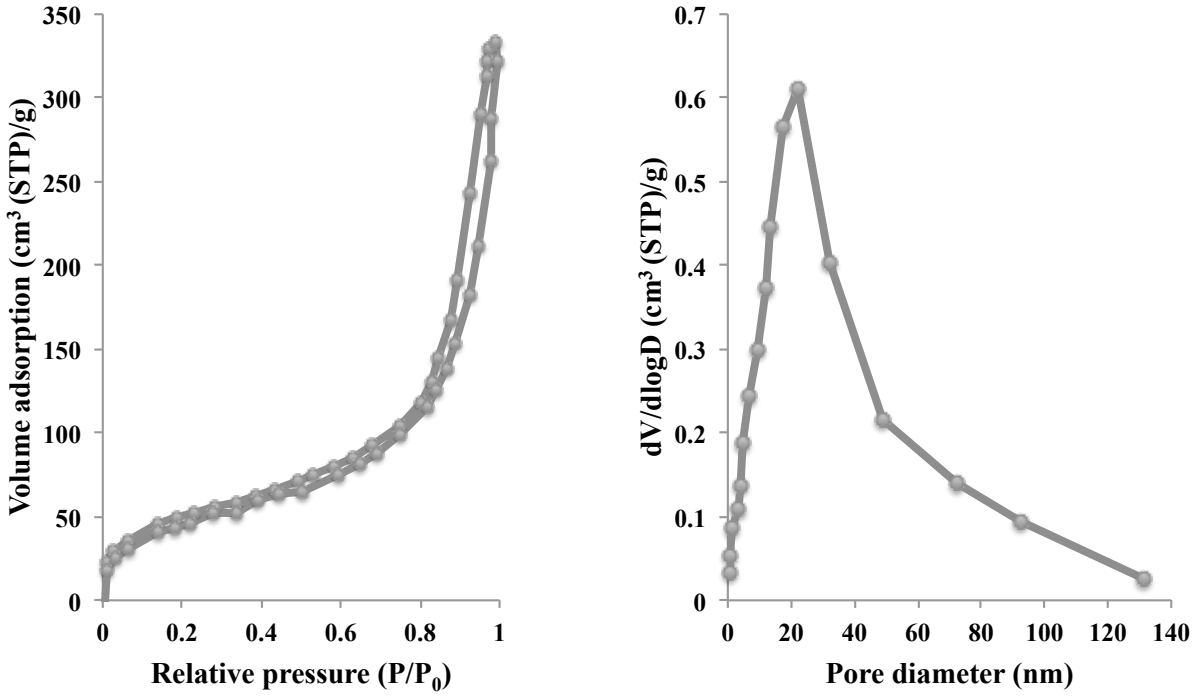

Figure 4.1. N_2 isotherms and pore size distribution of H-PDVB-SO_3H

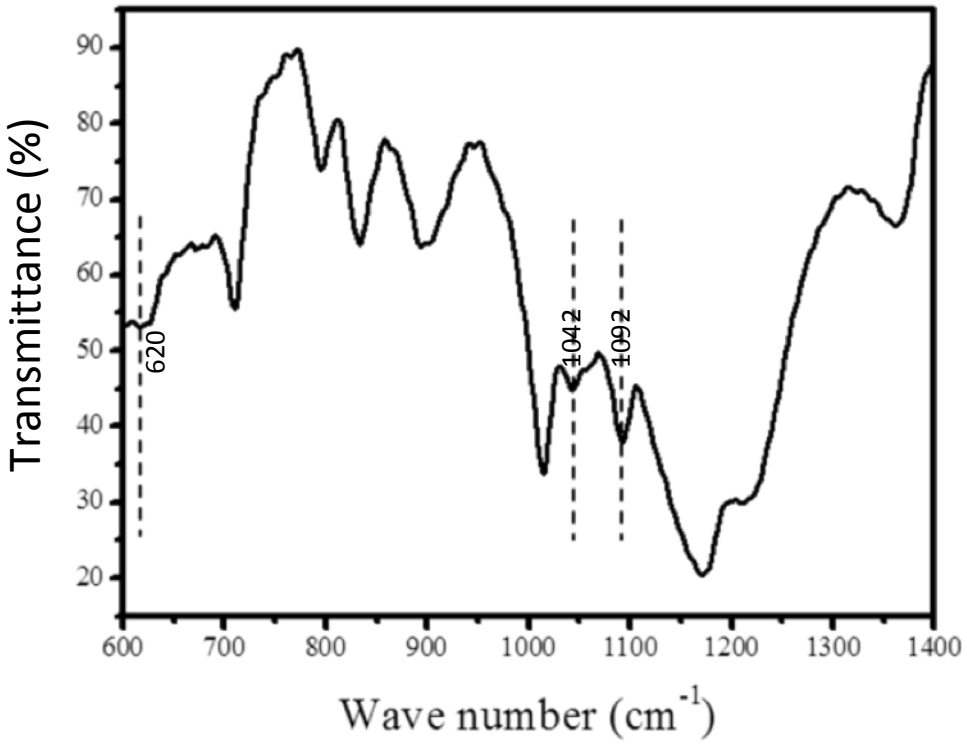

Figure 4.2. FT-IR spectrum of H-PDVB-SO_3H

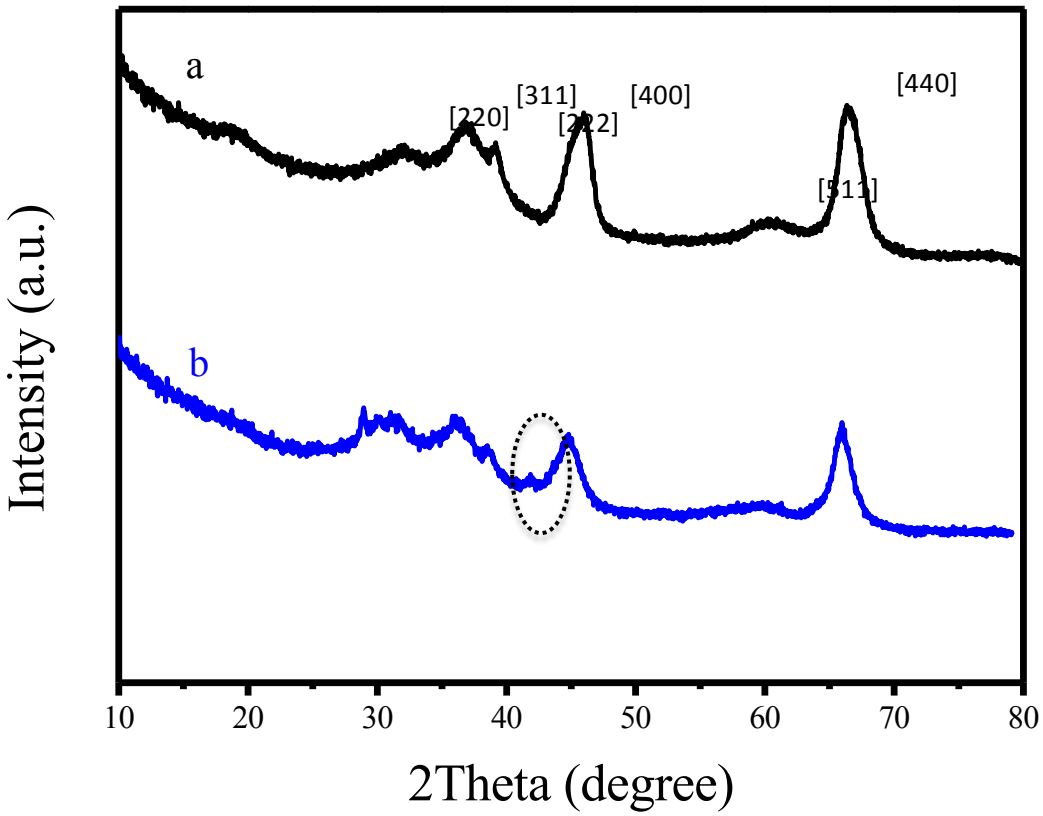

Figure 4.3. XRD patterns of a) crystalline mesoporous ɣ-Al_2O_3 templated and calcinated once, and b) crystalline mesoporous ɣ-Al_2O_3 after treatment with KF and calcinated a second time. The structural indices at the peaks in (a) indicate the crystal structure [22]. The dotted circle in (b) indicates the new peak near 42.7^o that appeared in the material illustrating the presence of the K_2O active site [24].

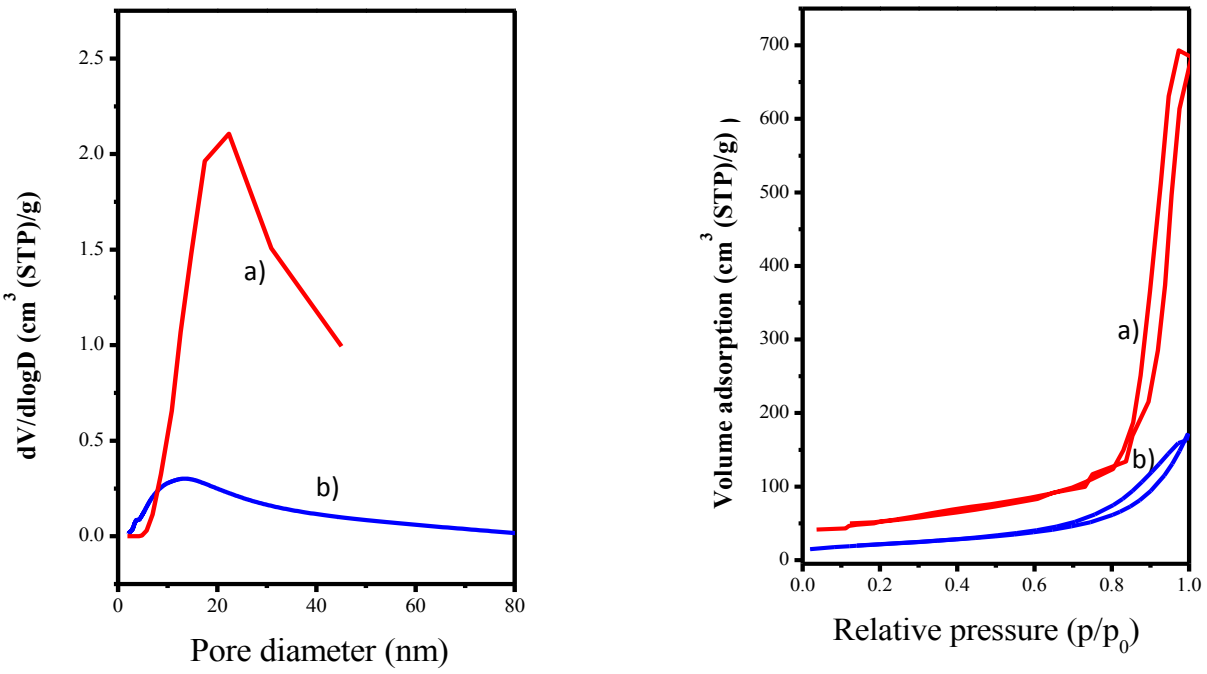

Figure 4.4. N_2 isotherms and pore size distribution of crystalline mesoporous a) γ-Al_2O_3 and b) ɣ-Al_2O_3-K_2O

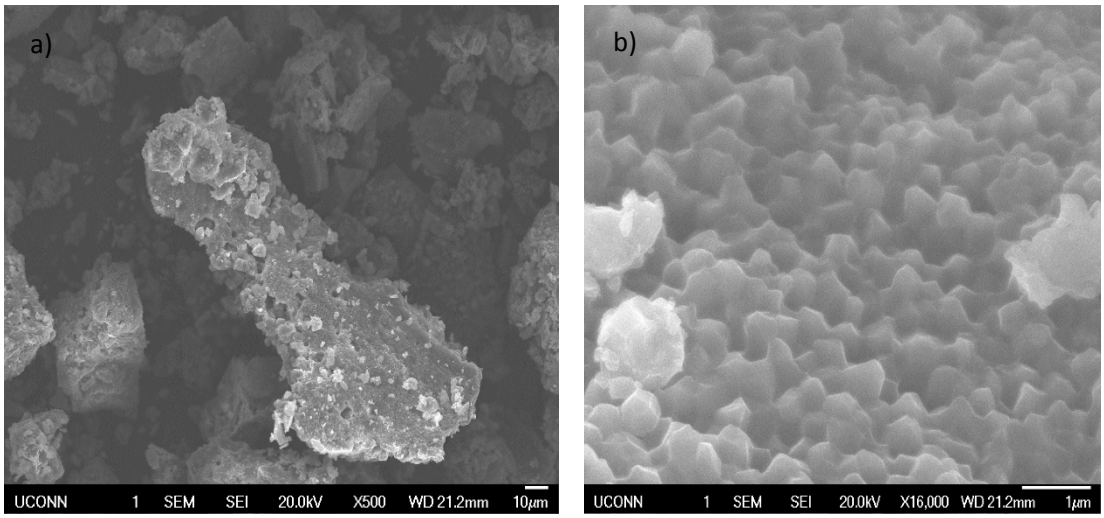

Figure 4.5. SEM Images of ɣ-Al_2O_3- K_2O a) 500X b) 16000X

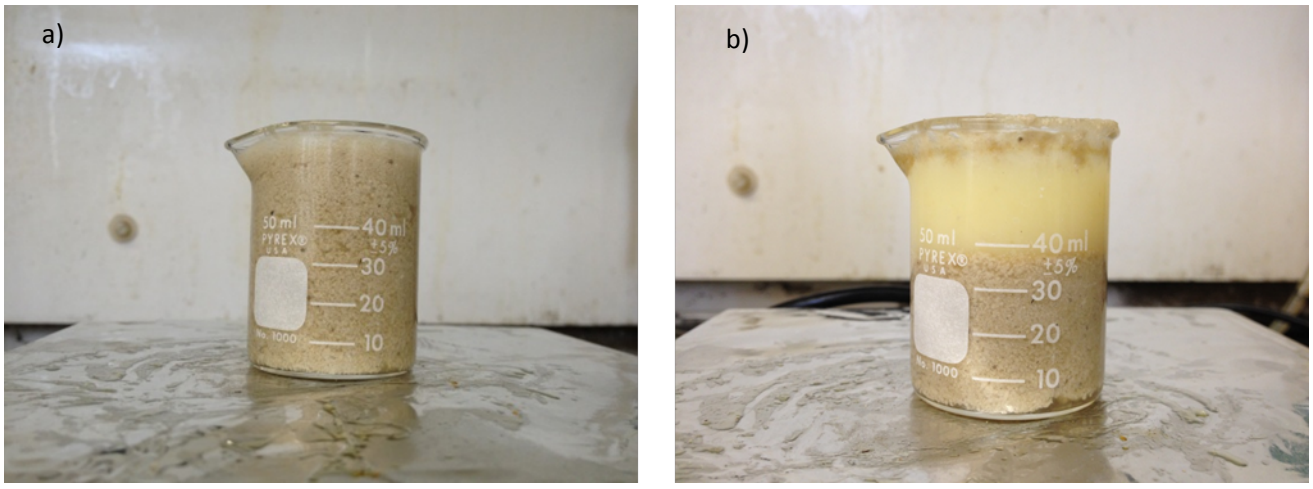

Figure 4.6.Oil separation from dewatered acidulated bone by heating at temperature of 35ºC for 16hr: (a) acidulated bone prior to separation; (b): separated layers of dewatered acidulated bone after being heat treated at 35ºC for 16 hours.

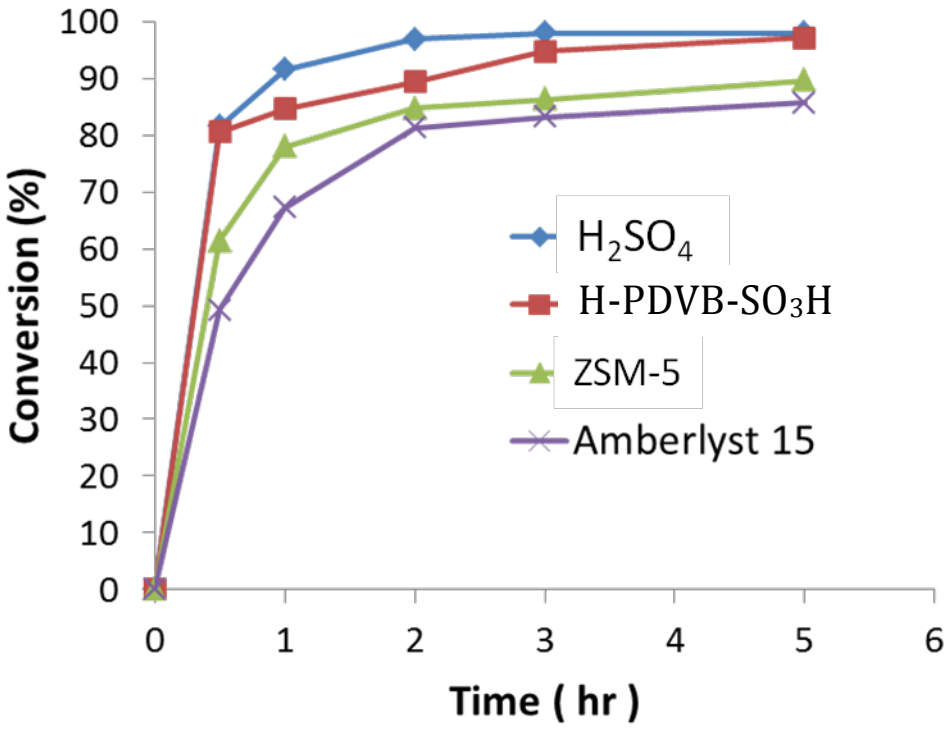

Figure 4.7. Catalytic activity of H-PDVB-SO_3H on esterification of oleic acid. (Temperature=65ºC, methanol:oil=9, catalyst 5wt% relative to oil)

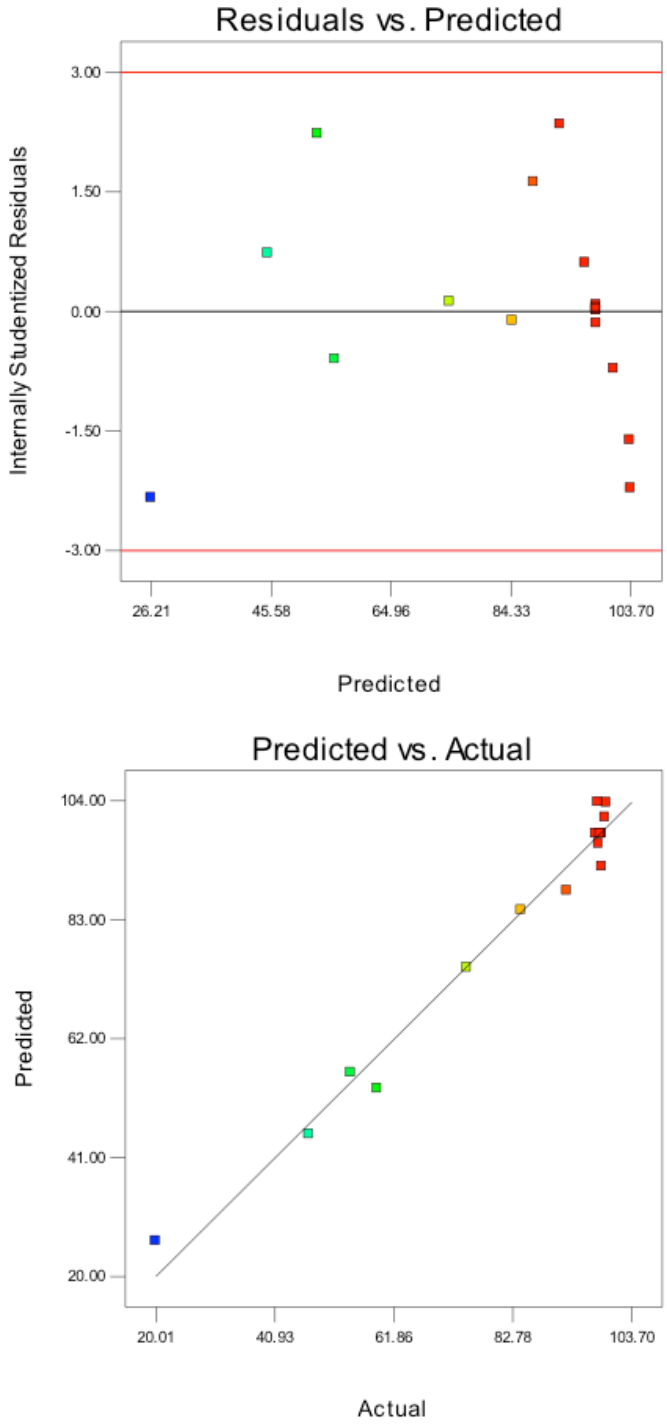

Figure 4.8 (a) The studentized residuals and predicted response plot (b) The actual and predicted plot

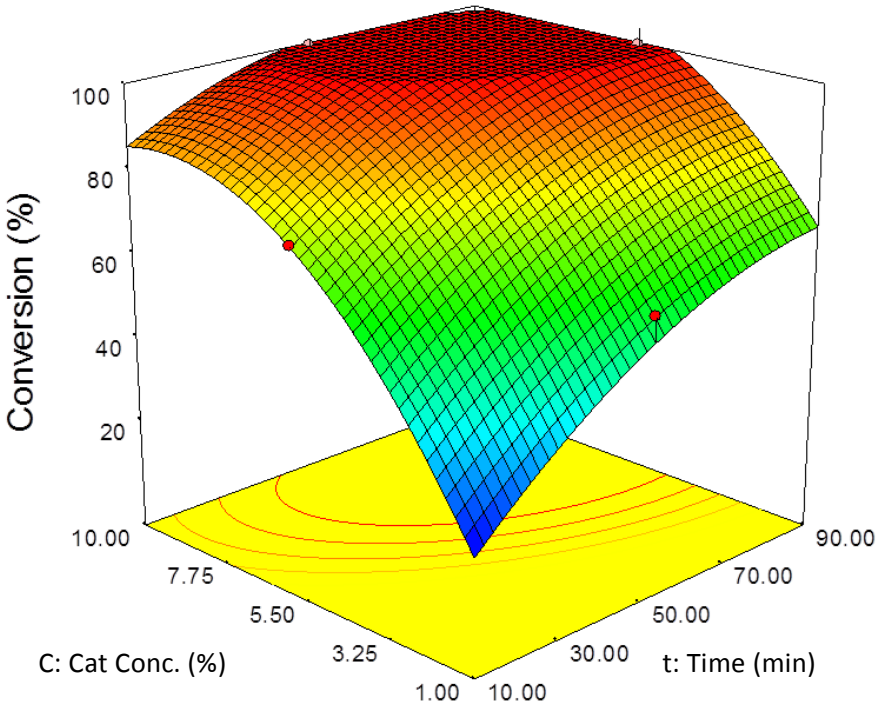

Figure 4.9. The effect of catalyst concentration (wt% relative to oil) and reaction time on oil conversion, for reaction temperature of 60ºC.

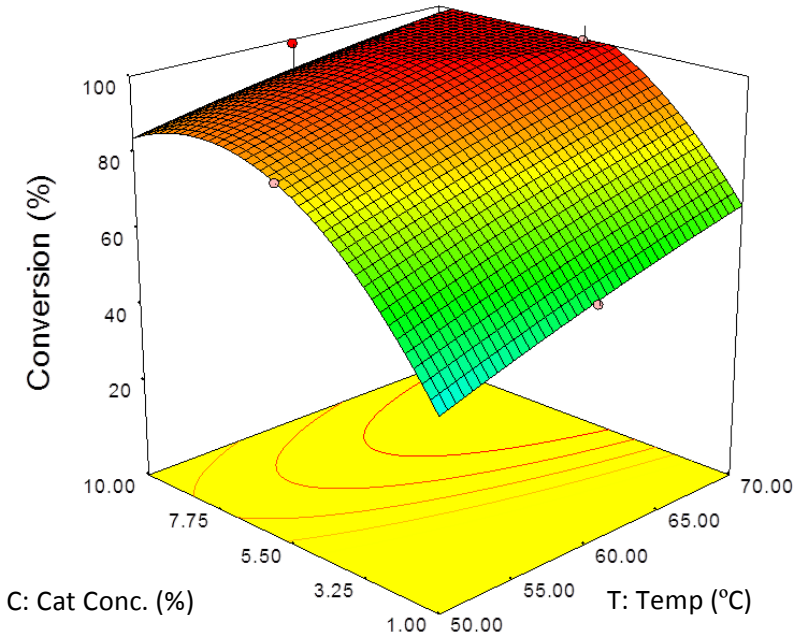

Figure 4.10 The effect of catalyst concentration (wt% relative to oil) and reaction temperature on oil conversion, for reaction time of 50 min.

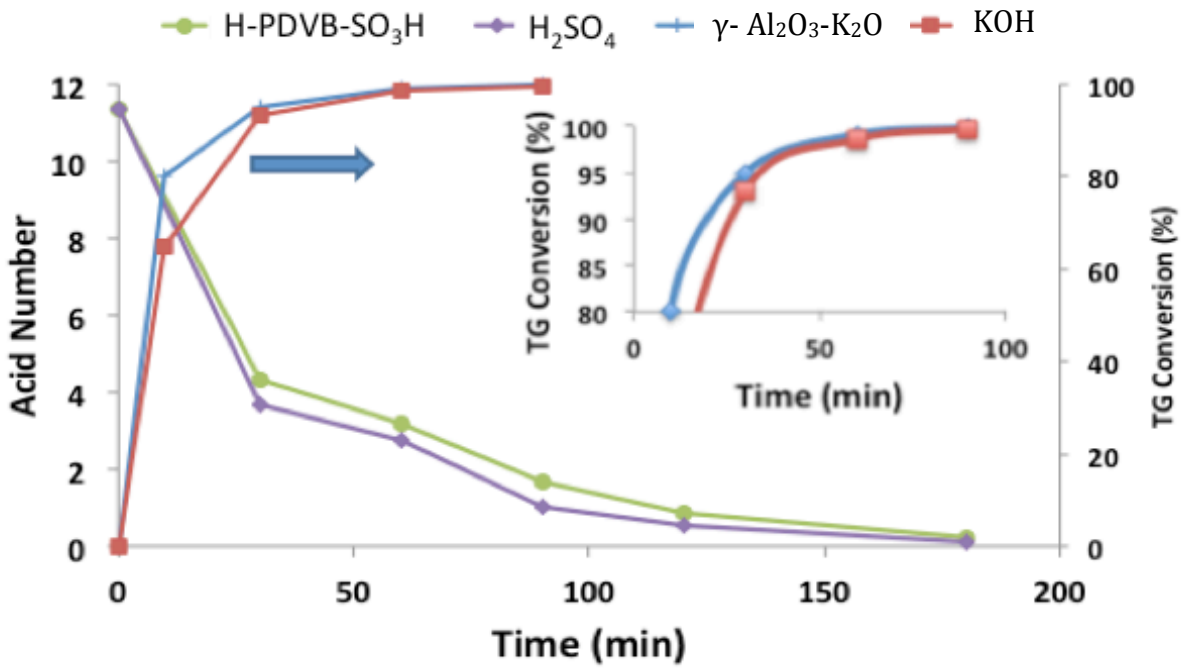

Figure 4.11 H-PDVB-SO_3H Esterification and ɣ-Al_2O_3-K_2O transesterification of acidulated bone oil

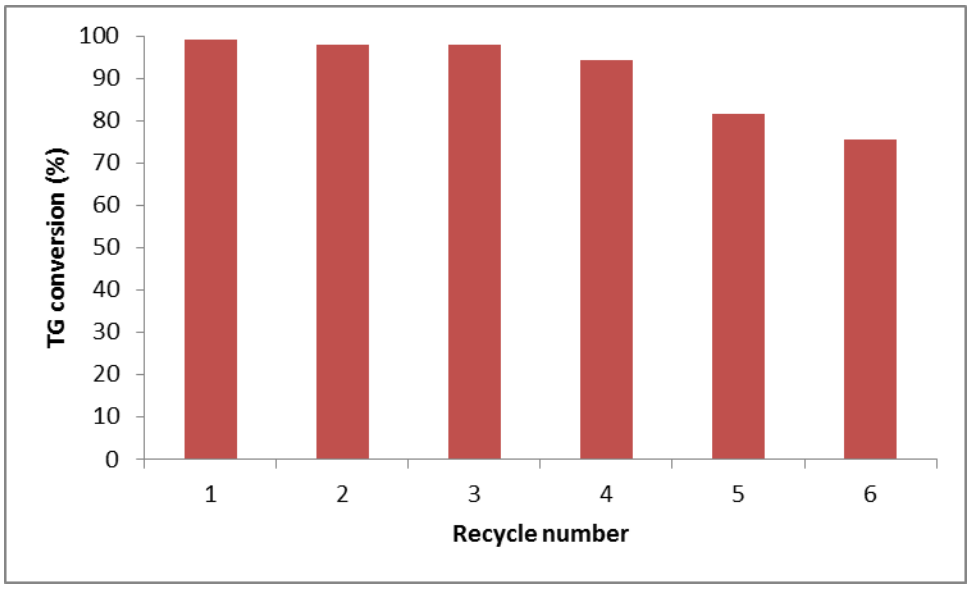

Figure 4.12 ɣ-Al_2O_3- K_2O catalyst recyclability for transesterification of TG with methanol

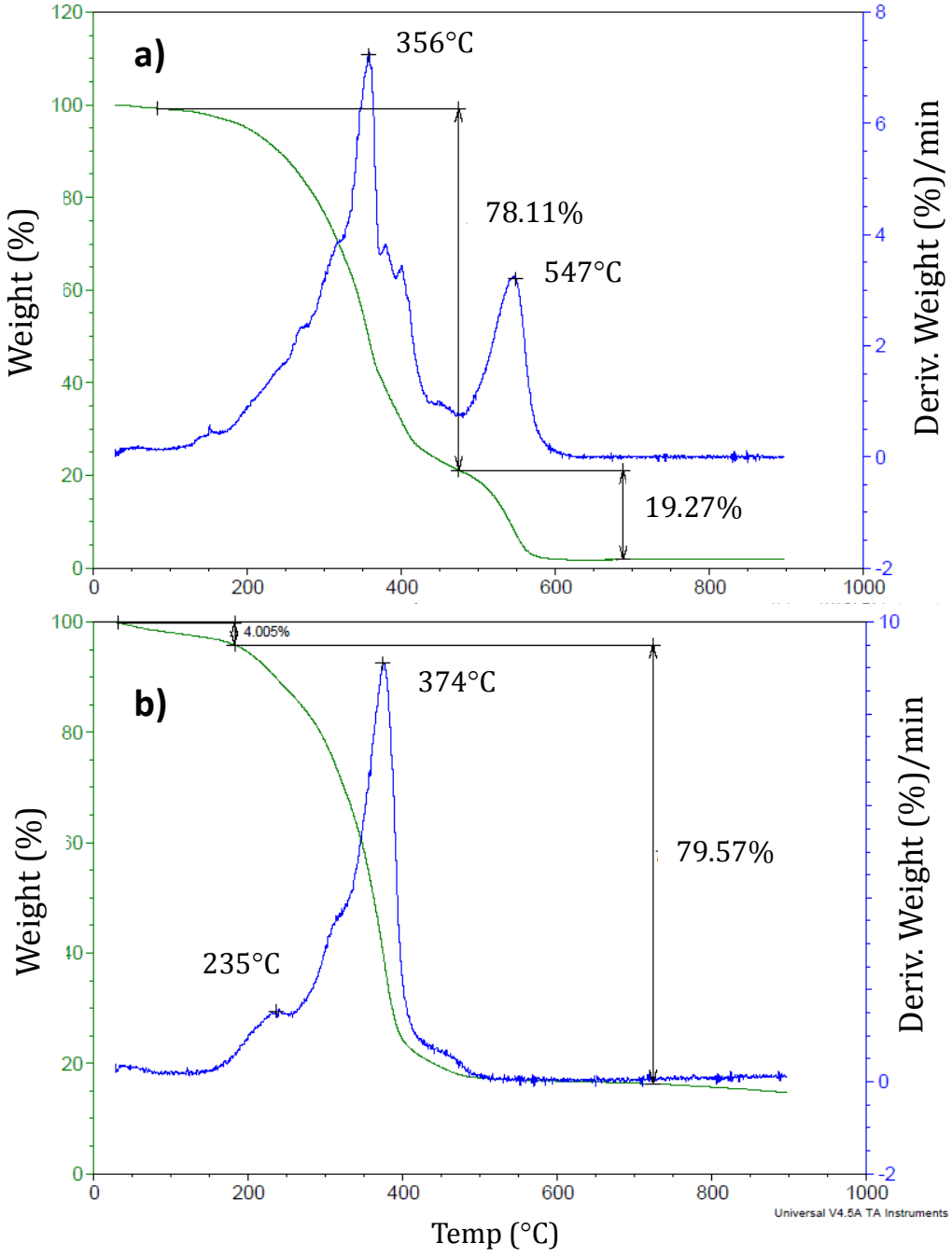

Figure 4.13 Thermogravimetric analysis (TGA) of biosolid in (a) air and (b) nitrogen

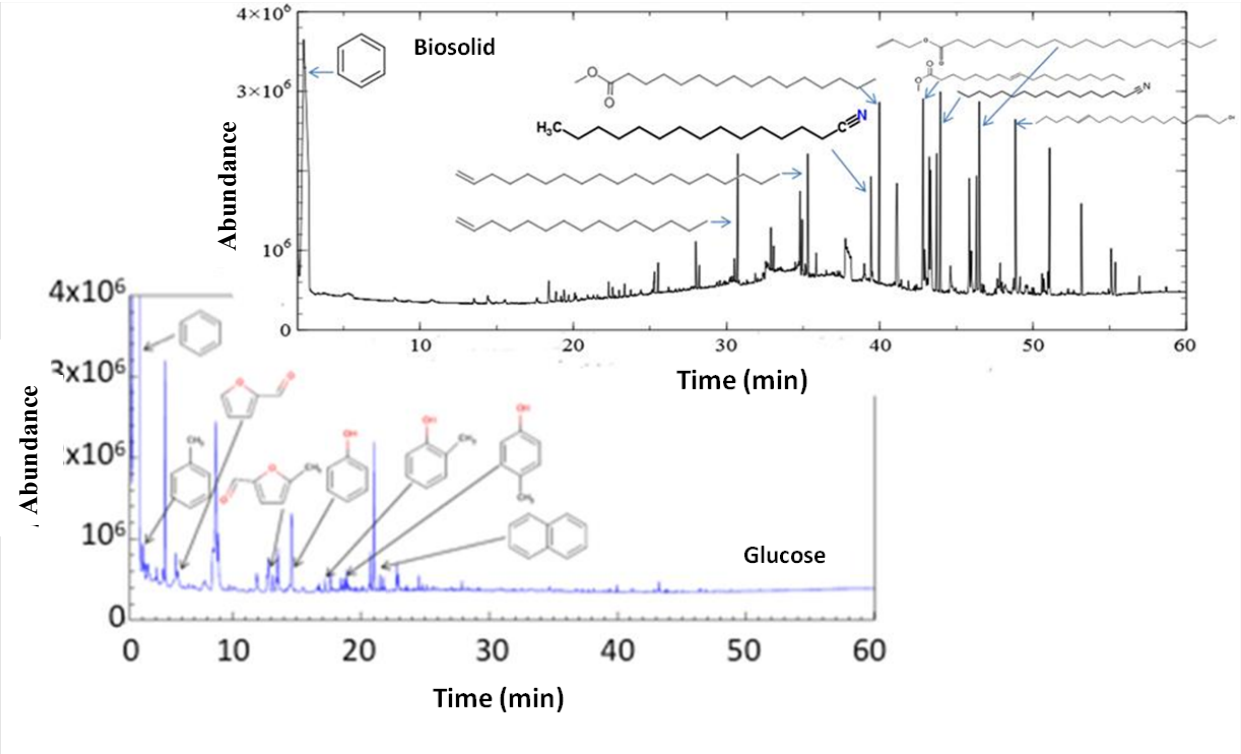

Figure 4.14 GC-MS chromatograms of glucose and biosolid pyrolysis

Table 4.1 The textural and acidic parameters of various solid acid catalysts

Samples	S content (mmol/g) [a]	Acid sites (mmol/g) [b]	S_{BET} (m^2/g)	V_p (cm^3/g)	D_p (nm) [c]
H-PDVB -SO_3H	1.3	1.8	171	0.52	21.5
Amberlyst 15	4.30	4.70	45	0.31	40
H-ZSM-5	-	0.92	368	0.31	14.5
H_2SO_4	10.2	20.4	-	-	-

[a] Measured by elemental analysis

[b] Measured by acid-base titration

[c] Pore size distribution estimated from BJH model

Table 4.2 Experimental design results for transesterification of Canola oil

Run	Temperature (ºC)	Time (min)	Cat Conc. (wt% to oil)	Conversion (%)
1	50	50	10	97.82
2	60	50	5.5	98.23
3	50	90	5.5	84.3
4	50	50	1	46.98
5	70	50	1	59.01
6	60	50	5.5	97.43
7	60	50	5.5	98.38
8	60	90	10	98.51
9	70	50	10	99.07
10	70	90	5.5	99.30
11	60	10	1	20.01
12	60	90	1	54.34
13	60	50	5.5	98.21
14	70	10	5.5	74.76
15	60	10	10	97.94
16	60	50	5.5	98.52
17	50	10	5.5	92.35

Table 4.3 ANOVA for the regression model and respective model terms

Source	Sum of Squares	Df	Mean Square	F Value	p-value Prob>F	
Model	8978.11	9	997.56	35.58	<0.0001	significant
T (Temperature)	14.28	1	14.28	0.50	0.4984	
t (time)	330.11	1	330.11	11.77	0.01	
C (Catalyst %)	5671.12	1	5671.11	202.28	<0.0001	

$R^2 = 0.9786$ $R^2_{adj} = 0.9511$

Table 4.4 Acidulated bone oil biodiesel specification

	Acid Number (ASTM limit: <0.5)	Free glycerin (ASTM limit <0.02)	Total glycerin (ASTM limit <0.24)
Two-step process	0.28	0.01	0.21

Table 5: Elemental analysis of bio-solid, pine and glucose (mol%, dry basis)

Feedstock	**N**	**C**	**H**	**O***	**H/C**	**O/C**	**H/C_{eff}**
Bio-solid	1.97	37.7	49.36	10.97	1.30	0.29	1.00
Pine	0.20	34.52	46.33	18.95	1.34	0.55	0.25
Glucose	0.00	25.00	50.00	25.00	2.00	1.00	0.00

* Oxygen content was calculated by difference

Table 6. Liquid product selectivity from fast pyrolysis of glucose and bio-solid

R.T. (min)	Glucose	R.T. (min)	Bio-solid	R.T. (min)	Bio-solid (Continued)
2.75	Benzene	2.40	Benzene	39.44	Pentadecanenitrile
3.31	Toluene	18.40	Phenol	39.97	Hexadecanoic acid, methyl ester
5.56	Furfural	19.40	5-Undecene	41.87	Hexadecanoic acid, 14-methyl, methyl ester
13.12	2-Furancarboxaldehyde, 5-methyl	22.31	1-Dodecene	43.11	9,12-octadecadienoic acid (Z,Z)-, methyl ester
14.59	Phenol	22.58	Dodecane	43.23	8-Octadecenoic acid, methyl ester
17.63	Phenol, 2-methyl	25.30	1-Tridecene	43.32	Heptadecanenitrile
18.48	Phenol, 4-methyl	25.53	Tridecane	43.71	Octadecanoic acid , methyl ester
18.75	Bicyclo [2.2.1]hept-5-ene, 2-acetyl	28.01	2-Tetradecene	46.32	Octadecanoic acid, 2-propenyl ester
21.75	Naphthalene	28.22	Tetradecane	47.67	9-Octadecenamide, (Z)-Erucylamide
22.79	1,4:3,6-Dianhydro-alpha-d-glucopyranose	30.53	1-Pentadecene	47.86	1-Nonadecene
		33.07	Hexadecane	47.98	1-Docosene
		34.80	8-Heptadecene	48.20	Octadecanamide
		34.93	1-Octadecene	39.44	Pentadecanenitrile
				39.97	Hexadecanoic acid, methyl ester
				41.87	Hexadecanoic acid, 14-methyl, methyl ester
				43.11	9,12-octadecadienoic acid (Z,Z)-, methyl ester
				43.23	8-Octadecenoic acid, methyl ester

Annexure:

Sulphur Estimation results from AmSpec LLC.

AmSpec

Certificate of Analysis

Vessel / Object:		Job No:	41-13-00498
Location:		Date Sampled:	10/29/2013
Job Type:	Submitted	Date Tested:	11/5/2013
Product Grade:	Biodiesel	Date Reported:	11/5/2013
Client Reference:			

Sample Number:	411300498-001	Sample ID & Desc:	Biodiesel HCl - T. Program
		Sample Type:	

Method	Test	Result	Units
ASTM D5453	Total Sulfur	29.98	mg/kg

Sample Number:	411300498-002	Sample ID & Desc:	Biodiesel HCl - Raney-Ni 75C, 16 Hr.
		Sample Type:	

Method	Test	Result	Units
ASTM D5453	Total Sulfur	18.02	mg/kg

Sample Number:	411300498-003	Sample ID & Desc:	Biodiesel HCl - Raney-Ni 140C. 8Hr.
		Sample Type:	

Method	Test	Result	Units
ASTM D5453	Total Sulfur	8.83	mg/kg

Sample Number:	411300498-004	Sample ID & Desc:	Biodiesel HCl - IL
		Sample Type:	

Method	Test	Result	Units
ASTM D5453	Total Sulfur	Out of Range	mg/kg

Reported By: Mike Bailey
Title: Laboratory Manager

AmSpec Services, LLC - 30 Commercial St - Everett, MA 02149 - (617) 389-7272
RESULTS ARE VALID "AS AT" DATE AND LOCATION LISTED

Page 1 of 1

AmSpec

Certificate of Analysis

Vessel / Object:	Submitted Biodiesel	Job No:	41-14-00417
Location:	RPM	Date Sampled:	5/29/2014
Job Type:	Submitted	Date Tested:	6/7/2014
Product Grade:	Bio Diesel	Date Reported:	6/9/2014
Client Reference:			

Sample Number:	411400417-001	Sample ID & Desc:	Solid Acid Treated Biodiesel from Br. Grease
		Sample Type:	

Method	Test	Min	Max	Result	Units
ASTM D5453	Total Sulfur			109.97	mg/kg

Sample Number:	411400417-002	Sample ID & Desc:	Brown Grease
		Sample Type:	

Method	Test	Min	Max	Result	Units
ASTM D5453	Total Sulfur			354.62	mg/kg

Reported By: Mike Bailey
Title: Laboratory Manager